AD NUMBER

AD805438

NEW LIMITATION CHANGE

TO

Approved for public release, distribution unlimited

FROM

Distribution authorized to U.S. Gov't. agencies and their contractors; Critical Technology; NOV 1966. Other requests shall be referred to Air Force Materials Laboratory, Wright-Patterson AFB, OH 45433.

AUTHORITY

afml ltr, 7 dec 1972

(9) Final ... technical rept.) 1 Jun - 31 ... 1965

(18) (17) AF ML-TDR-64-173-Pt-4
~~Part IV~~

AD 805438

(6) HIGH TEMPERATURE PROTECTIVE COATINGS FOR GRAPHITE.

(10) J. M. Criscione,
S. Sarian,
H. F. Volk,
R. A. Mercuri
J. W. Nuss
~~F. W. Meszaros~~

(15) AF 33(657)-1125

(16) AF-7350

(17) 735002

(40) (1) Union Carbide Corporation
Carbon Products Division

TECHNICAL DOCUMENTARY REPORT NO. ML-TDR-64-173, Part IV

(11) Nov[redacted] 1966

(12) 101 p.

This document is subject to special export controls and each transmittal to foreign governments or foreign nationals may be made only with prior approval of the Metal and Ceramics Division, Air Force Materials Laboratory (MAMC), Wright-Patterson Air Force Base, Ohio 45433.

Air Force Materials Laboratory
Research and Technology Division
Air Force Systems Command
Wright-Patterson Air Force Base, Ohio

NOTICES

When Government drawings, specifications, or other data are used for any purpose other than in connection with a definitely related Government procurement operation, the United States Government thereby incurs no responsibility nor any obligation whatsoever; and the fact that the Government may have formulated, furnished, or in any way supplied the said drawings, specifications, or other data, is not to be regarded by implication or otherwise as in any manner licensing the holder or any other person or corporation, or conveying any rights or permission to manufacture, use or sell any patented invention that may in any way be related thereto.

Copies of this report should not be returned to the Research and Technology Division unless return is required by security considerations, contractual obligations, or notice on a specific document.

FOREWORD

This Summary Technical Report was prepared by Union Carbide Corporation, Carbon Products Division, Technical Center, Parma, Ohio 44130, under USAF Contract No. AF 33(657)-11253. This contract was initiated under Project No. 7350, "Refractory Inorganic Nonmetallic Materials," Task No. 735002, "Refractory Inorganic Nonmetallic Materials: Graphite." The title of the project is "High Temperature Protective Coatings for Graphite." This work is being administered under the direction of the Air Force Materials Laboratory, Research and Technology Division, Air Force Systems Command, Wright-Patterson Air Force Base, Ohio, with W. C. Simmons, Captain, USAF, Project Engineer.

This report covers the work conducted from 1 June 1965 to 31 May 1966. The manuscript was released by the authors in November 1966 for publication as a technical report.

The authors would like to express their thanks to Drs. M. Stern and R. Kebler of the Union Carbide Research Institute for aid in obtaining materials for the carbon diffusion studies. Acknowledgment is made for guidance and helpful suggestions from Mr. J. C. Bowman, Director of Research, Dr. A. W. Searcy, and H. Eyring, consultants to Union Carbide Corporation, Carbon Products Division.

This technical report has been reviewed and is approved.

W. G. RAMKE
Chief, Ceramics and Graphite Branch
Metals and Ceramics Division
Air Force Materials Laboratory

ABSTRACT

The final annual report of a three-year program concerning basic factors controlling the oxidation behavior of high temperature protective coatings for graphite is presented.

The work includes: the permeability of Al_2O_3, ZrO_2 in contact with ZrB_2, and ThO_2 in contact with ZrB_2 to oxygen; the iridium-carbon eutectic temperature; the thermal expansion of ZrB_2, HfB_2, and various composites of ZrB_2 and HfB_2 with one of the rare earth hexaborides, CeB_6, YB_6, or LaB_6; the deposition of ZrB_2 on graphite via the decomposition of $Zr(BH_4)_4$; the diffusion of carbon in zirconium monocarbide and zirconium diboride; a review of the literature concerning the vapor species in the iridium-oxygen system and mass spectrometric studies involving the dissociation of $CaZrO_3$ at temperatures to 1600°C and $HfSiO_4$ at temperatures to 2000°C.

TABLE OF CONTENTS

ILLUSTRATIONS

ILLUSTRATIONS (Cont'd)

ILLUSTRATIONS (Cont'd)

ILLUSTRATIONS (Cont'd)

I. INTRODUCTION

The severe operational requirements of missiles and space vehicles require structural components that must withstand temperatures of 2000°C and higher. Graphite, because of its exceptional high temperature strength and stability, is extensively used for aerospace applications. In oxidizing atmospheres, however, graphite must be protected from oxidation. Silicon carbide coatings are now available which will give adequate protection for substantial time periods at temperatures to 1700°C. The present research program was aimed at finding materials which may afford protection for graphite to 2200°C.

To achieve this goal, fundamental information concerning various factors which control the oxidation protection of graphite has been sought. As illustrated in Figure 1, there are several factors which should be considered in selecting a protective coating for graphite. The coating must be mechanically and chemically compatible with both graphite and oxygen, it must have a low volatility, and it must prevent diffusion of oxygen inwards and of carbon outwards.

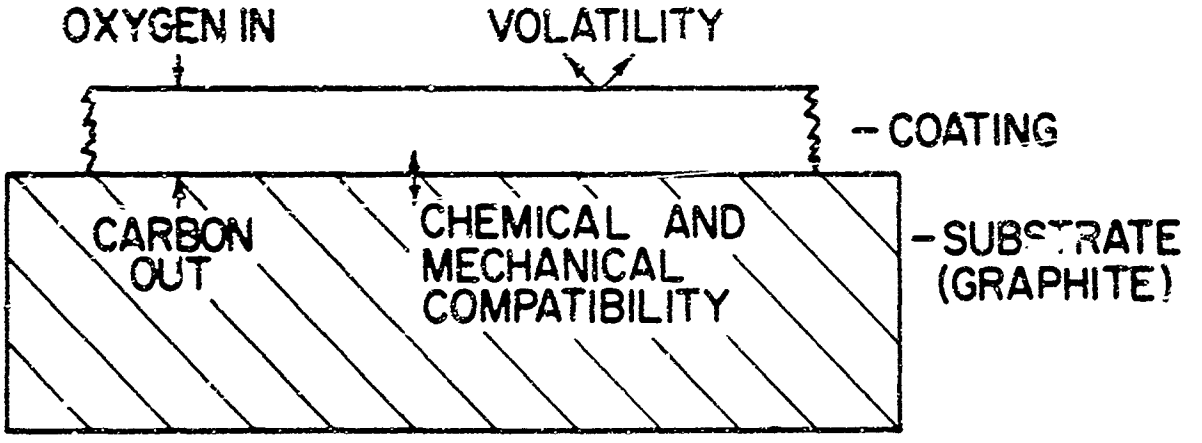

Figure 1. Factors Controlling the Oxidation Protection of Graphite

This report describes the third and final year of research directed toward evaluating coating materials for the oxidation protection of graphite at temperatures to 2200°C. Specifically, it deals with studies of the permeation of oxygen through oxides, the mechanical compatibility of potential coating systems, the diffusion of carbon through refractory carbides and diborides, the gaseous oxides of iridium, and the dissociation of mixed oxides at high temperatures.

II. SUMMARY

1. PREVIOUS WORK

A review of the previous state of the art concerning protective coatings for graphite, a description of the basic factors controlling the oxidation protection of graphite, and a review of existing information on the diffusion of oxygen and carbon through coating materials, the volatility, the chemical stability, and the mechanical compatibility of coating materials were presented in report number ML-TDR-64-173, Part I, released for publication June 1964. It was concluded that a considerable amount of research was needed to evaluate coating materials for the protection of graphite from oxidation at temperatures of 2000°C or higher.

A comprehensive program to provide fundamental information concerning various factors controlling the behavior of protective coating systems for graphite at temperatures to 2200°C and the research effort for the first year of this program are described in ML-TDR-64-173, Part II, covering the period 1 June 1963 to 31 May 1964. The work includes: the evaporation of iridium in the presence of oxygen and water vapor to temperatures of 1300°C; the results of studies involving carbon diffusion through iridium and rhodium and of oxygen diffusion through ZrO_2, HfO_2, and ThO_2 at temperatures to 2000°C; the coating of graphite with iridium and the reactions of iridium and rhodium with ZrB_2, HfB_2, ZrC, HfC, and ThC_2; the kinetics of the carbothermic reduction of ZrO_2, HfO_2, and ThO_2 to temperatures in excess of 2000°C; the chemical reactions of graphite with ZrB_2 and HfB_2; and arc plasma oxidation tests of iridium coated graphite. The practical implications of the experimental results are also discussed.

The research effort for the second year of the program was presented in ML-TDR-64-173, Part III, covering the period 1 June 1964 to 31 May 1965. Work presented includes: the oxidation kinetics of iridium and rhodium; the permeability of $ZrSiO_4$, ZrO_2, ThO_2, Al_2O_3, and BeO to oxygen; an investigation of the iridium-carbon system by means of high temperature X-ray diffraction techniques, the deposition of iridium on graphite and the volatility of HfO_2, ZrO_2, ThO_2, $ThZrO_4$, $SrZrO_3$, $BaZrO_3$, $ZrSiO_4$, and $HfSiO_4$ in the presence of water vapor; the kinetics of the carbothermic reduction of ZrO_2, ThO_2, HfO_2, $ThZrO_4$, and $HfSiO_4$; the kinetics of the reaction of ZrO_2, HfO_2, and ThO_2 with ZrC, HfC, and ThC_2, respectively; the chemical reactions of HfO_2, ZrO_2, ThO_2 with HfB_2 and ZrB_2; initial work on carbon diffusion through diborides and carbides; and the mechanical compatibility of components of multilayer coatings for graphite. Practical implications of the research results are also presented.

2. RESEARCH RESULTS

A summary of the results of the final year effort (1 June 1965 to 31 May 1966) of the program is included in the following sections.

a. Permeability of Various Aluminum Oxides to Oxygen

Oxygen permeability measurements have been made on various commerical polycrystalline aluminas and on single crystal sapphire over the temperature range 1700° to 2000°C. In polycrystalline material, the permeability is a strong function of crystallite size and purity. At 1900°C, the permeability constant $P\ell$ [g cm^{-1} sec^{-1}] to 50 torr of oxygen ranged from 1×10^{-10} to 1×10^{-8}, the activation energy ranged from 105 to 135 kcal, and the permeability varied with the one-fourth power of the oxygen pressure. In single crystal sapphire, the permeability was below the detection limit. At 2015°C, $P\ell$ of sapphire is less than 4×10^{-13} g cm^{-1} sec^{-1}.

b. Mechanical Compatibility of Iridium With Graphite

The iridium-carbon eutectic temperature was redetermined: melting occurred in the 2250° to 2280°C range. The presence of metallic impurities (one percent Fe and trace quantities of Si, Cr, Ni, and Al) lowered the melting point to 2110°C.

c. Mechanical Compatibility of Multilayer Coatings With Graphite

(1) Thermal Expansion Measurements

The thermal expansion of ZrB_2, ZrB_2-CeB_6, ZrB_2-LaB_6, ZrB_2-YB_6, and an experimental grade of graphite was determined in the range 900° to 2000°C. The thermal expansion of 78 percent dense ZrB_2 is in agreement with existing expansion information for single crystal ZrB_2. Values for thermal expansion of HfB_2, HfB_2-CeB_6, HfB_2-LaB_6, and HfB_2-YB_6 also were determined in the temperature range 900° to 2000°C. The thermal expansion of 76 percent dense HfB_2 is in agreement with values obtained from existing data for single crystal HfB_2.

The thermal expansion of all the borides investigated exhibited a close match with that of an experimental grade of graphite. Curves showing the linear expansion as a function of temperature are presented.

ZrC-coated graphite and HfC-coated graphite exhibited excellent thermal shock resistance when cycled from 25° to 2000°C.

(2) Coating Experiments

As a precursor to the vapor deposition of ZrB_2 on graphite, the thermal decomposition of zirconium borohydride, $Zr(BH_4)_4$, was investigated in the 400° to 800°C range. At low temperatures (<600°C), the decomposition products, zirconium, boron, and hydrogen, were detected in quantities consistent with

$$Zr(BH_4)_4 \rightarrow Zr + 8H_2 + 4B .$$

Above 600°C, ZrB_2, H_2, and B_2H_6 were detected among the decomposition products.

A 1-mil coating of ZrB_2 on an experimental grade of graphite (one matching the thermal expansion of the diboride) remained dense and adherent even after thermal cycling several times between 400°C and 2000°C. The zirconium diboride coatings formed on Union Carbide Corporation Grades ATJ and ZTA graphite were found to exhibit poor adherence and large macrocracks when cooled from 1750°C in the deposition experiments.

d. Carbon Diffusion Studies

The volume diffusion coefficient of carbon in ZrC is

$$1.62 \times 10^2 \exp\left(-\frac{113,200}{RT}\right) cm^2/sec.$$

The "apparent" diffusivity for diffusion-controlled phase boundary motion is about

$$2.4 \exp\left(-\frac{86,000}{RT}\right) cm^2/sec$$

and is probably the value which should be used in calculating the flux of carbon through a zirconium carbide barrier layer.

e. Studies on Multilayer Coatings - Oxygen Permeability

Both calcia- and yttria-stabilized zirconia tubes were coated with ZrB_2 to determine the effect of the latter on the permeability of ZrO_2 to oxygen, i.e., the permeability of a multilayer coating to oxygen. The calcia-stabilized zirconia tubes were destabilized during heat treatment in the presence of ZrB_2, and, as a result, either shattered or developed leaks. Yttria-stabilized zirconia was not destabilized but became oxygen deficient and, as a result, exhibited a great affinity for oxygen. After complete reoxidation of the tubes, and simultaneously, oxidation of the ZrB_2 coating, the permeability of the yttria-stabilized tubes was found to be identical with the permeability determined on the same tubes prior to the coating application.

Oxygen permeability measurements were also carried out on thoria tubes coated with ZrB_2. Initially, a threefold increase in permeability over that of uncoated ThO_2 was detected; however the permeability decreased to that of the uncoated thoria after continued exposure to oxygen. The permeability increase is attributed to an oxygen deficiency caused by the vacuum sintering of the ZrB_2 coating on thoria.

f. Oxidation of Iridium - Gaseous Oxides of Iridium

As a portion of the subcontract work on iridium oxidation performed at Rice University, a critical review of the literature concerning the vapor species in the iridium-oxygen system is presented in Appendix A. Apparently, three and possibly four gaseous oxides of iridium are present: IrO_3, IrO_2, IrO, and Ir_2O_3; IrO_3 apparently is the major species at low temperatures and IrO_2 and IrO became significant above 2000°K. The $Ir_2O_3(g)$ is probably formed exothermally and is usually a minor species; however, at high O_2 pressures and low temperatures, it is possible for $Ir_2O_3(g)$ to be the major species.

g. Vaporization of Mixed Oxides at High Temperatures

This portion of the program (Appendix B) also was subcontracted to Rice University. The vaporization of $CaZrO_3$ was investigated at temperatures to 1600°C with the aid of a Bendix time-of-flight mass spectrometer. The vaporization occurs through the dissociation of $CaZrO_3$ into gaseous CaO and solid ZrO_2. No stable $CaZrO_3(g)$ species were observed.

The vaporization of $HfSiO_4$ was investigated at temperatures to 2000°C in a magnetic mass spectrometer. In this case, the vaporization occurs through dissociation of $HfSiO_4$ into SiO and SiO_2 gaseous species and solid HfO_2. Again, no ternary gaseous oxide molecular species were detected in this study.

III. PRACTICAL IMPLICATIONS

The Practical Implications Section is presented mainly to stimulate the application of program findings. The interpretations and implications may in some cases be somewhat tenuous; however, they may motivate others to use the information presented here for the solution of coatings problems in general.

1. SINGLE LAYER COATINGS ON GRAPHITE

a. Iridium Coatings

In previous reports,[1,2] single layer coatings for the oxidation protection of graphite have been adequately discussed. It was concluded that iridium was the only single component material that would offer complete protection of graphite from oxidation at temperatures of 2000°C and above. The "life" of the coating is limited by its rate of ablation in oxygen and not by the interdiffusion of oxygen and carbon. Temperature limitations are determined primarily by the carbon-iridium eutectic temperature, which in the absence of impurities is of the order of 2250° to 2280°C. However, small amounts of impurities, e.g., Fe, Si, B, can lower the eutectic temperature by as much as 100° to 150°C. These impurities should be carefully excluded if iridium coated graphite is to be utilized at temperatures above 2100°C.

b. Single Layer Oxide Coatings

The refractory oxides and mixed oxides are not suitable for use as a coating directly on graphite when protection over an extended period of time is desired. As already discussed in previous reports,[1,2] rapid carbothermic reduction reactions limit the practical use of a single layer coating on graphite to only a few minutes. For this reason, the oxides should be considered primarily for applications in a multilayer coating system where a reaction barrier separates the oxide coating from the graphite substrate.

2. MULTILAYER COATINGS ON GRAPHITE

The concept of a multilayer coating consists of an outer layer of a refractory oxide which acts as an oxygen barrier; the oxide is prevented from reacting with the graphite substrate by means of an intermediate layer, which may consist of a refractory carbide, a refractory boride, or of iridium. The intermediate layer also serves to retard the outward diffusion of carbon to the oxide coating. The multilayer coating concept, therefore,

requires consideration of the chemical and mechanical compatibility of the intermediate layer materials with the graphite substrate and with the refractory oxides (outer layer); consideration of the oxygen permeability through the refractory oxides; and consideration of the permeability of the intermediate layer materials to carbon.

a. Chemical Compatibility of Refractory Oxides with Refractory Carbides, Borides, and Iridium

The chemical stability of ThO_2, ZrO_2, and HfO_2 with respect to various borides and carbides has been discussed extensively in a previous report.[2] Briefly, ThO_2 was found to be stable against both ZrB_2 and HfB_2 at all temperatures to 2200°C. Similarly, there was no reaction between ZrO_2 and ZrB_2 and between HfO_2 and HfB_2. This stability, however, refers only to the absence of phase changes detectable by X-ray diffraction. Minor reactions leading, e.g., to an oxygen deficient oxide can occur. These reactions would not be expected to lead to structural coating failure and their significance is discussed below in the section on oxygen diffusion.

The refractory carbides, ZrC and HfC, were found to react with ThO_2, ZrO_2, and HfO_2.[2] However, in a closed system, the reaction leads to an equilibrium and comes to a stand-still when the partial pressure of CO attains values in the order of 10^{-2} mm of mercury. In a coating system, CO formed at the oxide-carbide interface should have little or no chance to escape; the use of ZrC or HfC as intermediate barrier material appears therefore feasible.

Iridium is nonreactive with respect to both graphite and the refractory oxides and may, therefore, be used advantageously as a barrier material. Since the outer oxide coating would retard both the oxidation and evaporation of iridium, the barrier layer could be made much thinner than a single layer iridium coating.

b. Mechanical Compatibility

The adherence of a protective coating on graphite will depend strongly on the extent to which the coating and substrate are mechanically compatible. To obtain good coating adherence, it is necessary to match the thermal expansions of the various components of the coating system.

An exact definition of what constitutes an expansion "pair", i.e., a compatible coating and substrate, is difficult to obtain. Both should be isotropic and the difference in their thermal expansion should be minimal. According to R. A. Howard and E. L. Piper,[3] "General tests of several materials and substrates imply that the optimum performance is attained when the coating is under moderate compression, i.e., the thermal expansion of the substrate should be equal to or slightly higher than that of the coating."

Howard and Piper demonstrated that silicon carbide coatings (CTE range 4.4 to 5.9 in/in/°C)[4] are perfectly compatible with RVC isotropic graphite (CTE range 4.5 to 6.0 in/in/°C)[3], but will crack when applied to ATJ graphite (CTE 2.2 x 10^{-6} in/in/°C with grain and 3.42 x 10^{-6} in/in/°C across grain).[5] A number of RVC samples with various CTE's were coated with SiC and thermally cycled without coating failure, indicating that at least a 15 percent mismatch in CTE is tolerable and that possibly as much as 30 percent is acceptable. In similar experiments with silicon carbide coated ATJ, the coatings failed; however, in this case, there is a 50 percent mismatch.

The information gained concerning the thermal expansion behavior of ZrB_2 and HfB_2 containing rare-earth additives (CeB_6, YB_6, and LaB_6) allows one to predict that severe mechanical compatibility problems, due to thermal stresses, will not be encountered with these materials on high CTE graphite (5 to 6 x 10^{-6} in/in/°C). The rare-earth oxide formed on oxidation of the boride composites should serve to stabilize the ZrO_2 or HfO_2 and thus enhance its thermal shock resistance.

c. Stability and Volatility of Oxides

An oxide coating which is to function properly as an oxygen barrier must be stable and of reasonably low volatility. Thoria, alumina, stabilized zirconia and stabilized hafnia fulfill these conditions. The use of some mixed oxides, however, should be considered only with caution. Zirconium silicate was found to decompose and to soften in the 1700-1750°C temperature range. Mass-spectrometric investigations have shown that $HfSiO_4$ decomposes to gaseous SiO and SiO_2 and solid HfO_2. Similarly, $CaZrO_3$ dissociates into solid ZrO_2 and gaseous CaO.

d. Permeability of Oxides to Oxygen

In the multilayer coating concept, the primary function of the outer oxide layer is to act as an oxygen barrier. The permeability of the oxide to oxygen is, therefore, of critical importance. If a carbide is used as an intermediate barrier material, then oxygen diffusing through the coating will react to form carbon monoxide and the resulting pressure build-up at the carbide-oxide interface will ultimately lead to coating failure. If the barrier material consists of a boride, it will be converted to B_2O_3 and the respective metal oxide, again leading to ultimate coating failure when the reaction has proceeded to a point where the barrier material can no longer perform its proper function. If iridium is used as a barrier material, oxygen permeation through the oxide layer is less critical. The oxidation of iridium leads to an equilibrium and should cease at relatively low concentrations (partial pressures) of the iridium oxides. Since the iridium oxides cannot escape from the interface, an iridium barrier layer protected by a dense oxide coating

should last almost indefinitely. Coating failure will ultimately occur due to carbon diffusion through iridium and the build-up of CO pressure at the iridium-metal oxide interface.

Of all the oxides investigated, single crystal alumina exhibited by far the lowest permeability to oxygen. Coatings, however, would consist of polycrystalline alumina, which exhibits oxygen permeation via a grain boundary mechanism. The present work indicates that alumina coatings consisting of large grains with low impurity content will have a substantially lower permeability than coatings of less pure alumina and/or small grain size. At 1800°C, a representative value for the permeability of a 10-mil coating of polycrystalline alumina to 50 torr of oxygen is 4×10^{-8} g cm^{-2} sec^{-1}. The oxygen permeability through a similar coating of beryllia is less than 1×10^{-8} g cm^{-2} sec^{-1}, and beryllia appears, therefore, to be equal or somewhat better than polycrystalline alumina. The oxygen permeability of thoria, stabilized zirconia, and stabilized hafnia is higher than the permeability of polycrystalline alumina. At 1800°C, the permeability of a 10-mil layer of thoria to 50 torr of oxygen on one side and 10^{-3} torr on the other side is 3×10^{-6} g cm^{-2} sec^{-1}. The corresponding values for yttria stabilized zirconia, calcia-stabilized zirconia, and calcia-stabilized hafnia are 1×10^{-5}, 5×10^{-6}, and 6×10^{-6} g cm^{-2} sec^{-1}, respectively. The oxygen permeability in thoria, hafnia, and the various types of zirconia was not affected by grain growth. It can, therefore, be concluded that the permeability through these materials is primarily due to bulk diffusion.

The exact boundary conditions can have a significant influence on the oxygen permeability, particularly in oxides such as ThO_2, HfO_2, and ZrO_2, which can exhibit significant variations from stoichiometric composition. At 1700°C in vacuo or an inert atmosphere, coating ZrO_2 with ZrB_2 by sintering causes a slight (approximately one percent) oxygen deficiency in the oxide. Similarly, heating ThO_2 in contact with ZrB_2 at 1800°C in vacuo also resulted in a slight reduction of the oxide, although the extent of the oxygen deficiency could not be determined. The oxygen permeability of ZrB_2-coated ZrO_2 and ThO_2 was substantially higher than that of the uncoated oxides. This can be qualitatively explained on the basis of thermodynamic considerations. The equilibrium oxygen pressure in the presence of ZrB_2 at 1500°C is of the order of 10^{-6} atmospheres and vacuum sintering results in oxygen deficient oxides. The oxygen vacancy concentration gradient and the oxygen permeability are therefore correspondingly large at the beginning of the permeation experiments. Under dynamic conditions, that is when oxygen is permeating through the oxide, the thermodynamic equilibrium considerations no longer apply. The vacancy concentration gradient is then determined by how fast oxygen is removed by reaction with ZrB_2. The permeation rate decreases with time but remains enhanced as long as some unreacted boride is present. After complete oxidation of the ZrB_2 coating, the oxygen permeability is identical to that of the uncoated oxides.

The effect of ZrB_2 on the oxygen permeability was far more severe with ZrO_2 than with ThO_2. This was expected, since ZrO_2 exhibits wider variations from the stoichiometric composition. The ZrO_2 tubes also contained

approximately eight percent Y_2O_3 or stabilizer, and the presence of yttria may have contributed to the observed results.

Caution must therefore be exercised in using oxygen permeation data. The present results do not, however, automatically eliminate the use of ZrB_2 as a barrier layer on graphite. Under dynamic conditions, the oxygen permeation rate is dependent on the rate of removal of oxygen by reaction with ZrB_2. This depends on the structure, density and composition of the ZrB_2 layer as well as on the structure and composition of the oxidation product. The recently developed oxidation resistant ZrB_2 and HfB_2 compositions may well be suited for use in oxidation protective coatings on graphite.

The free energies of formation of iridium oxides are apparently so low that the use of iridium as a barrier layer does not effect the stoichiometry of the refractory oxides. The presence of iridium should therefore have no influence on the oxygen permeability of ZrO_2, HfO_2, or ThO_2.

e. Carbon Diffusion Through Intermediate Layers

The function of the intermediate layer is to prevent the reaction of the oxide with the graphite substrate. The rate of carbon diffusion through this layer, therefore, needs to be considered. The actual rates of carbon diffusion will again depend on the particular boundary conditions. The steady-state rate of carbon permeation through a plane sheet of thickness, l, whose surfaces, $x = 0$ and $x = 1$, are maintained at concentrations C_1 and C_2, respectively, is given by

$$J = D \frac{C_2 - C_1}{l} .$$

For ZrC at 1800°C, in the absence of grain boundary enhanced material transport, $D = 1.2 \times 10^{-10}$ cm^2/sec and if we take C_1 and C_2 as those concentrations for ZrC in equilibrium with pure carbon and carbon saturated metal, then the flux through a one-mil thick coating is about 1.4×10^{-8} g/cm^2-sec. If the grain boundary contribution is appreciable, the appropriate diffusivity is about 1.2×10^{-5} cm^2/sec and the flux is larger by an order of magnitude. The permeability of an iridium coating to carbon is of the same order of magnitude, i.e., a one-mil thick iridium coating will exhibit a permeability of 8×10^{-8} g cm^{-2} sec^{-1}.

IV. PROGRAM MANAGEMENT

Official award of Contract No. AF 33(657)-11253 was made on 1 June 1963 to the National Carbon Company (renamed the Carbon Products Division of Union Carbide Corporation on 1 September 1963). Union Carbide , as Prime Contractor of this program, is to provide a detailed description of the major parameters controlling the oxidation behavior of selected protective coating systems for graphite at temperatures as high as 2200°C. The research was carried out as a group effort with Dr. J. M. Criscione as Principal Investigator and Technical Coordinator.

The research on all tasks except those outlined in ML-TDR-64-173, Part II, was performed by personnel at the Union Carbide Corporation, Carbon Products Division, Parma Technical Center.

Research on the oxidation of rhodium, a portion of the research on the oxidation of iridium, and the vaporization of compound oxides were subcontracted to Dr. J. L. Margrave at Rice University, Houston, Texas, beginning 1 January 1964.

Captain W. C. Simmons served as Project Engineer for the Air Force Materials Laboratory, Research and Technology Division.

V. OXYGEN PERMEABILITY STUDIES

TASK A3-3

1. PERMEABILITY OF VARIOUS ALUMINUM OXIDES TO OXYGEN

a. Introduction

Alumina has recently received much attention as a component in coating systems for the high temperature oxidation protection of graphite and refractory metals. To better assess its value as a barrier to oxygen, information is needed regarding the rate of transport of oxygen through alumina and the influence of microstructure and purity on this transport rate. Published data on the diffusivity of oxygen in alumina could be used to calculate the oxygen permeation from a consideration of Fick's first law,

$$P = -D \frac{dc}{dx}, \qquad (1)$$

where P = the permeability,
D = the diffusivity,
and $\frac{dc}{dx}$ = the concentration gradient.

However, since the concentration gradient, dc/dx, is generally unknown and since D is not necessarily independent of dc/dx, one cannot calculate permeabilities from the measurements of the diffusivity alone. The results of direct oxygen permeability measurements on various grades of alumina are reported here for the purpose of evaluating alumina as a coating material.

b. Experimental

The oxide samples were in the form of impervious tubes closed at one end. Their imperviousness was frequently checked, and all reported results are on tubes which showed no detectable permeability of argon at any of the temperatures of the investigation.

The experimental procedure was essentially identical with that previously reported.[1, 2] However, it was found that graphite susceptors reacted with alumina forming aluminum oxicarbide Al_4O_4C[6]; an iridium susceptor was therefore used for heating the sample. The change in susceptor material also reduced the background pressure, resulting in a 100-fold increase in the sensitivity of the measurements. The iridium susceptor was coated with a three-mil layer of ThO_2 which effectively reduced the reaction between iridium and oxygen. Measurements were made with oxygen either on the inside or on the outside of the tube while the other side was being continuously evacuated. The pressure on the downstream side varied between 10^{-2} and 10^{-5} torr depending on the quantity of oxygen permeating through the tubes. Data taken with oxygen inside the tube required a correction for the small

(~20 percent) quantity of oxygen which, after permeating through the tube, reacted with the iridium susceptor and thus escaped measurement in the detection system. This correction was determined for various temperatures and flow rates in independent calibration runs. Data taken with oxygen outside the tubes required no correction.

To obtain the maximum sensitivity, an omegatron mass spectrometer was used for detecting permeation rates smaller than $Pl = 5 \times 10^{-11}$ (gm/cm sec).

(1) Materials Characterization

(a) COORS PORCELAIN Alumina

The samples were in the form of 9-inches long x $^3/_8$-inch O.D. x $^9/_{32}$-inch I.D. impervious alumina tubes, manufactured by the COORS PORCELAIN Company. The density of this alumina, determined from its buoyancy in water, was 3.74 gm/cm^3. Comparing this density with that of sapphire [7] (3.97 gm/cm^3) gives a porosity of approximately six percent. The manufacturer's typical chemical analysis is given in Table 1 and our own spectrographic analysis in Table 2.

TABLE 1

TYPICAL CHEMICAL ANALYSIS OF COORS PORCELAIN ALUMINA

Compound	Percent
Al_2O_3	99.5
SiO_2	0.3
CaO, MgO, Fe_2O_3	Balance

TABLE 2

SPECTROGRAPHIC ANALYSIS OF COORS PORCELAIN ALUMINA

Element	Percent
Al	greater than 0.1
Si	greater than 0.1
Fe	0.01 to 0.1
Mg	0.01 to 0.1
Mn	0.01 to 0.1
Ni	0.01 to 0.1
Cu	0.01 to 0.1
Cr	less than 0.01
V	less than 0.01
Ag	less than 0.01
Zn	less than 0.01
Na	less than 0.01
Ti	less than 0.01

Photomicrographs of the COORS PORCELAIN alumina hot and cold zones are shown in Figure 2 at a magnification of 500 X. No secondary phases are present in agreement with the high purity of this material. Heating to 1800°C caused considerable grain growth and some aggregation of the small pores into larger ones. The very high apparent pore volume in the photomicrograph of the hot zone is, however, due to some "pull-out" caused by polishing; this was unavoidable because the material was highly strained and extremely brittle.

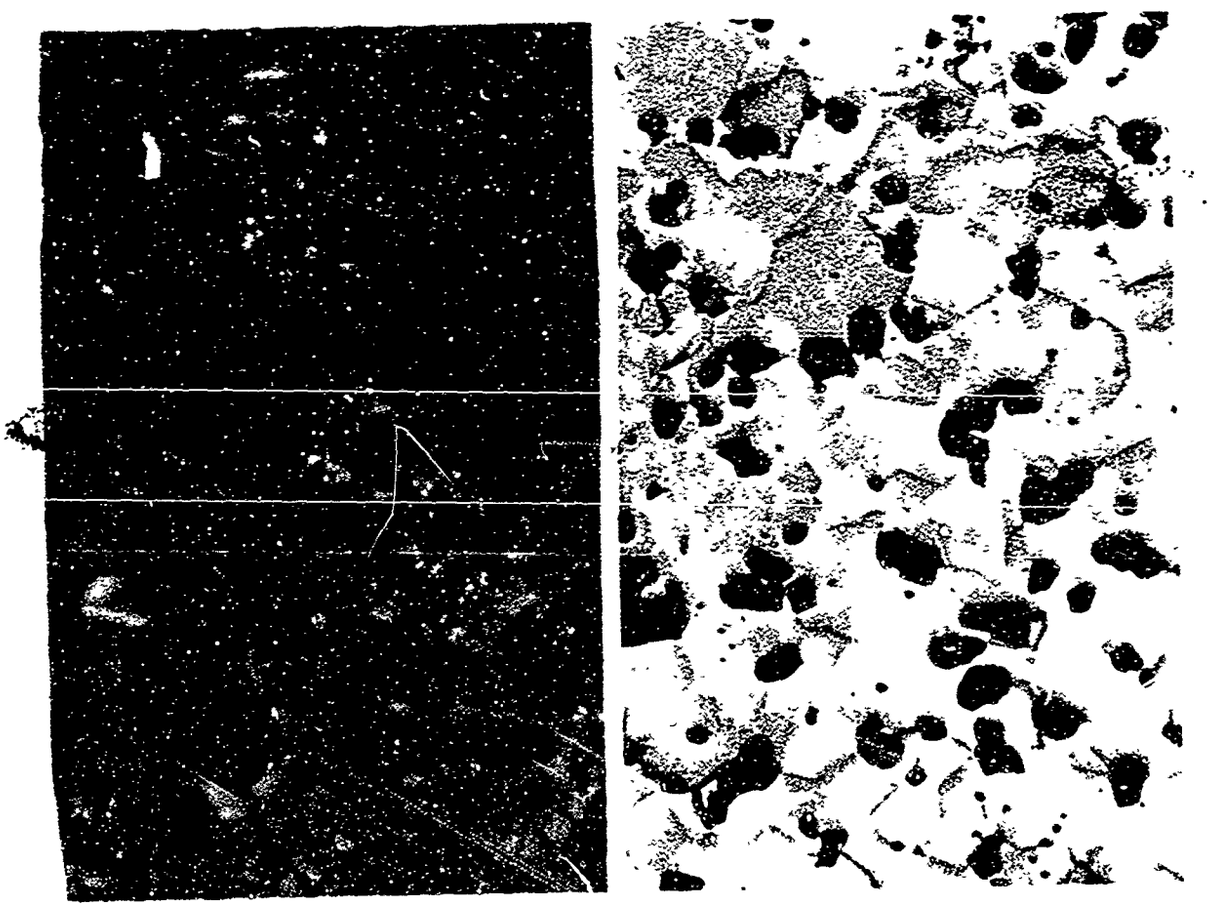

2a. Cold Zone

2b. Hot Zone

Figure 2. Photomicrographs of Cross Sections of COORS PORCELAIN Alumina (500 X Magnification)

(b) McDANEL AV30 Alumina

The specimens consisted of 9-inches long x $^3/_8$-inch O. D. x $^3/_{32}$-inch I. D. impervious alumina tubes, manufactured by the McDANEL Refractory Porcelain Company. The manufacturer's typical chemical analysis is given in Table 3 and our own spectrographic analysis in Table 4.

TABLE 3

McDANEL REFRACTORY PORCELAIN COMPANY'S TYPICAL CHEMICAL ANALYSIS OF AV30 ALUMINA

Compound	Percent
Al_2O_3	95.5
SiO_2	3.0
MgO	1.1
CaO	.22
Na_2O_3	.06
Fe_2O_3	.1

TABLE 4

SPECTROGRAPHIC ANALYSIS OF McDANEL AV30 ALUMINA

Element	Percent
Al	greater than 0.1
Si	greater than 0.1
Mg	greater than 0.1
Fe	0.01 to 0.1
B	0.01 to 0.1
Cu	0.01 to 0.1
Na	0.01 to 0.1
Mn	0.01 to 0.1
V	less than 0.01
Ni	less than 0.01
Ca	less than 0.01
Ag	less than 0.01
Zn	less than 0.01
Ti	less than 0.01
Cr	less than 0.01
Sn	less than 0.01

The density of this material was 3.73 gm/cm^3, corresponding to a porosity of approximately six percent.

A photomicrograph (500 X Magnification) of the cold zone (as received material) is shown in Figure 3a. The fine grain and small pore size are readily apparent. The gray areas show a secondary phase, a condition which is consistent with the fact that this material is only 95.5 percent pure. The structural changes which occurred on heating to 1916°C are depicted in Figure 3b, a photomicrograph of the hot zone (500 X Magnification).

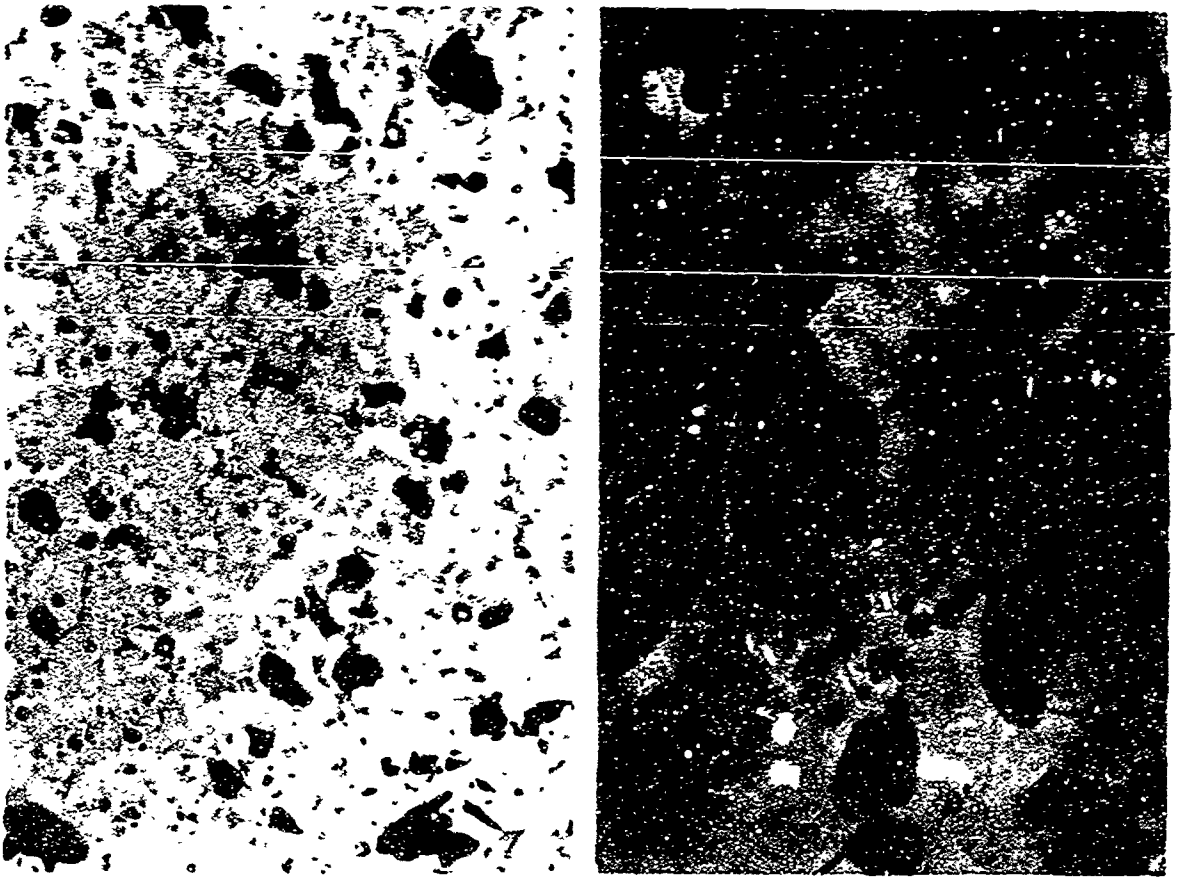

3a. Cold Zone 3b. Hot Zone

Figure 3. Photomicrographs of Cross Sections of McDANEL AV30 Alumina (500 X Magnification)

The grains have become considerably larger, and most of the small pores have combined to form larger ones. The light spots are merely reflections from pores immediately below the surface and do not depict a secondary phase. The broad dark lines separating the grains are not cracks; rather, they result from the various grain facets polishing at different rates. Attention should be drawn to the numerous areas where small crystals can be seen completely surrounded by pores. It is possible that these areas depict a congregation of impurities and, thus, a secondary phase.

(c) McDANEL AP35 Alumina

Impervious alumina tubes, 9-inches long x $^{3}/_{8}$-inch O.D. x $^{9}/_{32}$-inch I.D., manufactured by the McDANEL Refractory Porcelain Company, were used. The manufacturer's typical chemical composition is given in Table 5 and the spectrographic analysis performed at this Laboratory in Table 6.

TABLE 5

McDANEL REFRACTORY PORCELAIN COMPANY'S TYPICAL CHEMICAL ANALYSIS OF AP35 ALUMINA

Compound	Percent
Al_2O_3	99.
SiO_2	.7
MgO	.07
Na_2O	.05
Fe_2O_3	.07
CaO	.03

The manufacturer's reported density was 3.7 g/cm^3 and the value determined at this Laboratory by the water buoyancy technique was 3.81 g/cm^3. Comparing the latter density with that of sapphire (3.97 g/cm^3) indicates a porosity of four percent.

TABLE 6

SPECTROGRAPHIC ANALYSIS OF McDANEL AP35 ALUMINA

Element	Percent
Al	greater than 0.1
Si	greater than 0.1
Mg	0.01 to 0.1
Na	0.01 to 0.1
Fe	0.01 to 0.1
B	0.01 to 0.1
Cu	0.01 to 0.1
Ca	less than 0.01
V	less than 0.01
Cr	less than 0.01
Ni	less than 0.01
Sn	less than 0.01
Ti	less than 0.01
Mn	less than 0.01
Ag	less than 0.01
Zr	less than 0.01

Photomicrographs of the hot and cold zone cross sections (Figure 4, 500 X Magnification) show that the grains have become larger in the hot zone and that the pore structure has also changed; most of the smaller pores have combined to form larger ones. A secondary phase present in the cold zone has congregated along the grain boundaries in the hot zone. The white spots are pores which show through the polished alumina.

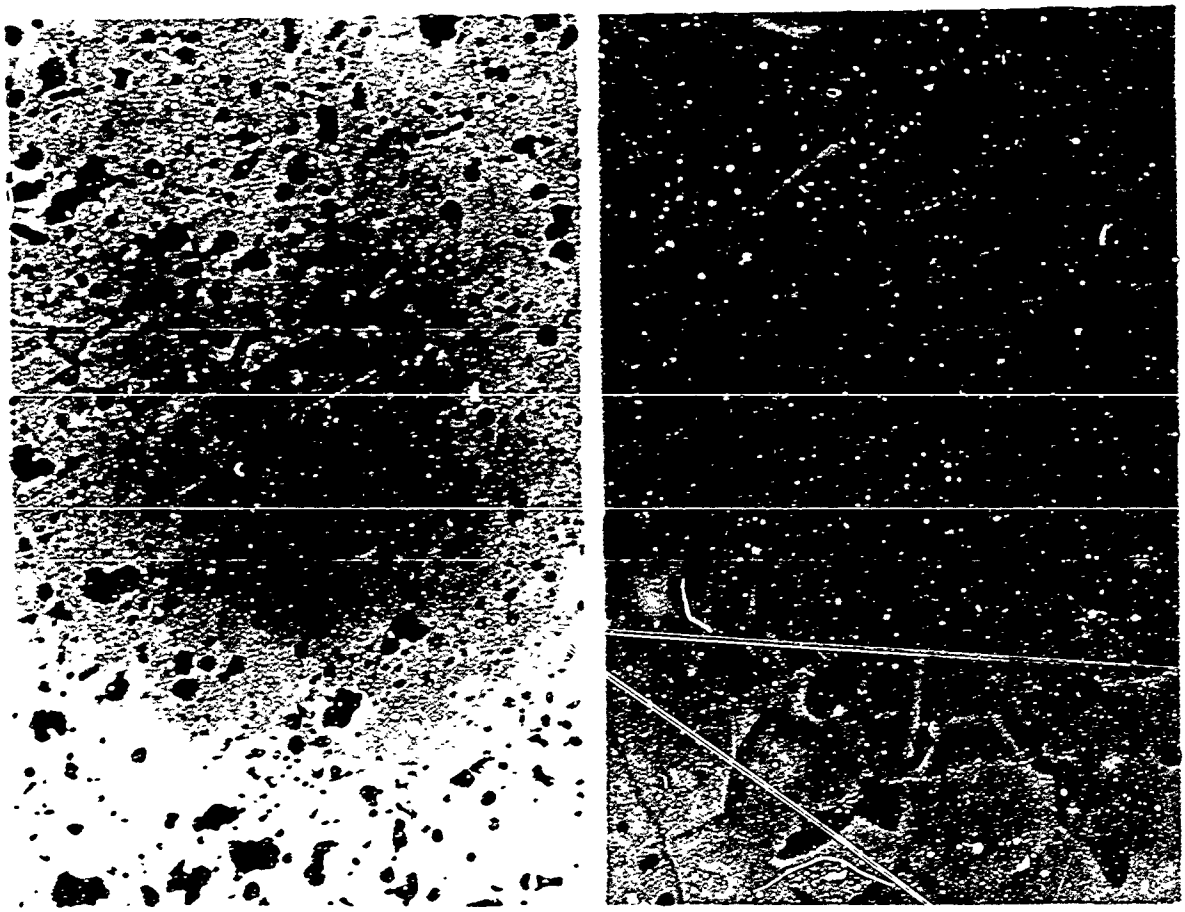

4a. Cold Zone

4b. Hot Zone

Figure 4. Photomicrographs of Cross Sections of McDANEL AP35 Alumina (500 X Magnification)

(d) McDANEL 997 Alumina

Impervious alumina tubes, 9-inches long x $^3/_8$-inch O.D. x $^9/_{32}$-inch I.D., manufactured by the McDANEL Refractory Porcelain Company, were used. The typical composition as reported by the manufacturer is given in Table 7; a semiquantitative spectrographic analysis performed at this Laboratory confirmed the high purity of this material.

TABLE 7

McDANEL REFRACTORY PORCELAIN COMPANY'S TYPICAL CHEMICAL ANALYSIS OF GRADE 997 ALUMINA

Compound	Percent
Al_2O_3	99.7
SiO_2	.05 to .1
MgO	.05 to .1
Na_2O	.005 to .05
Fe_2O_3	.03
CaO	.03
Ga_2O_3	.01
B_2O_3	less than .001
CdO	less than .001
MnO	less than .0007
ZnO	less than .0005
CuO	less than .0005
Cr_2O_3	less than .0005
V_2O_5	less than .0005

The manufacturer's reported density was 3.8 g/cm^3 and the value measured at this Laboratory was 3.86 g/cm^3, corresponding to a porosity of approximately three percent.

Photomicrographs of the McDANEL 997 alumina hot and cold zones are shown in Figure 5 at a magnification of 500 X. The grains have become larger in the hot zone and the smaller pores have combined to form larger ones. A secondary phase present in the cold zone has congregated in pores and grain boundaries in the hot zone.

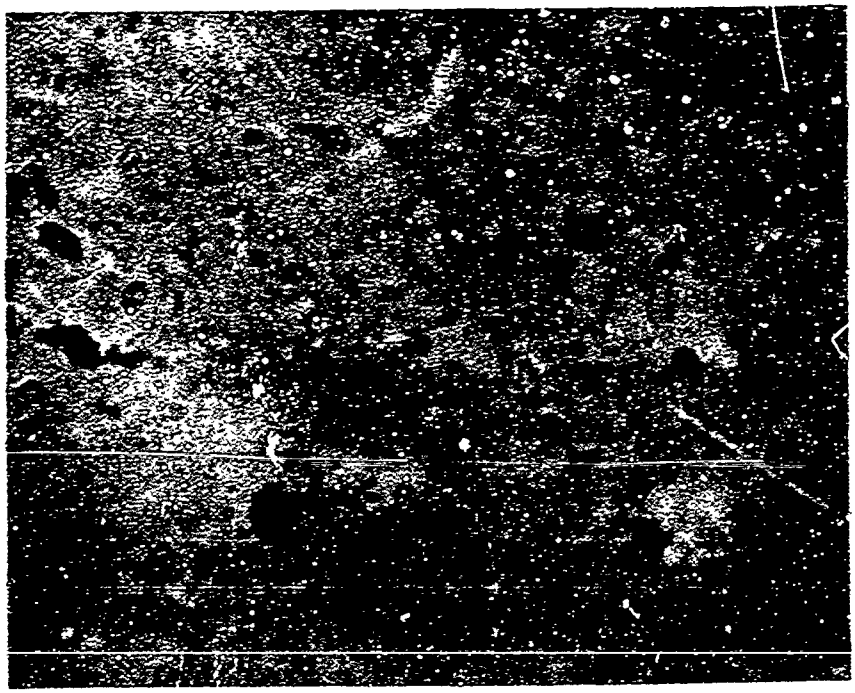

5a. Cold Zone

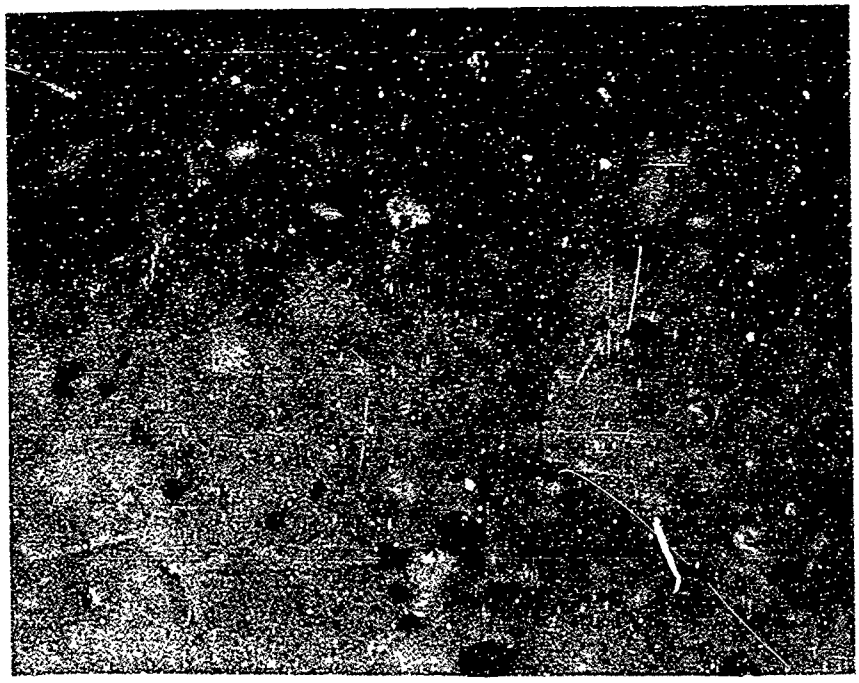

5b. Hot Zone

Figure 5. Photomicrographs of Cross Sections of McDANEL 997 Alumina (500 X Magnification)

(e) LINDE Sapphire

The single crystal sapphire, obtained from the LINDE Division of Union Carbide Corporation, was of theoretical density with an impurity content (mainly silica) of less than 50 parts per million.

A $^3/_8$-inch O.D. x $^1/_4$-inch I.D. x 4-inches long closed-end tube was drilled from the crystal. Difficulties encountered in drilling the sapphire rod limited the length of the sample to four inches. To avoid overheating of the Swagelok connection between the tube and vacuum system, the sample must have a length of at least eight inches; an extension tube, joined to the sapphire by means of a high-temperature, vacuum-tight seal, was therefore required. A LUCALOX tube was joined to the sapphire using Code 1731 glass sealing frit, made by Corning Glass Works. The seal was vacuum tight and serviceable to 1300°C.

The temperature was measured by sighting down the inside of the sample with an optical pyrometer. Since sapphire is translucent, sighting through the sapphire onto the susceptor had to be avoided. This problem was minimized by coating the outside of the sapphire with a thin layer of porous high purity alumina. To check on the accuracy of our temperature measurements, the sample was melted after we had made our permeability measurements. Since the sample melted at a measured temperature of 2043°C and the melting point of sapphire is 2050°C [8], the error in our temperature measurement was very small. Figure 6 is a photograph showing the sample after the end of the sapphire had been melted. The smaller diameter tube is the sapphire sample and the larger one is the LUCALOX tube.

c. Results and Discussion

(1) Permeability of COORS PORCELAIN Alumina to Oxygen

The temperature dependence of the permeability of COORS PORCELAIN alumina to 50 torr of oxygen is shown in Figure 7, and is expressed by

$$P\ell = 1.57 \times 10^2 \, e^{-104,000/RT} \text{ (gm/cm sec)}.$$

Measurements were made in the temperature range from 1745°C to 1830°C; below 1745°C, the quantity of oxygen diffusing through the sample was too small for accurate determination; above 1830°C, the samples became pervious.

Figure 6. The Sapphire Tube After Melting

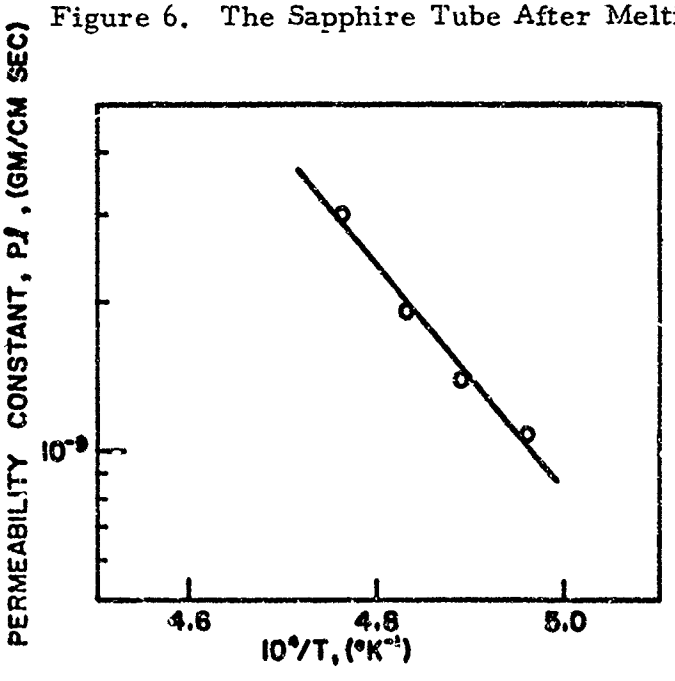

Figure 7. Temperature Dependence of Permeability Constant, Pl, of COORS PORCELAIN Alumina to 50 torr of Oxygen

Oxygen pressure dependence measurements were attempted, but each time the sample developed a leak during the runs. Altogether, three tubes were used for the temperature dependence measurements. Two tubes developed leaks after two runs each and could not be used further. The third tube remained impervious for eight runs and then also developed a leak. Figure 8 shows all of the experimental data obtained on the three samples. The numbers beside some of the points refer to the runs with the third sample and indicate the order in which the measurements were taken. It is clearly evident from Figure 8 that sample number 3 tightened up considerably on heating to 1800°C during the first series of four runs. Runs No. 1 to 4 were therefore disregarded in drawing the permeability curve.

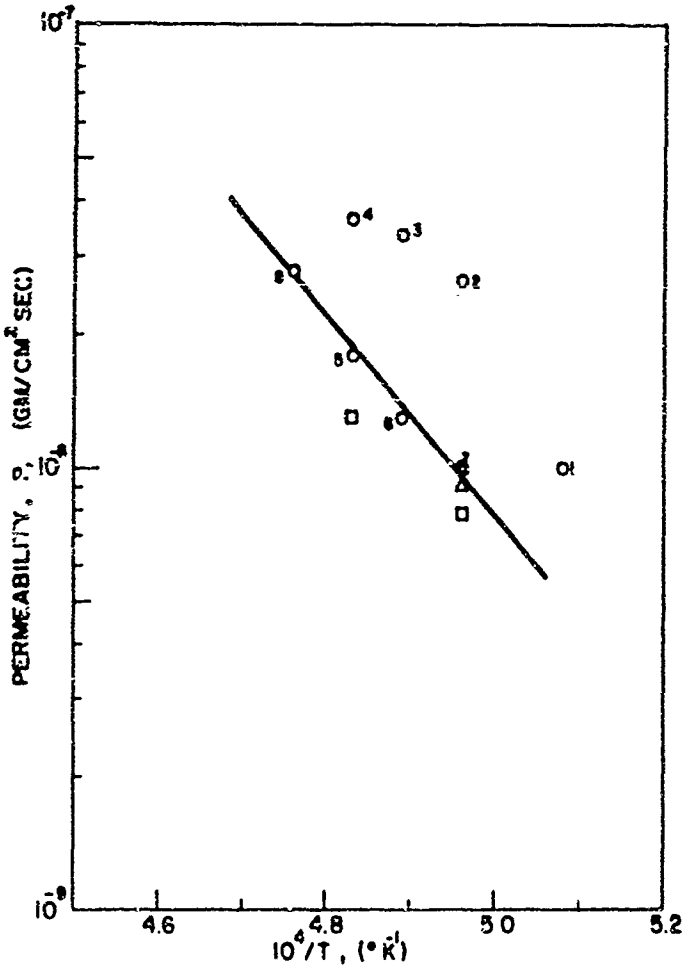

Δ Sample No. 1
□ Sample No. 2
O Sample No. 3

Figure 8. Permeability, P, of COORS PORCELAIN Alumina to Oxygen at 50 torr

(2) Permeability of McDANEL AV30 Alumina to Oxygen

The temperature dependence of the permeability constant for McDANEL AV30 alumina at 50 torr oxygen is drawn in Figure 9 and given by

$$Pl = 3.45 \times 10^3 \, e^{-110,000/RT} \text{ (gm/cm sec)}$$

in the range 1700°C to 1920°C. The numbers beside the data points refer to the order in which the measurements were made.

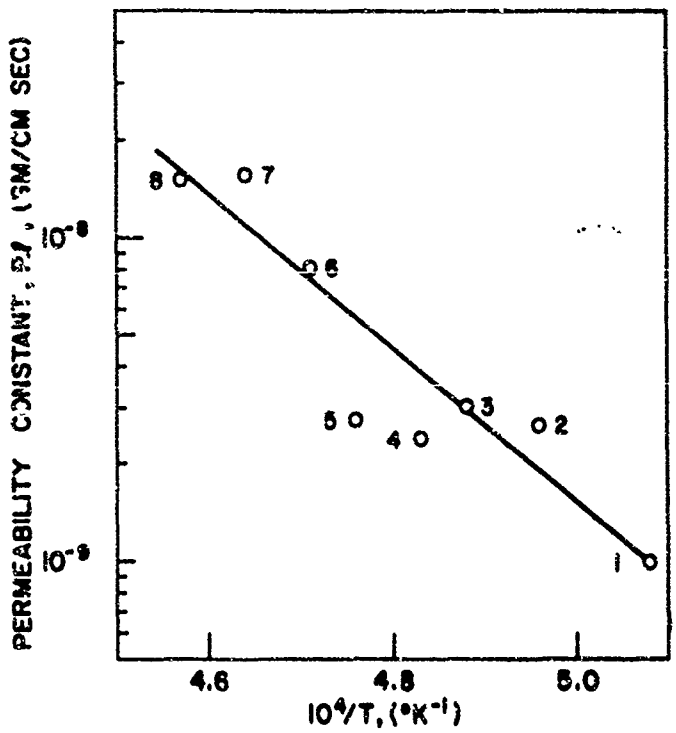

Figure 9. Temperature Dependence of Permeability Constant, Pl, of McDANEL AV30 Alumina to 50 torr of Oxygen

As shown in Figure 10, the McDANEL AV30 alumina exhibited an oxygen permeability which varied with the .36 power of the oxygen pressure.

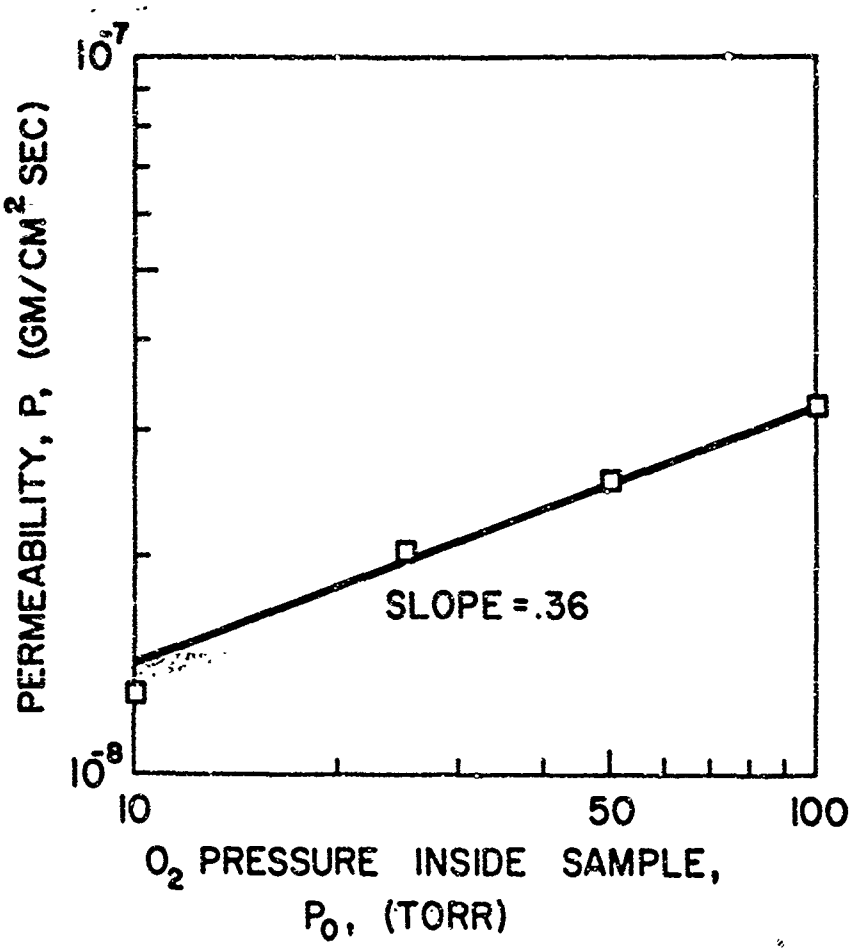

Figure 10. Pressure Dependence of Permeability, P, of McDANEL AV30 Alumina to Oxygen at 1745°C

(3) Permeability of McDANEL AP35 Alumina to Oxygen

Due to grain growth, the permeability of this material was a strong function of prior heat-treatment temperature, i.e., the permeability decreased rapidly on heat-treatment to above 1750°C. This phenomenon had been observed on other types of alumina, although to a much lesser extent. Two samples of this material were studied. The permeability of the first sample decreased continuously during a series of six runs, after which the tube developed a leak. No meaningful results can be reported on this sample. The second tube was heat treated for several hours at 1750°C to 1800°C before the diffusion measurements were made. Even then, the measurements were poorly reproducible; the scatter in the data points is too large to permit calculation of an equation for Pℓ; the results are shown in Figure 11. The squares represent measurements with oxygen inside the tube and the triangles represent data taken with oxygen on the outside of the sample.

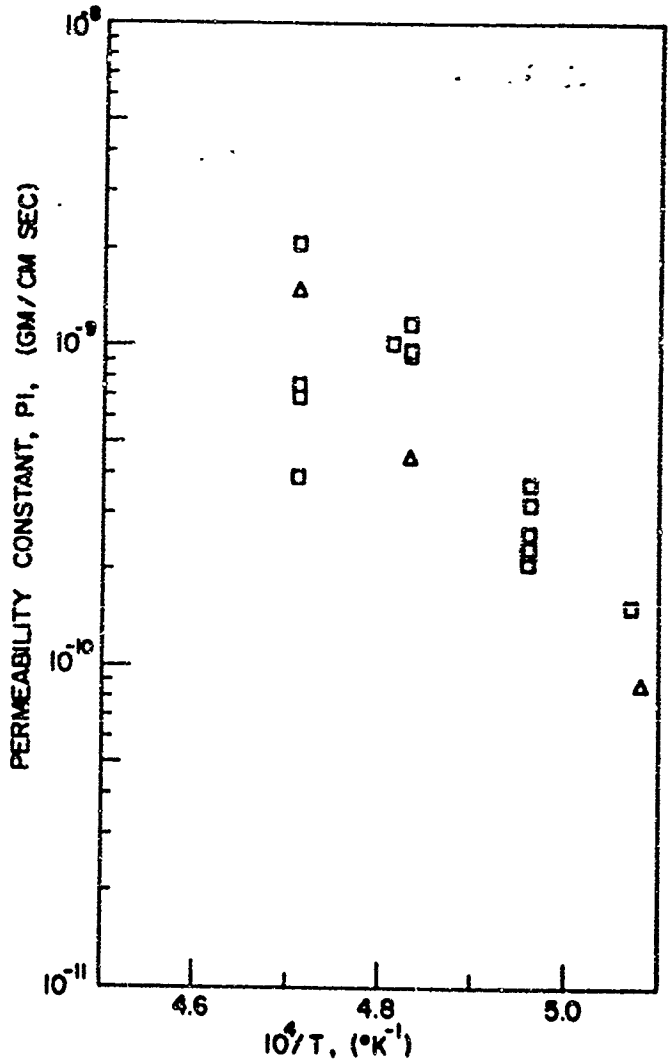

Figure 11. Temperature Dependence of Permeability Constant, $P\ell$, of McDANEL AP35 Alumina to 50 torr of Oxygen

As shown in Figure 12, the McDANEL AP35 alumina exhibited an oxygen permeability which varied with approximately the $^1/_4$ power of the oxygen pressure.

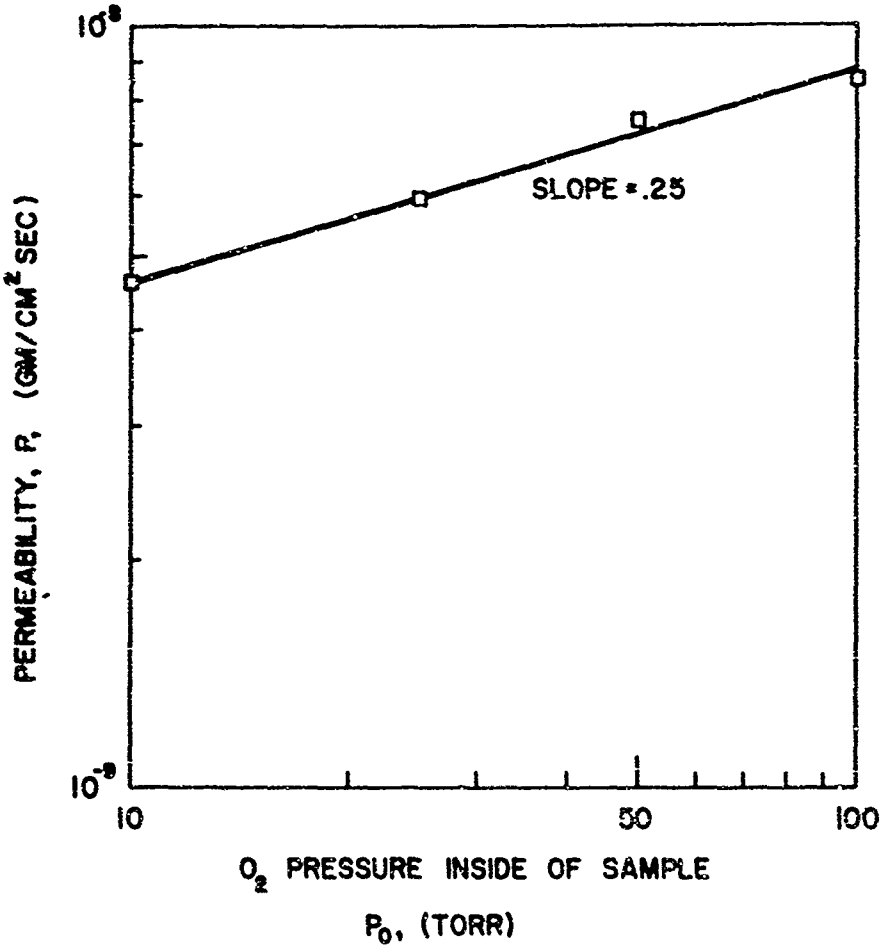

Figure 12. Pressure Dependence of Permeability, P, of McDANEL AP35 Alumina to Oxygen at 1745°C

(4) Permeability of McDANEL 997 Alumina to Oxygen

Oxygen permeability measurements were made on polycrystalline alumina grade McDANEL 997, a high-purity, low-porosity material. The permeability was again found to be a very strong function of heat-treatment, time, and temperature. During one week of continuous heat treatment of 1900°-1930°C, the permeability constant, $P\ell$ (50 torr of oxygen), decreased from 1×10^{-8} to 1×10^{-10} gm/cm sec at 1915°C. Even then, the permeability was still decreasing; however, at this point, the sample developed

a leak. The two orders of magnitude drop in oxygen permeability is undoubtedly related to the pronounced grain growth exhibited by this material, as shown in the Materials Characterization Section of this report.

(5) Permeability of LINDE Sapphire to Oxygen

The permeability of single crystal alumina (sapphire) to oxygen was investigated using the omegatron mass spectrometer as a detection device. The sample, at a temperature of 2015°C, was exposed to 50 torr of oxygen for three hours, and no detectable oxygen permeation was observed; therefore, an upper limit for the permeability constant can be calculated: Pl is less than 4×10^{-13} gm/cm sec at 2015°C.

d. Conclusions

Figure 13 shows all of the alumina data plotted on one graph. The MORGANITE and LUCALOX data from the Second Summary Report[2] have been added for completeness.

The rate of oxygen permeation through polycrystalline alumina is determined primarily by grain size and purity. High purity grades have the lowest permeability in part because they also exhibit more pronounced grain growth. However, the activation energy determined on less pure grades is lower than that for high purity material; this result suggests that, in the presence of substantial amounts of impurities, the diffusion mechanism even at 1850°C is not yet entirely determined by intrinsic oxygen ion motion[9].

The effect of closed pore porosity on the permeability was found to be negligible. A dense grade such as LUCALOX exhibits a permeability comparable with that of somewhat porous materials. The results of the present study may be compared with those of Oishi and Kingery.[10] Extrapolating the single crystal data of these authors to 2015°C gives a diffusivity of approximately 10^{-11} cm^2 sec. Assuming a 0.1 percent difference in oxygen concentration between the high pressure and the low pressure side, one would calculate Pl for sapphire at 2015°C to be of the order of 10^{-14} gm/cm sec, i.e., below the detection limit of our system. The permeation rate was indeed too small to be observed. Similar calculations for polycrystalline alumina yield permeabilities which are 4 to 5 orders of magnitude below the experimentally determined values. Fryer, Budworth, and Roberts[11] have attributed this discrepancy to the existence of an impervious skin on the outer or inner surface of the alumina, with the bulk of the material pervious to gas flow. We were, however, unable to detect such a skin on our samples. Moreover, to obtain agreement with Oishi and Kingery, the skin thickness would have to be of the order of 10^{-4} to 10^{-5} cm, orders of magnitude less than the average grain size. We prefer the alternative explanation that impurities segregating at the grain boundaries provide a preferential diffusion path. In addition, the diffusivity measured in the presence of a

concentration gradient may well be higher than that determined by isotope exchange experiments.

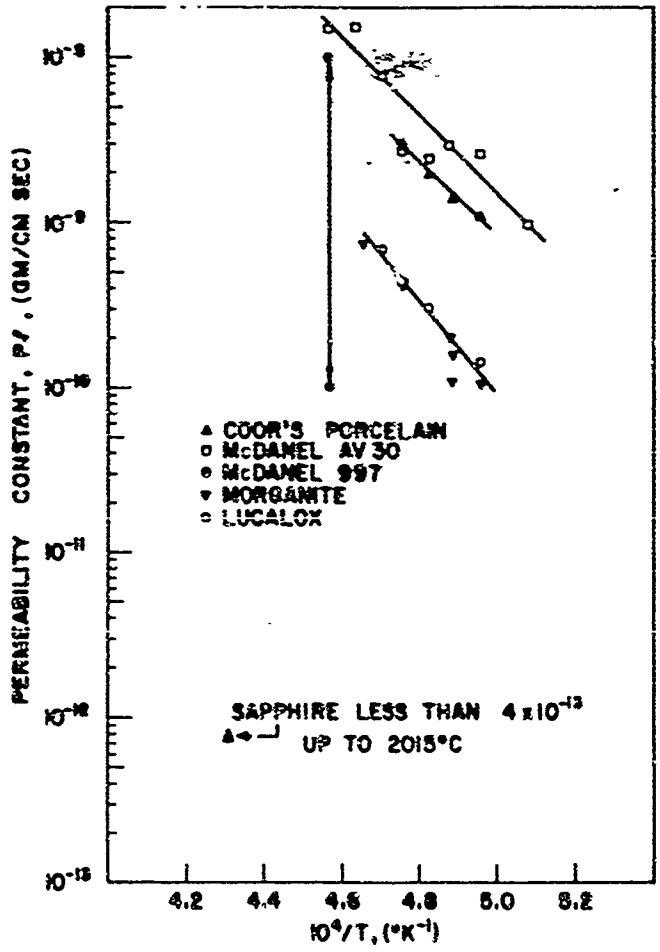

Figure 13. Temperature Dependence of Permeability Constant, Pℓ, to 50 torr of Oxygen for Various Grades of Alumina

In conclusion, the permeability of single crystal alumina to oxygen is so low that, with the possible exception of beryllia, sapphire appears to be the best oxygen barrier of all the refractory oxides. The permeability of polycrystalline alumina, although substantially higher than that of sapphire, still compares favorably with the oxygen permeabilities of zirconia, hafnia, and thoria.[1,2] Thus, alumina deserves increased attention as an oxygen barrier in coatings for refractory metals or graphite to temperatures up to 2000°C.

VI. MECHANICAL COMPATIBILITY OF IRIDIUM WITH GRAPHITE

TASK B1-2

1. REDETERMINATION OF THE IRIDIUM-CARBON EUTECTIC TEMPERATURE

The iridium-carbon eutectic temperature was redetermined. For iridium containing approximately 0.1 percent Fe, 0.05 percent Rh, and traces of Si, Cr, Ni, and Ag totaling about 0.02 percent, the eutectic temperature was found to be between 2250°C and 2280°C.

The experiments were done with commercial (Engelhard Industries) iridium powder that had been fused in a spectroscopically pure graphite crucible at 2450°C in an argon atmosphere. The fused button was sliced on a diamond saw, each section boiled in aqua regia and hydrofluoric acid, washed with distilled water, and wrapped in plastic until used. The eutectic temperature was determined by packing the iridium sample in spectroscopically pure (Grade SP-1) graphite powder contained in a graphite capsule of like purity and heating in a purified graphite tube furnace in an argon atmosphere. A new iridium specimen was used for each run. The first indications of melting (rounded corners) were observed after the sample had been heated to 2250°C and held there for three hours. Complete melting was observed after heating to 2280°C and holding at that temperature for three hours. The analysis given in the introductory paragraph was obtained on the sample which had been heated to 2250°C.

A piece of slurry-dipped iridium coating was similarly packed and heated. Complete melting was observed when the sample was heated to 2150°C. Semiquantitative spectroscopic analysis indicated an iron content of approximately 1 percent and 0.1 percent each of Si, Cr, Ni, and Al. These impurities are apparently picked up during the preparation of the slurry by wet-milling in a steel mill with stainless steel balls.

The discrepancy between the present and previous [1] eutectic temperature determination is probably due to previously insufficient furnace purification which may have led to impurity pick-up, particularly of silicon and boron.

VII. MECHANICAL COMPATIBILITY OF MULTILAYER COATINGS WITH GRAPHITE

TASKS C2-2 AND D-3

1. THERMAL EXPANSION

The adherence of a protective coating on graphite will depend strongly on the extent to which the coating and substrate are mechanically compatible, a factor controlled largely by the thermal properties of the coating constituents and substrate. In this phase of the program, the oxides ThO_2, HfO_2 and ZrO_2 and the carbide and diboride of hafnium and zirconium are being considered for components of multilayer coatings on graphite.

The thermal expansion of the oxides and the carbides has been adequately investigated. A review of the data for the oxides has been presented previously[2]; a review of the carbide data is included here. On the other hand, the thermal expansion data for the diborides were derived largely from lattice parameter measurements and thus pertain to single crystals. Polycrystalline materials of less than theoretical density could conceivably have considerably different thermal expansion coefficients (CTE). Bulk thermal expansion measurements were, therefore, carried out in this phase of the program.

In addition to the thermal expansion measurements on pure ZrB_2 and HfB_2, the coefficients of thermal expansion of HfB_2 and ZrB_2 doped with alkaline earth or rare-earth boride were determined. These additives make it possible to adjust the thermal expansion characteristics of the diborides and to increase coating adherence and density.

a. Previous Work on the Thermal Expansion of the Carbide and Diborides

The thermal expansion of hafnium diboride in the range 25° to 2040°C has been recently investigated by Keihn[12] using X-ray diffraction methods. Houska and Keplin[13] by the same techniques measured the lattice parameters for ZrB_2 in the range 25° to 2040°C. Using the data reported by these investigators, the average CTE of completely dense polycrystalline HfB_2 and ZrB_2 was calculated. This information is presented in Table 8.

TABLE 8

COEFFICIENTS OF THERMAL EXPANSION OF HfB_2 AND ZrB_2, CALCULATED FROM LATTICE PARAMETER DETERMINATIONS

Temperature °C	CTE of HfB_2[12] in/in/°C x 10^6	CTE of ZrB_2[13] in/in/°C x 10^6
25- 600	6.4	6.7
600-1400	8.3	8.4
1400-2000	8.3	8.3

The most recent thermal expansion data on the carbides of hafnium[14-16] and zirconium[14,16-18] are shown in Figures 14 and 15 and listed in Table 9. High purity fine grain graphites are now available from many sources* with CTE's in the range of 6.8 (±2) x 10^{-6}/°C (room temperatures to 1650°C) with an anisotropy of less than 1.2 units. Figure 16 shows an upper limit for these materials.

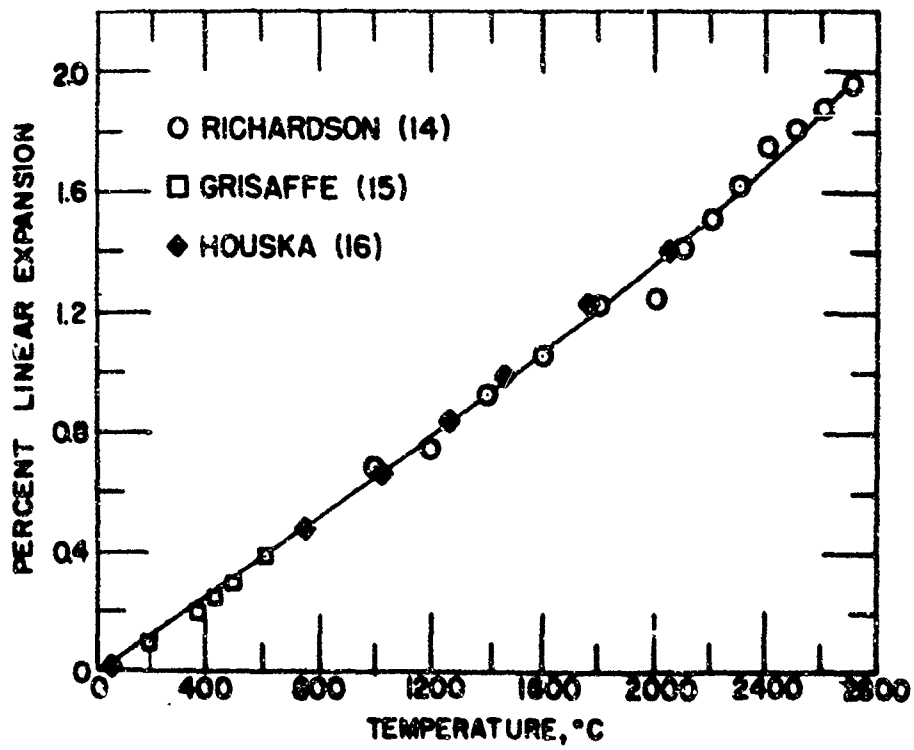

Figure 14. Thermal Expansion of Hafnium Carbide

* Macklin, B.A., Redmond, J.R., "Development of Improved Methods of Depositing Iridium Coatings" PR 1 AF33(615)-3617

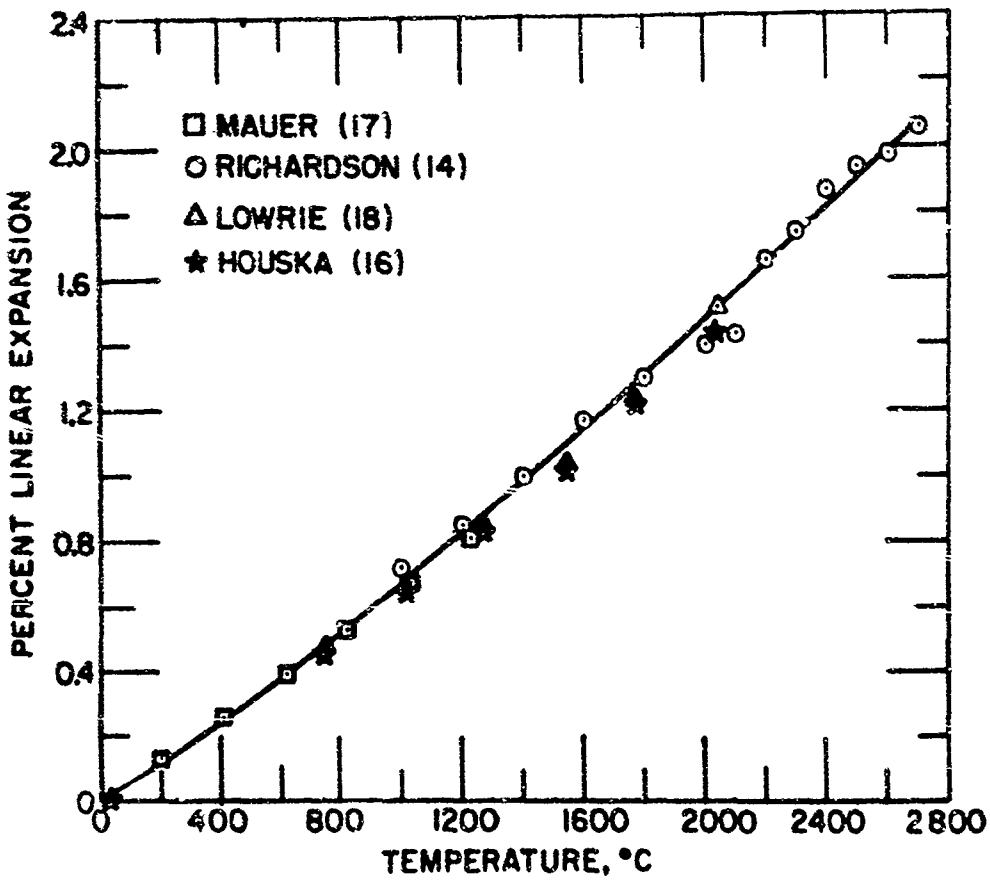

Figure 15. Thermal Expansion of Zirconium Carbide

TABLE 9

THERMAL EXPANSION* OF HfC AND ZrC

Temperature, °C	CTE of HfC in/in/°C x 10^6	CTE of ZrC in/in/°C x 10^6
25- 600	6.5	6.3
600-1400	6.9	7.4
1400-2000	7.2	8.5

* From Figures 1 and 2

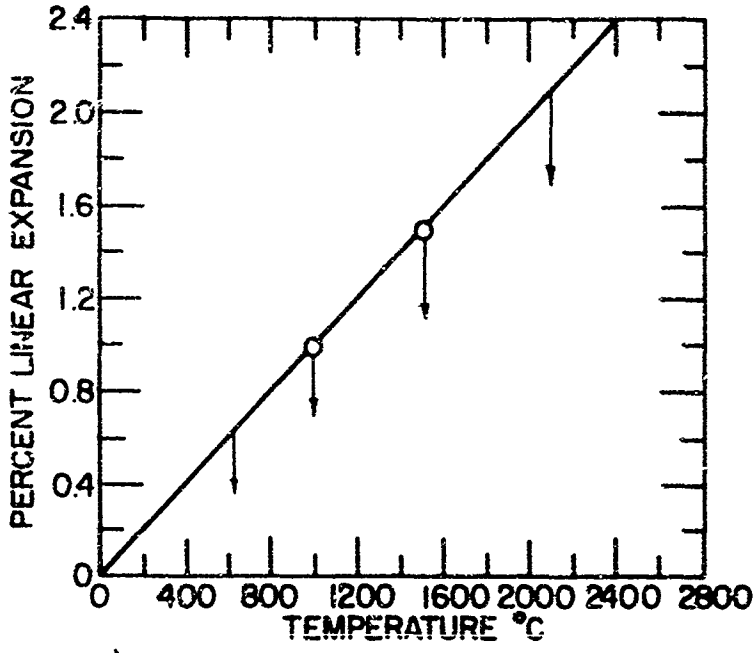

Figure 16. Thermal Expansion of High CTE Experimental Graphites (Line Shows Upper Limit of Presently Available Commerical Grades)

b. Experimental

(1) Materials Characterization

The ZrB_2 obtained from Gallard-Schlesinger Chemical Manufacturing Corporation was 325 mesh powder containing 1.04 percent C and 1.16 percent O as major impurities; the X-ray diffraction pattern showed ZrB_2 and an unidentified impurity phase.

The HfB_2 was prepared from HfH_2 and boron (both materials 99+ percent pure). The mixture was milled and slowly heated in a graphite crucible to 2000°C for one hour, remilled and reheated in a similar manner; an X-ray diffraction pattern of the product showed hafnium diboride and a trace of HfC; the HfC intensity was less than that of a previous lot of HfB_2 which contained 0.36 percent carbon.

The CaB_6 was reagent grade material obtained from Fisher Scientific and showed no extraneous phases upon X-ray examination.

The CeB_6 was obtained from Cerac Incorporated. The manufacturer reported a 99.1 percent total Ce plus B, only CeB_6 was detected by X-ray analysis.

The LaB_6 was obtained from Gallard-Schlesinger Chemical Manufacturing Corporation; their analysis reported 68.0 percent La, 31.5 percent B, 0.1 percent C, 0.07 percent O and 0.05 percent Fe; an X-ray diffraction pattern of this material showed only LaB_6.

The YB_6 was obtained from Cerac Incorporated. The manufacturer's analysis reported 42.4 percent B and 57.0 percent Y; an X-ray diffraction pattern showed a major phase of YB_6 and a minor amount of YB_4.

Samples of graphite coated with ZrC and HfC were obtained from High Temperature Materials, a Department of the Carbon Products Division of Union Carbide Corporation. The samples were prepared by passing the metal chloride over ATJ graphite at 1900° to 2100°C and pressures from 5 to 10 torr.

(2) Preparation of Samples

A bench scale vacuum hot press for preparing the samples for thermal expansion measurements is shown in Figure 17. The assembly consists of water-cooled brass bottom and top plates, a vacuum line, an optical sight tube, water-cooled ram, a graphite (Union Carbide Corporation Grade AGW) die, graphite (Union Carbide Corporation Grade ATJ) plungers, graphite felt (Union Carbide Corporation Grade WDF) insulation, and a quartz envelope. The induction heated system is capable of 2500°C under a vacuum of < 1 mm of Hg. The pressure capability is determined by the strength of the die (4000 to 6000 lb/in^2).

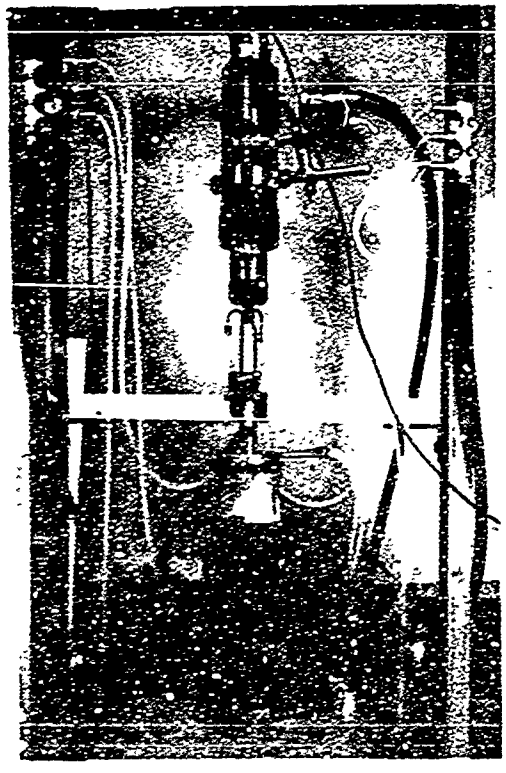

Figure 17. Hot Press Assembly

The mixed boride rods were prepared by porcelain ball milling each sample 16 hours and vacuum (< 1 torr) hot pressing for 0.5 hours at 1800°C and 2000 lb/in^2. Table 10 lists the composition and density of each sample. The compositions prepared included the pure diborides (ZrB_2 and HfB_2) as well as mixtures of the diborides with one of the hexaborides from the group CaB_6, LaB_6, YB_6, and CeB_6 in amounts of about 20 mole percent. The density of the mixed boride rods, as determined from the buoyancy of the sample immersed in water, was in most cases quite high; in fact, it exceeded in some areas the theoretical density based on the simple rule of mixtures indicating either some phase change or, possibly, hexaboride loss during hot pressing.

TABLE 10

COMPOSITION AND DENSITY OF MIXED BORIDE RODS (3/4-INCH DIAMETER TIMES ~1-INCH LONG) HOT PRESSED FOR 0.5 HOURS AT 1800°C

Sample No.	Diboride	Hexaboride	Density	% of Theo. Density*
65-18	ZrB_2	none	4.85	78
58	ZrB_2	CaB_6 (10.5 m/o)	5.47	100
56	ZrB_2	CaB_6 (15.5 m/o)	5.25	100
59-2	ZrB_2	CeB_6 (22.5 m/o)	5.50	100
67-31	ZrB_2	LaB_6 (22.5 m/o)	5.04	100
61-12	ZrB_2	YB_6 (20 m/o)	5.20	99**
83	HfB_2	none	10.11	90
75	HfB_2	none	8.56	76
78	HfB_2	CeB_6 (22.5 m/o)	8.05	95
72	HfB_2	LaB_6 (22.5 m/o)	6.93	100
76	HfB_2	YB_6 (20 m/o)	8.48	100

* Based on rule of mixtures
** Hot pressed at 2030°C

(3) Thermal Expansion Measurements

A high temperature dilatometer (Figure 18) was constructed for the thermal expansion measurements. It consists of a 1-inch O.D. x 5/8-inch I.D. graphite tube (closed on the bottom), a 1/2-inch O.D. graphite plunger rod, and a mechanical gauge accurate to 1 x 10^{-4} inches. The tube containing the sample is joined to the gauge by means of a water-cooled joint; the plunger is placed on the sample so that any movement of the sample will cause a deflection in the gauge. The induction furnace used to heat the dilatometer consists of a 2-inch I.D. x 8-inch long graphite susceptor contained in an argon-flushed quartz envelope and insulated with (Grade WDF) 1/4 inch graphite felt. The system is heated by means of a 6 KW AJAX-Northrup sparkgap-type converter, and the temperature is monitored optically with a Leeds and Northrup optical pyrometer.

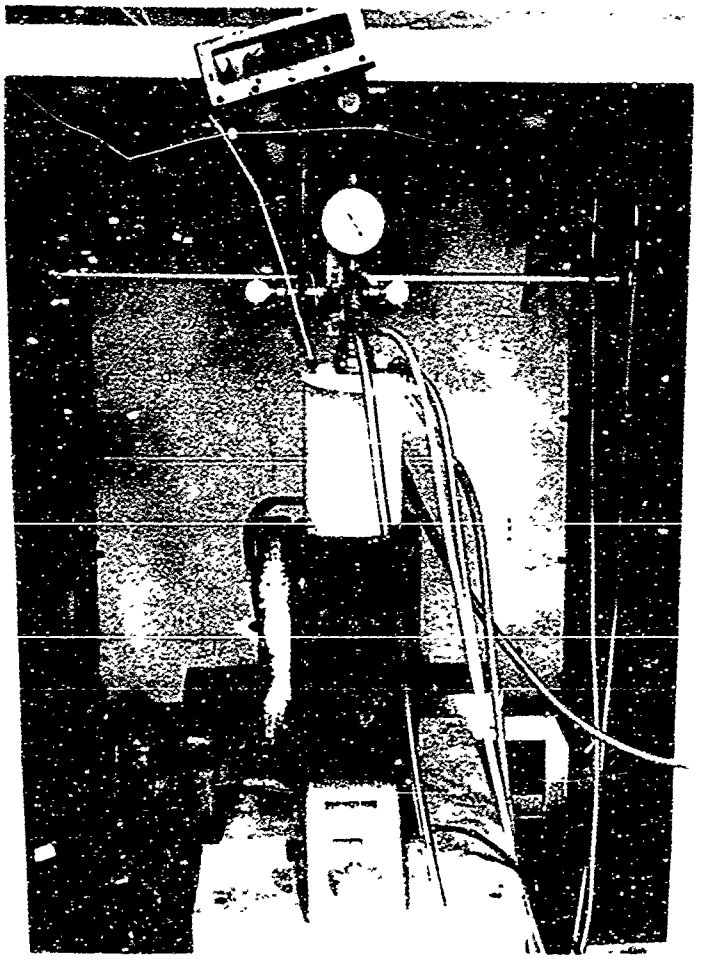

Figure 18. High Temperature Dilatometer

The dilatometer measures the difference in the thermal expansion of the sample and of the sample-containing tube, which was constructed from Union Carbide Corporation's Grade AGW graphite. The apparatus was calibrated against molybdenum,[19] tungsten,[19] and quartz,[19] all of which have well known thermal expansion coefficients. The calibration data shown in Figure 19 agree well with the with-grain thermal expansion curve of Grade AGW graphite as determined by an alternate technique.

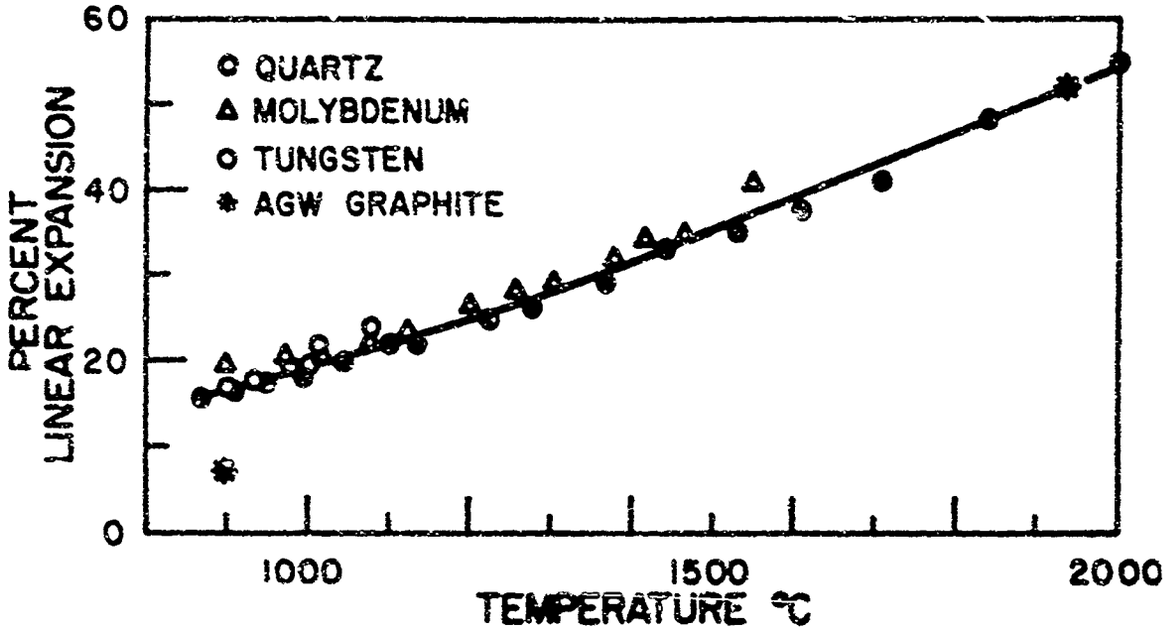

Figure 19. Calibration Correction for AGW Graphite Dilatometer Calibrated With Tungsten, Molybdenum, and Quartz

c. Results and Discussion

Thermal expansion measurements were made on eight boride compositions: ZrB_2 of 78 percent density, ZrB_2-22.5 mole percent CeB_6, ZrB_2-22.5 mole percent LaB_6, ZrB_2-20 mole percent YB_6, HfB_2 of 76 percent density, HfB_2-22.5 mole percent CeB_6, HfB_2-22.5 mole percent LaB_6, and HfB_2-20 mole percent YB_6.

The thermal expansion data on all of these materials are summarized in Table 11.

TABLE 11

THERMAL EXPANSION OF BORIDE COMPOSITES

Material	Density	Expansion in/in/°C x 10^6 0-1000°C	1000-1400°C	1400-1800°C
ZrB_2	*	(7.1)	(8.2)	(8.2)
ZrB_2	78%	6.8	8.2	8.7
$ZrB_2 + CeB_6$	~100%	6.7	8.5	9.5
$ZrB_2 + LaB_6$	~100%	7.5	9.2	11.2
$ZrB_2 + YB_6$	~100%	6.1	8.7	8.5
HfB_2	*	(6.8)	(8.0)	(8.0)
HfB_2	76%	6.6	8.2	9.7
Experimental Graphite		6.0	9.2	9.5
$HfB_2 + CeB_6$	~ 95%	7.2	9.5	9.5
$HfB_2 + LaB_6$	~100%	7.3	9.5	10.2
$HfB_2 + YB_6$	~100%	5.6	7.8	7.8

* () Calculated from single crystal data for a completely dense polycrystalline material based on the work of Houska, Keihn, and Keplin of the Union Carbide Research Institute [1,2]

The thermal expansion of ZrB_2 is shown in Figure 20. The points represent our data on 78 percent dense material and the circles show the results of Houska and Keplin [13] on single crystal ZrB_2 (averaged over the two a and one c direction). The excellent agreement in the thermal expansion of single crystal and 78 percent dense polycrystalline zirconium diboride suggests that, at least for this material, the thermal expansion is independent of porosity.

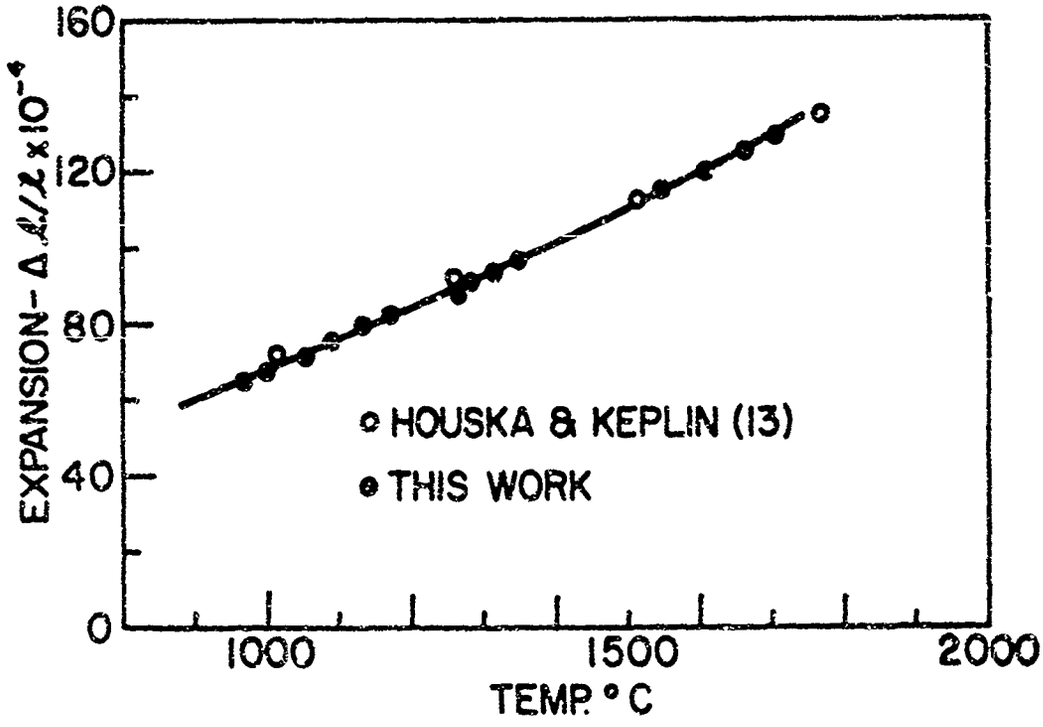

Figure 20. Thermal Expansion of 78 Percent Dense ZrB_2

Figure 21 is a photomicrograph of the 78 percent dense ZrB_2 sample.

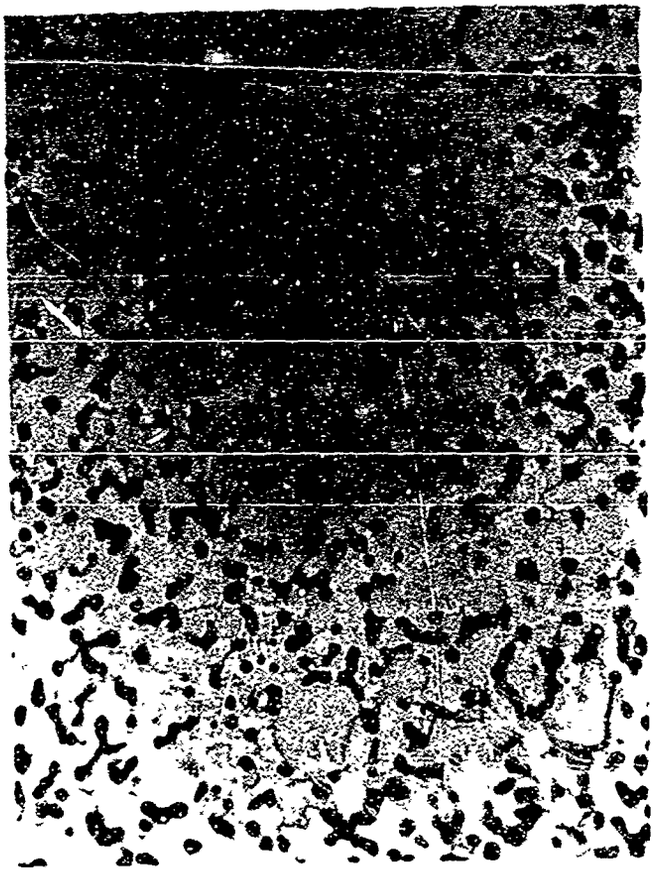

Figure 21. Photomicrograph of 78 Percent Dense ZrB_2 (500 X Magnification)

The thermal expansions of the three zirconium diboride composites (ZrB_2-CeB_6, ZrB_2-LaB_6, ZrB_2-YB_6) are shown in Figures 22, 23, and 24. The borides, with the possible exception of the ZrB_2-LaB_6 composite, have thermal expansion characteristics very similar to those of the graphite shown in Figure 16.

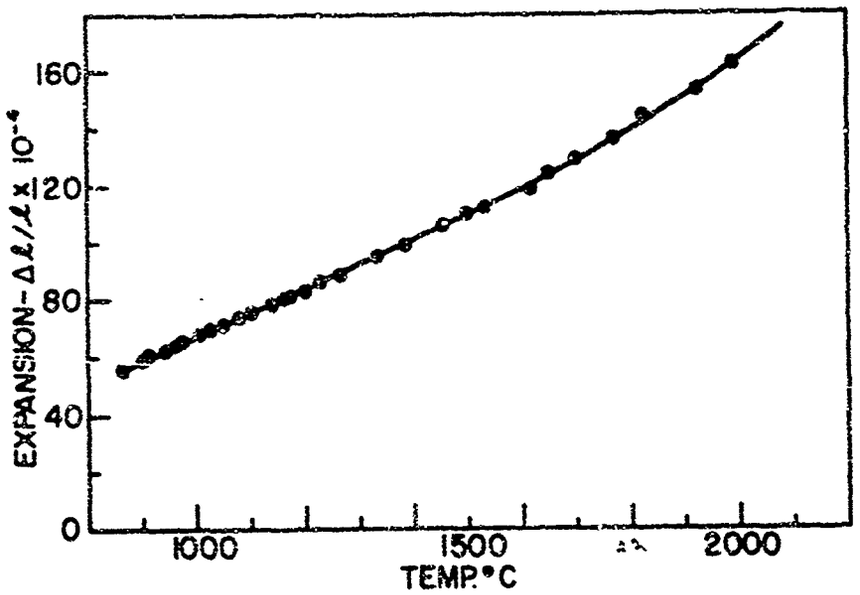

Figure 22. Thermal Expansion of ZrB_2-CeB_6 Composite

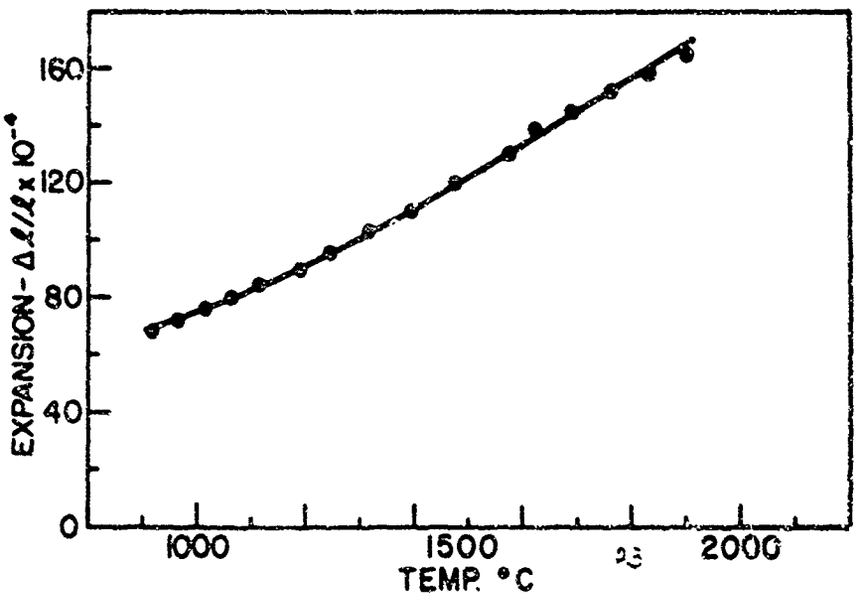

Figure 23. Thermal Expansion of ZrB_2-LaB_6 Composite

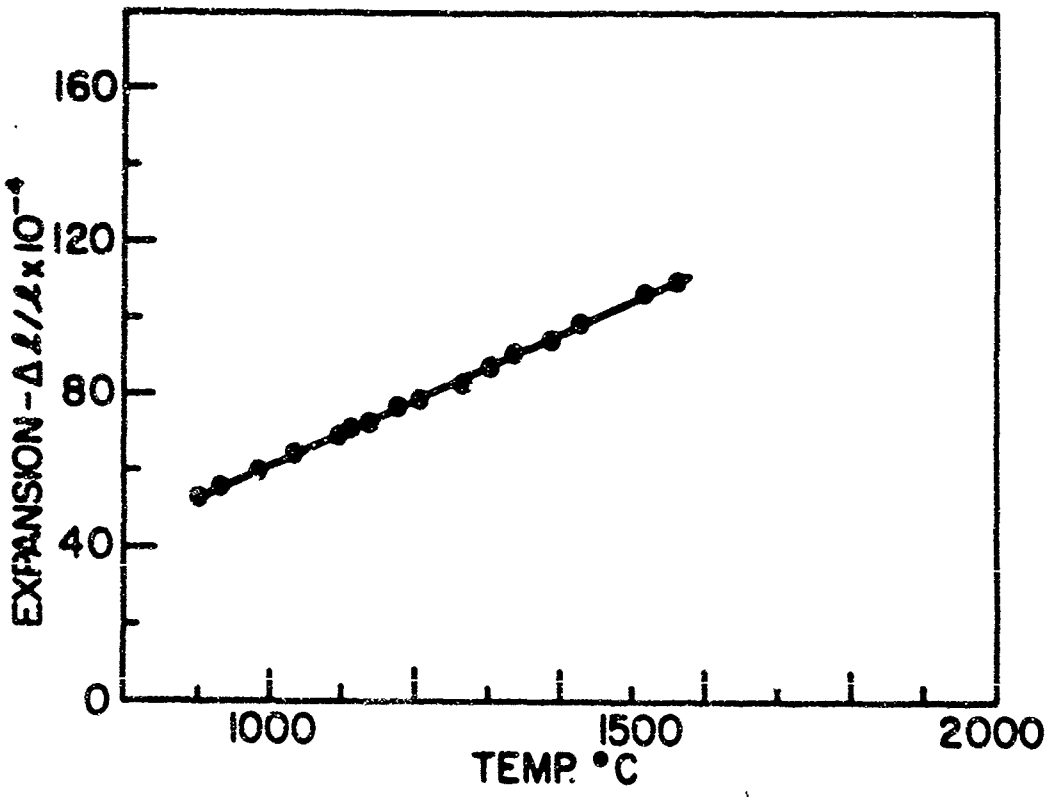

Figure 24. Thermal Expansion of ZrB_2-YB_6 Composite

Metallographic examination of the ZrB_2 composites (Figures 25 through 28), before and after the thermal expansion measurements, showed that the thermal cycling caused a change in only one sample, the ZrB_2-YB_6. Heating (in this case, two cycles from room temperature to 2100°C) caused grain growth and further development of the matrix phase as shown in Figures 25 and 26. Debye-Sherer powder patterns before and after thermal cycling showed no difference; both samples contained ZrB_2, YB_6, and YB_4. During the work on ZrB_2-YB_6, some reaction occurred at the interface between boride and graphite at temperatures above 1600°C. An X-ray pattern of the reaction products was obtained but the products could not be identified. Since this reaction caused the boride rods to bond strongly to the graphite plunger, it may prove helpful in providing better coating adherence.

Photomicrographs of the remaining samples are shown in Figures 27 and 28. They represent the high density samples of ZrB_2-CeB_6 and ZrB_2-LaB_6, respectively. In both cases, the dark particles are in the hexaboride.

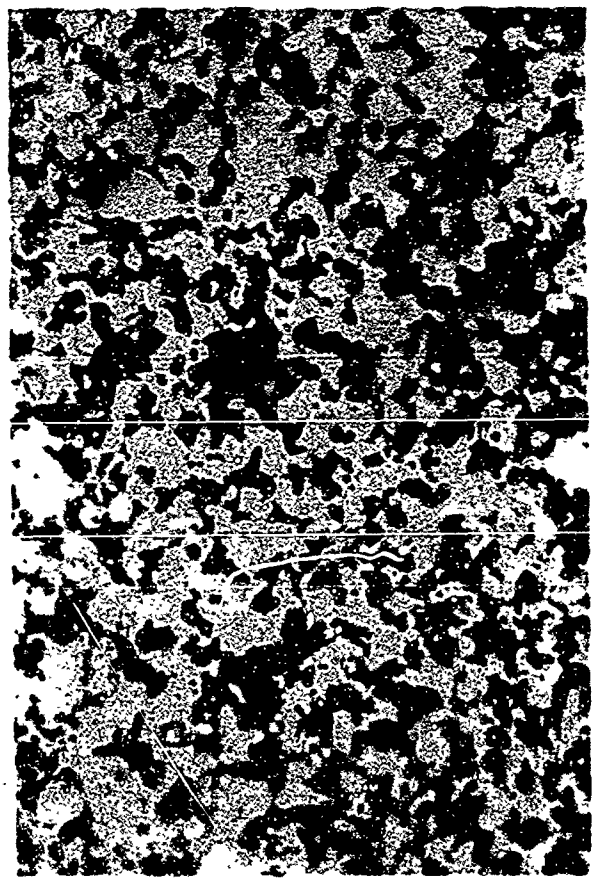

Figure 25. Photomicrograph of ZrB_2-YB_6 Composite as Hot Pressed (500 X Magnification)

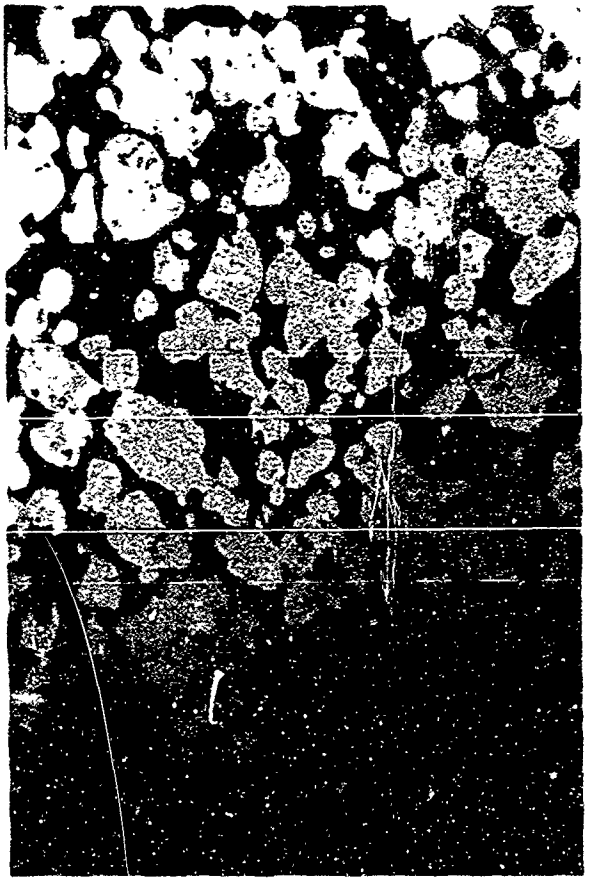

Figure 26. Photomicrograph of ZrB_2-YB_6 Composite After Thermal Cycling (500 X Magnification)

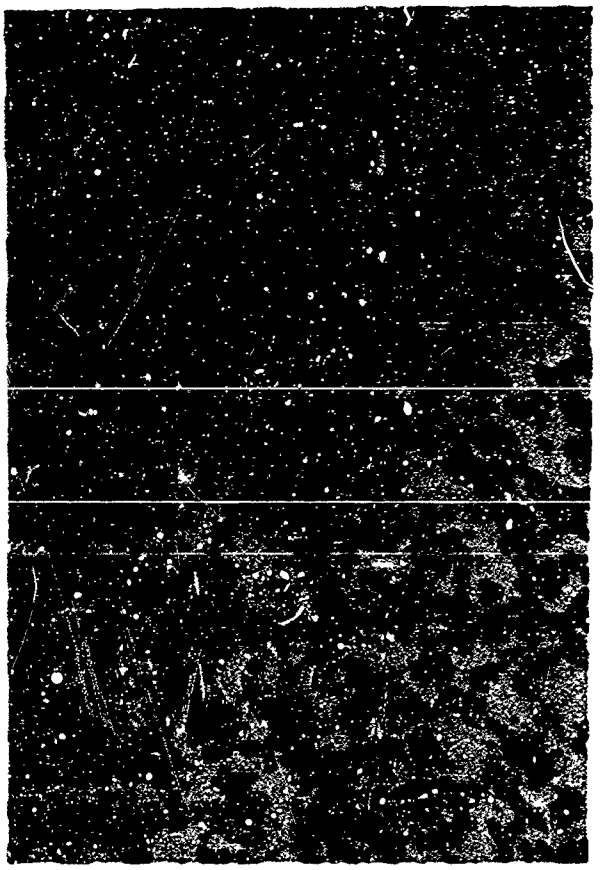

Figure 27. Photomicrograph of ZrB_2-CeB_6 Composite (500 X Magnification)

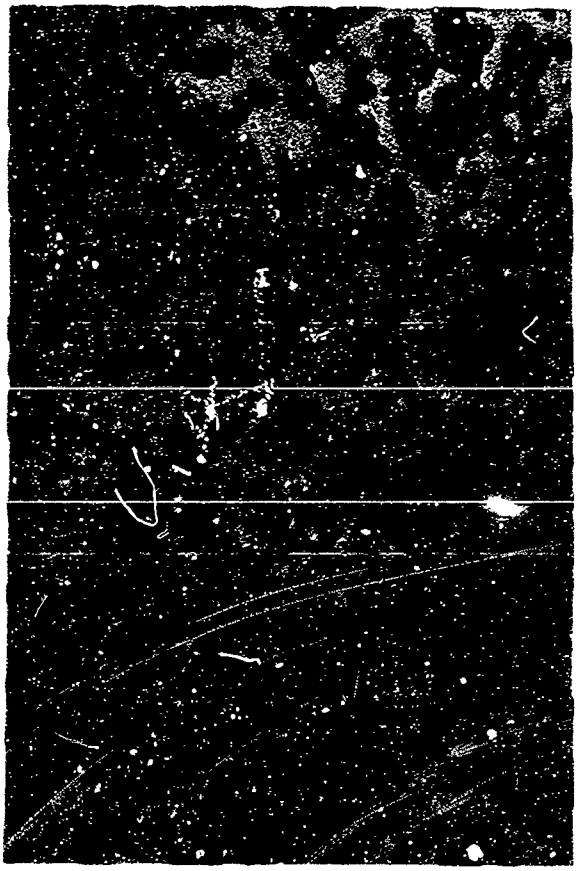

Figure 28. Photomicrograph of ZrB_2-LaB_6 Composite (500 X Magnification)

The thermal expansion of the HfB_2 samples is shown in Figure 29. The encircled points represent our measurements; the triangles and line represent the results of Keihn [12] on single crystal HfB_2 (averaged over the two a and one c direction). The agreement between the low density (76 percent) sample and the single crystal data was anticipated because of similar results obtained with ZrB_2.

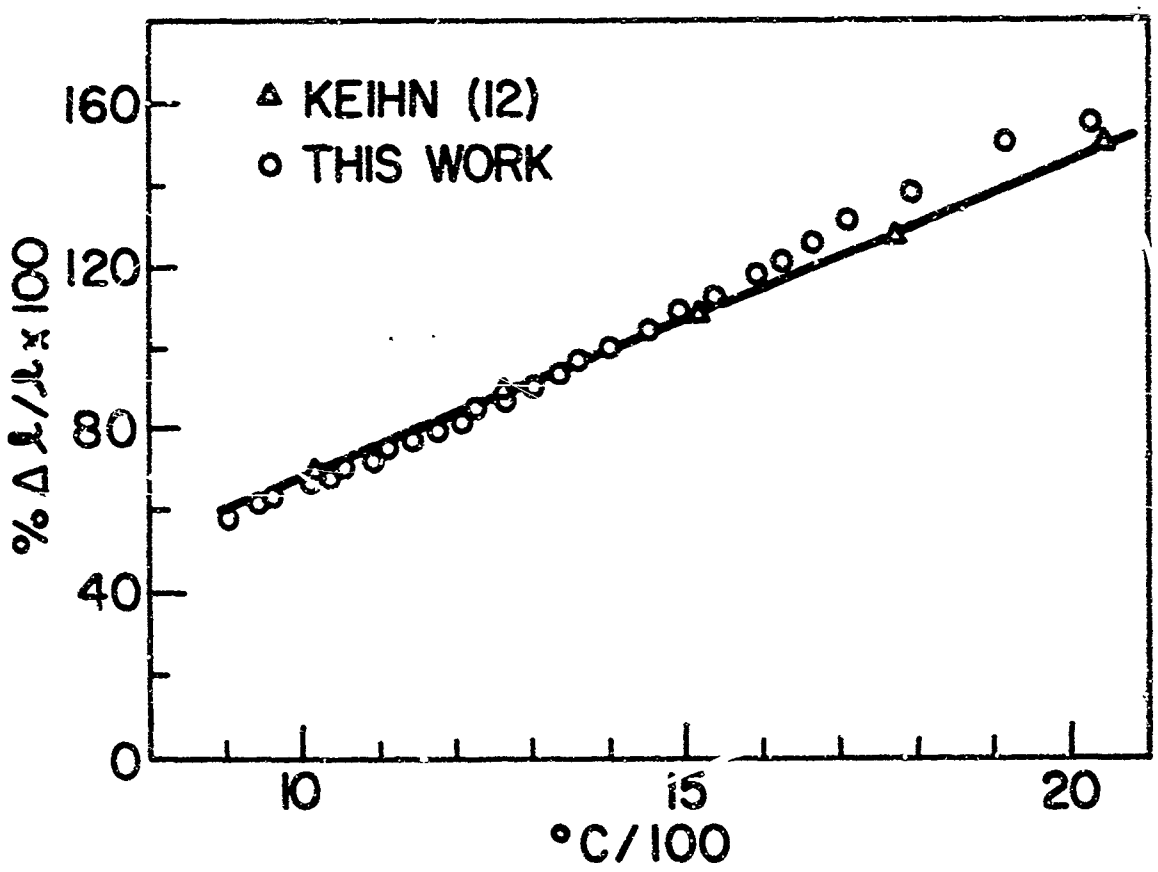

Figure 29. Thermal Expansion of 74.6 Percent Dense HfB_2

Thermal expansions for the three boride composites (HfB_2-CeB_6, HfB_2-LaB_6, and HfB_2-YB_6) are shown in Figures 30, 31, and 32.

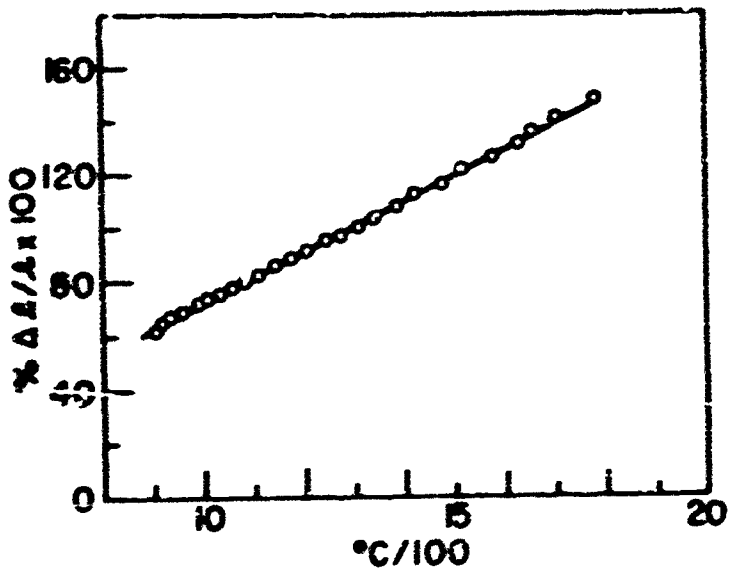

Figure 30. Thermal Expansion of HfB_2-CeB_6 Composite

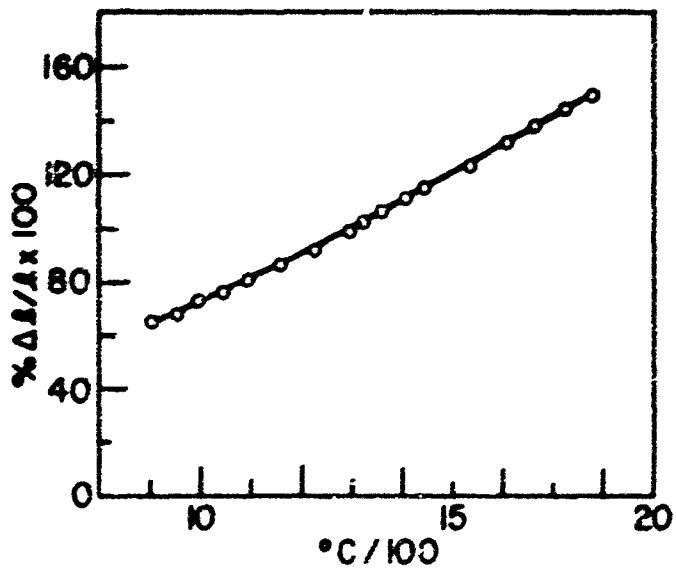

Figure 31. Thermal Expansion of HfB_2-LaB_6 Composite

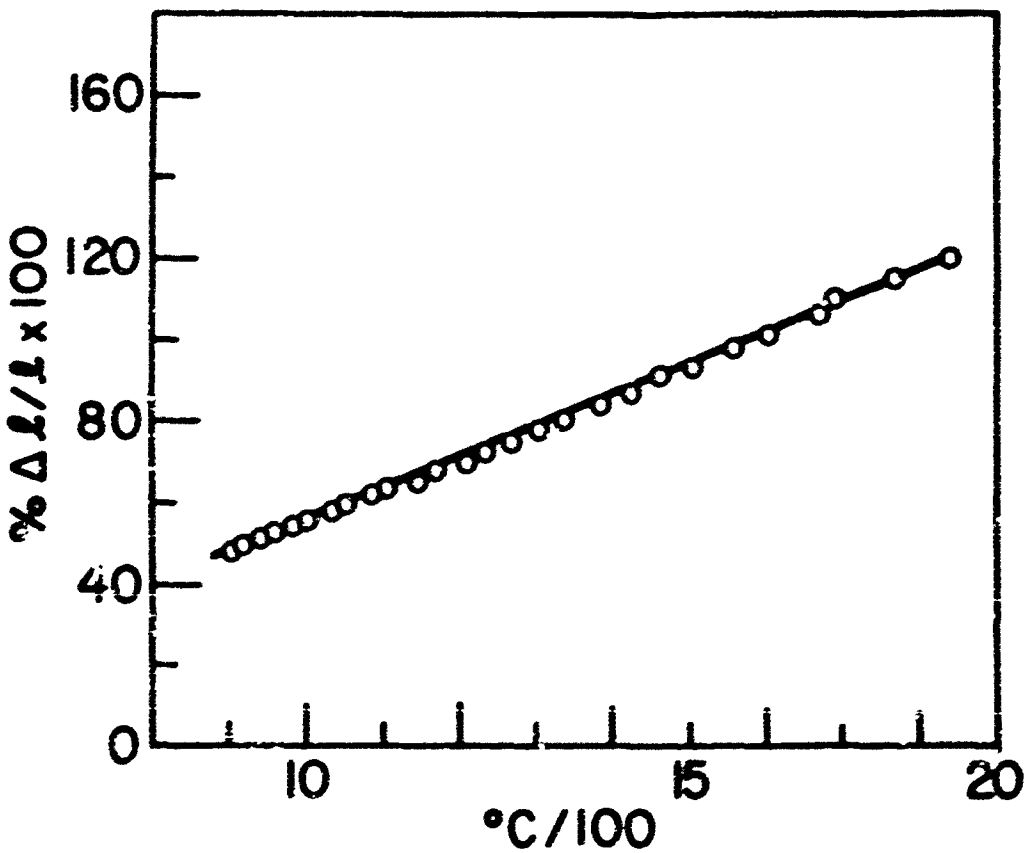

Figure 32. Thermal Expansion of HfB_2-YB_6 Composite

2. THERMAL SHOCK TESTS

A qualitative method for evaluating the effect of thermal cycling on coating adherence is to subject samples to thermal shock tests; samples of ATJ graphite vapor coated with HfC and ZrC were evaluated in this manner.

Thermal shock tests were accomplished by plunging cold samples into an argon-flushed furnace at 2000°C, holding in the furnace for 10 minutes, and then moving the samples into an argon-flushed cooling chamber. It took one minute for the samples to reach 1900°C and an additional 1.5 minutes to reach 2000°C; they cooled below red heat in 1.25 minutes.

Since the coefficient of thermal expansion of ATJ graphite, shown in Figure 33[5], is lower than that of the carbides, the samples crazed on cooling; however, the coating showed no sign of spalling. It has previously been demonstrated[1] that graphite can be tailored to high CTE materials and made sufficiently isotropic to be perfectly compatible with the coating materials.

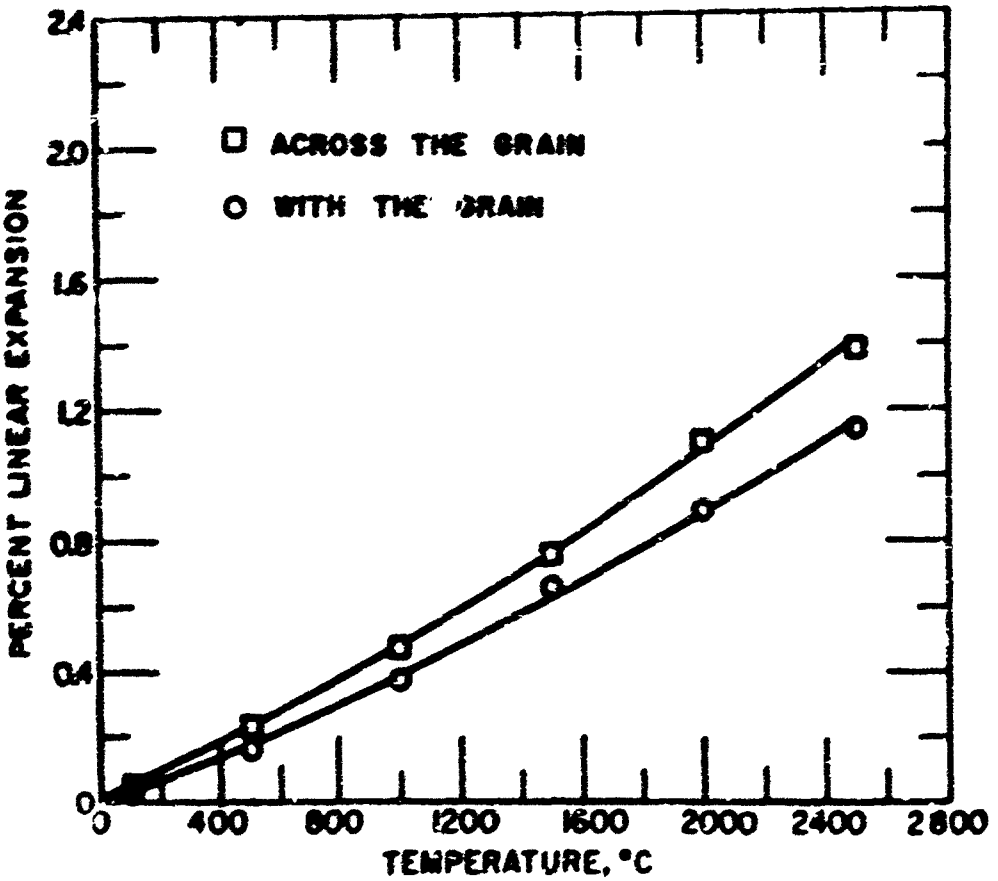

Figure 33. Thermal Expansion of ATJ Graphite

The 1 cm x 2 cm samples were subjected to three shock cycles. Figures 34 through 37 show clearly that no coating-substrate separation occurred; however, some additional crazing occurred in the ZrC sample.

As a result of information obtained from the thermal expansion studies, one can conclude that the borides and the carbides should not present serious mechanical compatibility problems when used with suitable graphite at temperatures to 2000°C.

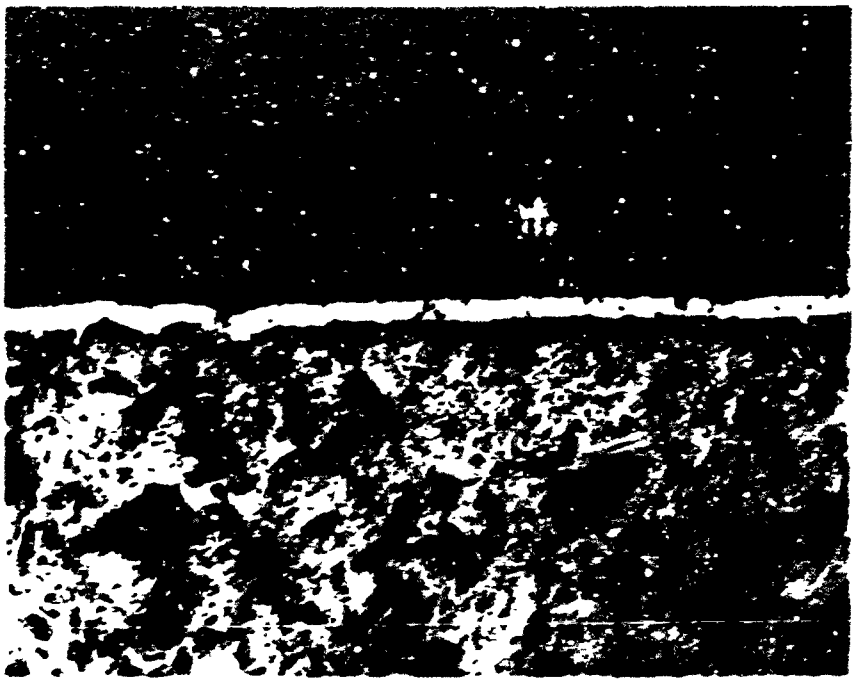

Figure 34. HfC Coating on Graphite Before Thermal Shock Tests (100 X Magnification)

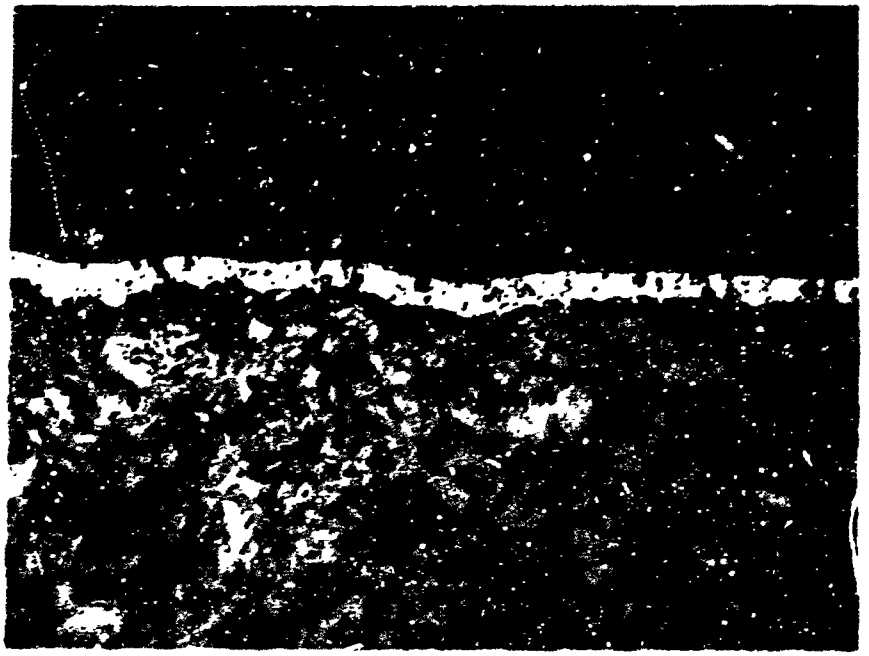

Figure 35. HfC Coating on Graphite After Thermal Shock Tests (100 X Magnification)

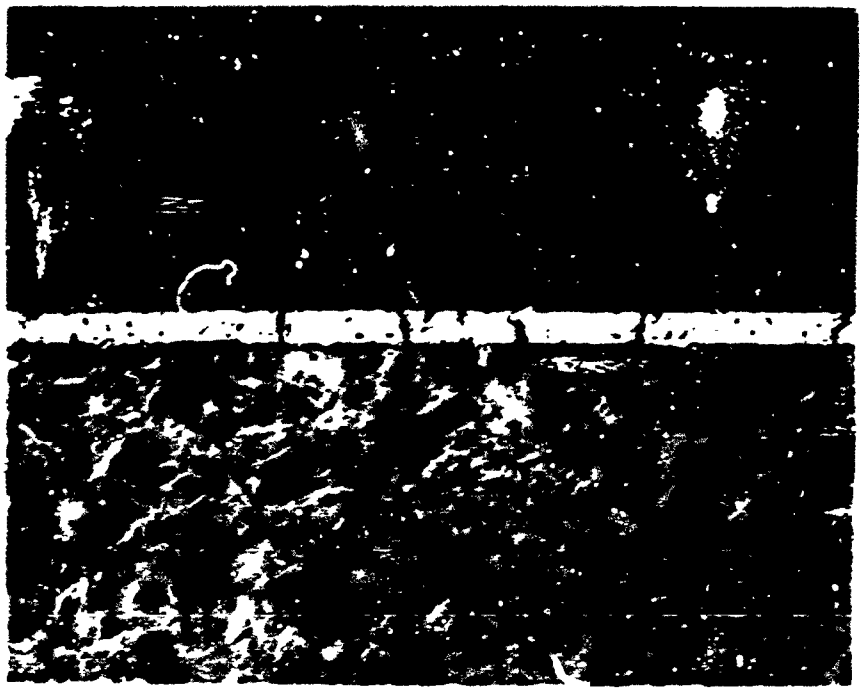

Figure 36. ZrC Coating on Graphite Before Thermal Shock Tests (100 X Magnification)

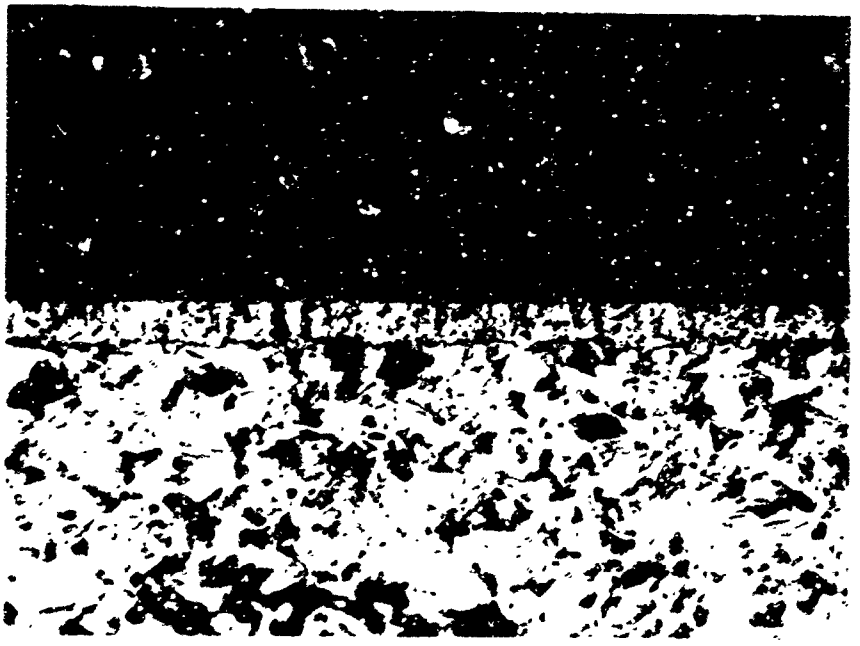

Figure 37. ZrC Coating on Graphite After Thermal Shock Tests (100 X Magnification)

3. VAPOR DEPOSITION OF ZrB_2 ON GRAPHITE

The technique of vapor deposition has been proven to be a very satisfactory method for applying pore-free, well-defined adherent coatings. Therefore, a review of volatile zirconium compounds containing boron was made; the tetraborohydride, $Zr(BH_4)_4$, was found to exhibit a vapor tension of 15.1 mm Hg at 25°C.[20] Since a study of its thermal decomposition had not been reported, the compound warranted further investigation as a possible precursor for zirconium diboride coatings.

These investigations of the thermal decomposition of $Zr(BH_4)_4$ demonstrated that the major product was ZrB_2, and experimental work was extended by coating several grades of graphite with ZrB_2 by the thermal decomposition of $Zr(BH_4)_4$.

a. Experimental

Zirconium tetraborohydride, $Zr(BH_4)_4$, was synthesized by mixing a four-mole excess of lithium borohydride, $LiBH_4$, with zirconium tetrachloride, $ZrCl_4$, in a glass bulb in a dry nitrogen atmosphere. Small nickel balls were used to aid mixing in the absence of a solvent. After an induction period of fifteen to twenty minutes, the reaction proceeded with the liberation of considerable heat. The reaction product, zirconium tetraborohydride, $Zr(BH_4)_4$, melted and the entire contents of the flask formed large cakes. The glass reaction chamber was transferred to a vacuum system and fractional crystallization through traps maintained 0°, -22°, and -196°C was effected. Pure zirconium tetraborohydride was retained in the -22°C trap; it exhibited 15.1 mm Hg vapor tension at 25°C and had a melting point of 30°C.

Zirconium tetraborohydride was condensed into a Pyrex container of known weight; the tube was then reweighed so that the quantity of zirconium tetraborohydride used in each experiment was known to within 0.0002 gms.

In a typical experiment the weighed sample was attached through a break-off seal to a quartz pyrolysis chamber and the entire system was evacuated to 10^{-6} torr. The pyrolysis chamber was brought to a predetermined temperature by means of a platinum wound tube furnace.

The temperature was controlled with a Variac and monitored with a thermocouple suitable for the working range.

The sample tube of zirconium tetraborohydride was cooled to 0°C in an ice bath to maintain a constant vapor pressure and thus rate of flow to the hot zone. The break-off was broken and the reaction products collected in traps maintained at -78°C and -196°C. The hydrogen formed was continually compressed into a known volume by means of an automatic Toepler pump. When the run was completed, the amount of hydrogen was determined, passed over copper oxide at 450°C, and the resulting water trapped and subsequently expanded as a

check on the purity of the hydrogen. The quartz tube was cooled and reweighed. The decomposed material was then scraped from the quartz tube, mixed with SP-1 graphite powder, and heated to 2000°C for one hour in vacuo to effect crystallization for X-ray examination.

The graphite substrates to be coated were heated by means of a 30 KW Thermionic generator coupled to a water-cooled copper flux concentrator, which was an integral part of a vacuum system. The graphite was degassed at 2000°C at 10^{-6} mm Hg pressure for one to two hours. The sample temperature was lowered to 1100°C, and zirconium tetraborohydride vapor was passed over the hot graphite. In a typical experiment, 0.4777 g of zirconium tetraborohydride (3.18 mmoles) deposited 0.160 g of zirconium diboride (1.06 mmoles) on a graphite substrate at 1100°C. The sample was then heated to 1950°C, held for one hour, and then cooled to room temperature by de-energizing the power supply.

The adherent coatings were subjected to thermal cycle tests in vacuo, heating from below red heat to 2000°C in three minutes, and then cooling to below red heat in two minutes.

b. Results and Discussion

The results of the various runs made on the thermal decomposition of zirconium tetraborohydride are presented in Table 12. At the lower decomposition temperature (< 600°C), zirconium metal and boron were the major products of the reaction. However, as the decomposition temperature was raised above 600°C, zirconium diboride was the major reaction product. The equations for these reactions at low and high temperatures may be written as follows:

$$Zr(BH_4)_4 \xrightarrow{<400^\circ C} 8H_2 + Zr + 4B$$

and

$$Zr(BH_4)_4 \xrightarrow{>600^\circ C} 8H_2 + ZrB_2.$$

TABLE 12

ANALYSIS ON THE THERMAL DECOMPOSITION OF ZIRCONIUM TETRABOROHYDRIDE

Weight of $Zr(BH_4)_4$ Grams	mmoles $Zr(BH_4)_4$	Environment	Temperature, °C	mmoles H_2	Ratio $H_2/Zr(BH_4)_4$	Wt. of Products in Quartz Tube Grams
0.090	0.602	Quartz Tube	400	4.57	7.6	
0.242	1.617	Quartz Tube	400	12.88	8.0	0.245
0.459	3.060	Quartz Tube	400	24.18	7.9	0.458
0.269	1.791	Quartz Tube	500	14.49	8.0	0.274
0.168	1.119	Quartz Tube	500	9.08	8.1	0.177
0.156	1.053	Quartz Tube	600	5.48	8.1	0.151
0.197	1.313	Quartz Tube	600	10.75	8.2	0.206
0.217	1.449	Quartz Tube	800	11.71	8.1	0.230

When graphite cloth was inserted into the quartz tube and zirconium tetraborohydride allowed to decompose thermally at 800°C, the ratio of H_2 to $Zr(BH_4)_4$ dropped to approximately 7.5 to 7.7, indicating either that some of the hydrogen was being consumed by the carbon or that another mechanism of decomposition was occurring. A white solid was also found in the -196°C trap, and its infra-red spectrum indicated boron-hydrogen bonding with no carbon-hydrogen bonding. A molecular weight determination gave a value of ~30. This product very probably is diborane, B_2H_6. The stoichiometry is tentatively summarized by:

$$Zr(BH_4)_4 \rightarrow ZrB_2 + B_2H_6 + 5H_2$$

with partial decomposition of the B_2H_6 to $B + H_2$.

The zirconium diboride coatings formed on Grades ATJ and ZTA graphite were found to have poor adherence and large macrocracks over the entire surface. The coating was easily removed with a sharp-edged knife. However, when an isotropic high coefficient of thermal expansion grade of graphite was used as the substrate, a dense adherent coating resulted. Figure 38 illustrates this point well. The right side of the figure demonstrates the poor adherence of a ZrB_2 coating on ZTA graphite; the left side of the figure demonstrates the excellent adherence of a ZrB_2 on the isotropic high CTE graphite. Figure 39 is a photomicrograph of the zirconium diboride coating (one mil thick) after thermal cycling to 2000°C several times. The coating remains dense and adherent, indicative of good bond formation between the boride and graphite.

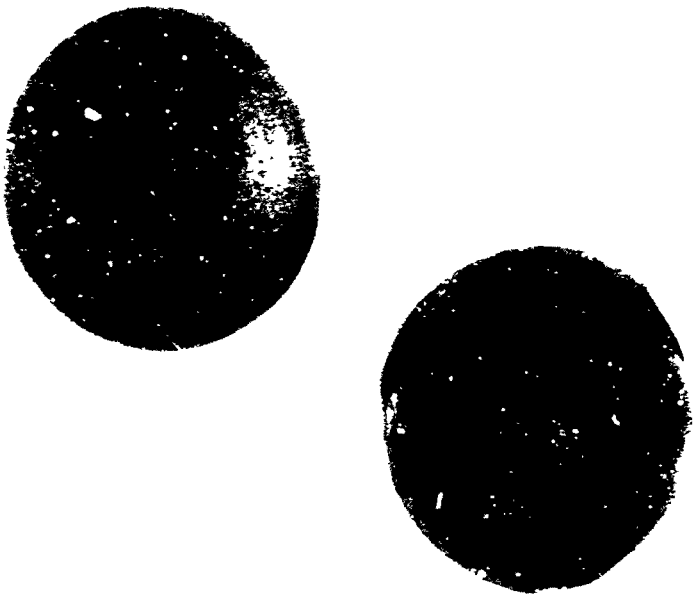

a) ZrB_2 on High CTE Graphite b) ZrB_2 on ZTA Graphite

Figure 38. Vapor Deposited ZrB_2 Coatings on Graphites

Figure 39. Vapor Deposited ZrB_2 Coating on Graphite After Thermal Cycling to 2000°C (1000 X Magnification)

VIII. CARBON DIFFUSION THROUGH ZIRCONIUM MONOCARBIDE AND ZIRCONIUM DIBORIDE

TASK D-1

1. CARBON DIFFUSION THROUGH ZIRCONIUM MONOCARBIDE

a. Introduction

There are a wide variety of methods, both direct, as in tracer studies, and indirect, such as in the measurement of phase boundary motion during diffusion-controlled layer growth, available for the study of diffusion coefficients. These techniques are well established and are described in the literature. In this investigation, the method of isotopic exchange between an initial plane source and a semi-infinite body was selected. In the absence of a macroscopic chemical gradient, if the diffusing isotope is initially present in concentration $C^*(0, 0)$ on a plane surface at the end of a semi-infinite specimen, then the concentration in a parallel plane at a distance, x, from the original interface, after a suitable annealing time, t, will be:

$$C^*(x, t) = \frac{C^*(0, 0)}{(\pi D^* t)^{1/2}} \exp\left(-\frac{x^2}{4D^* t}\right) \qquad (1)$$

where D^* is the tracer diffusion coefficient and is related to the self diffusion coefficient by the appropriate correlation factor.[21] Although ZrC shows a wide variation in composition,[22,23] the absence of a macroscopic chemical gradient and the boundary conditions which satisfy Eq. 1 can be achieved by utilizing carbon-12 saturated semi-infinite specimens and a thin plane source of carbon-14. For specimens which are lower in carbon content, other geometries such as a pair of butt-welded semi-infinite specimens identical in composition, except for the concentration of tracer in each half of the couple, must be used. Furthermore, in order to satisfy Eq. 1, the thickness of the isotope layer, h, must be small relative to the penetration depth. A good approximation for this requirement is that:[24]

$$h < 0.1 (D^* t)^{1/2} \qquad (2)$$

and this condition can be controlled by experiment.

b. Experimental

(1) Materials and Equipment

Both single crystal and polycrystalline samples were used. The fully dense specimens were provided by the Union Carbide Research Institute and were grown by an arc fusion technique. The polycrystalline specimen (approximately ½-inch D x 6 inches long) was composed of long columnar grains, about 0.2 mm x 0.2 mm x 3 mm (Figures 40 and 41).

Figure 40. Macrophotograph of the Polycrystalline ZrC Specimen Used in This Study. Note That the Long Axes of the Grains are Roughly Parallel to the Specimen Axis

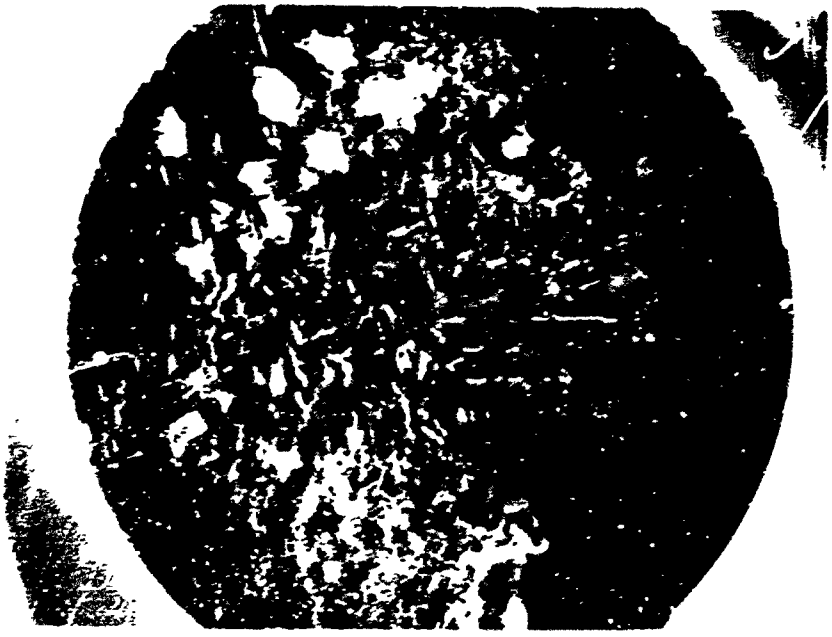

Figure 41. Macrophotograph of the Same Specimen Shown in Fig. 40. The Plane of the Figure is Normal to the Specimen Axis. Most of the Grains are Equiaxed

The long axes of the columnar grains were generally parallel to the specimen axis and the number of grains per unit area remained nearly constant throughout the length of the specimen. There appeared to be a small amount of free carbon (Figure 42) present which remained even after prolonged high temperature annealing (2 hours at 2650°C). Chemical analysis showed 49.1 atomic percent carbon, nearly that of carbon saturated ZrC

Figure 42. Photomicrograph of Polycrystalline ZrC Showing a Small Amount of Graphite in the Form of Flakes

The single crystal was ~$^3/_8$-inch D x 8 inches long; the long axis of the crystal was about 16.5° from the <110> and 20.5° from the <111> poles. Laue back-reflection photographs (Figure 43) showed some substructure and, in fact, at times some chemically polished specimens showed a low angle tilt (less than 1°) boundary running through the crystal. Other sections were free of boundaries. Chemically, the specimen was similar to the polycrystalline sample and contained 48.8 atomic percent carbon.

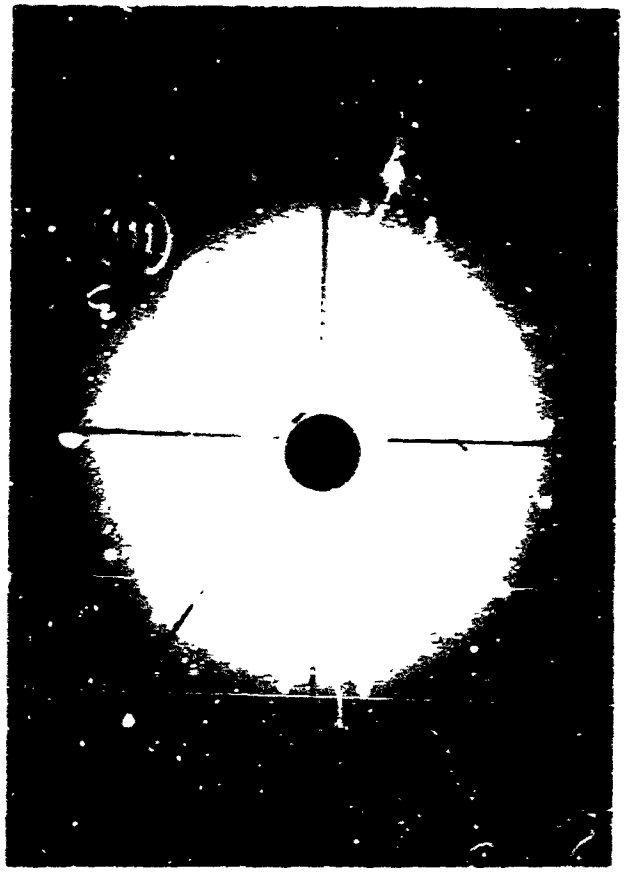

Figure 43. Laue Back-Reflection Photograph of the Single Crystal ZrC Specimen Used in This Study

The specimens were sectioned using a "Micro-Matic" precision wafering machine. The best results were obtained using a 240 grit, 100 concentration diamond wheel at a surface speed of 4,000 fpm. Downfeed was less than 0.005 inch per cut and cross feed was kept to less than 0.2-inch/minute. Grinding was done on the same unit using resin-bonded wheels with surface speeds of 4,000 fpm. The specimens were coarse ground with a 400 grit wheel and finished ground with an 800s grit wheel. The finished surfaces were comparable to those obtained by usual metallographic preparation.

Annealing was done in a tantalum tube resistor furnace and under a vacuum of 10^{-5} to 10^{-6} mm Hg. The time-to-temperature was less than one minute and cooling, under vacuum, from temperature to 1100°C was about two minutes. Temperature control was within ± 10°C at 2200°C and about ±2°C at 1200°C. Control was indirect, using a calibrated radiation pyrometer. However, the temperature was continuously monitored with a W-5 percent Re/W-26 percent Re thermocouple which was placed in close proximity to the specimen surface.

The specimen activity was measured with a low-level, low-background proportional counting system. The unit was equipped with an ultra thin window which allowed transmittance efficiencies of up to 35 percent for C^{14}. Background was less than 0.5 counts per minute.

(2) Experimental Methods

Cylindrical slabs, about 0.2 cm thick, were cut and the end faces ground parallel to $\pm$ 1 x 10^{-4} inches using a 400 grit resin-bonded diamond wheel. In the case of the polycrystalline specimen, the end faces were normal to the columnar grain while for the single crystal the end faces were cut parallel to the (110) plane. The sectioned specimens were then chemically polished using a solution of 2 parts HF, 8 parts HNO_3 and 15 parts H_2O to remove most of the disturbed surfaces. No annealing was attempted. C^{14} was deposited on the surfaces by means of the pyrolytic decomposition of radiomethane at 1000°C. Induction heating was employed and the elapsed time-at-temperature was of the order of two minutes. The radiomethane source was of two specific activities, 2mC/mM and 10mC/mM. The activity to be used depended on the intended annealing time and temperature. The usual procedure was to evacuate a quartz tube containing the specimen to less than 10^{-3} mm Hg, heat the specimen to 1000°C and introduce $C^{14}H_4$ to a pressure of about 50 mm Hg. Decomposition was instantaneous and the surfaces appeared as bright and shiny as when introduced into the chamber. The radioactive carbon was removed from all surfaces but one end face by grinding. In order to assure the presence of carbon of unit activity at all times during the vacuum anneal, the specimen was placed in a graphite crucible and packed with pure pyrolytic graphite powder.

After the appropriate anneal, 0.030 inch was removed from all surfaces, except the original hot face, to eliminate edge effects. The specimen was serially sectioned and the activity of each succeeding end face (looking into the low activity side of the penetration profile) was determined. No correction was made for the contribution of the layers beneath the surface but it has been estimated [25] that the ignoring of this effect leads to values of D which are too low by less than 10 percent.

Sectioning was done both mechanically and chemically. Mechanical sectioning was accomplished by abraiding with an 800s grit diamond wheel. Less than 2 x 10^{-4} inches were usually removed at one time. The amount removed was measured using a Starrett gauge which had divisions of 10^{-4} inches. Chemical sectioning was done using the chemical polish described earlier. It was found that uniform layer removal and minimization of spurious edge effects could be accomplished best by simply putting several drops of solution on the face to be etched and relying on surface tension to prevent spillage onto the sides of the specimen. Masking of the specimen with wax or using a variety of specimen holders made of teflon were not nearly as effective. Uniformity and amount of attack could be visually seen since the

etchant also stained the surface. This stain was removed with either hot concentrated H_2SO_4 or by washing with methyl alcohol. The latter was preferable and the usual procedure was to etch, rinse with distilled water, wash with reagent grade methyl alcohol and dry with a jet of dry air. As will be seen later, the agreement of the results between the mechanical and chemical sectioning techniques was well within the limits of experimental error.

(3) Penetration Curves

According to Eq. 1, the plot of ln activity versus the square of the penetration distance should be linear with the slope:

$$\frac{d \ln A(x,t)}{dx^2} = -\frac{1}{4D^*t} \qquad (3)$$

for bulk diffusion. In practice, several distinct regions of linearity as well as a curved "tail" may be observed.[24,26,27] These regions are usually described as near-surface, volume diffusion, and short-circuiting.[26] What is observed depends strongly upon the experimental conditions of time, temperature, and method of sectioning. For the case of short-circuiting by grain boundaries, the Fisher analysis[29] shows that a plot of ln A(x, t) varies as the first power of distance with the slope:

$$\frac{d \ln A(x,t)}{dx} = -\frac{(2)^{1/2}}{(\pi D_1^* t)^{1/4}(\delta D_b^*/D_1^*)^{1/2}} \qquad (4)$$

where: D^*_1 = the tracer lattice or volume diffusion coefficient

D^*_b = the tracer boundary diffusion coefficient

δ = the boundary width.

The assumptions of this model and the appropirate corrections by Whipple,[30] Levine and MacCallum[31] are well known and will not be delved into here.

A number of typical concentration profiles are shown in Figures 44 through 48. The scale factors refer to the abscissa only. These figures serve to illustrate the various regions usually observed. Under some conditions, the profiles for the single crystal and polycrystalline specimens are very much alike and in other instances, vastly different. Presumably, this variation is due to substructure or the lack of it. The in-deep region which is thought to be present because of short-circuiting,[25] is not always linear but often exhibits marked curvature. This region was observed in some single crystals but not in others. The near-surface region was observed only when chemical sectioning was employed. In addition, chemical sectioning revealed, in the case of the single crystals, the presence of a region intermediate between the near-surface and volume diffusion zones.

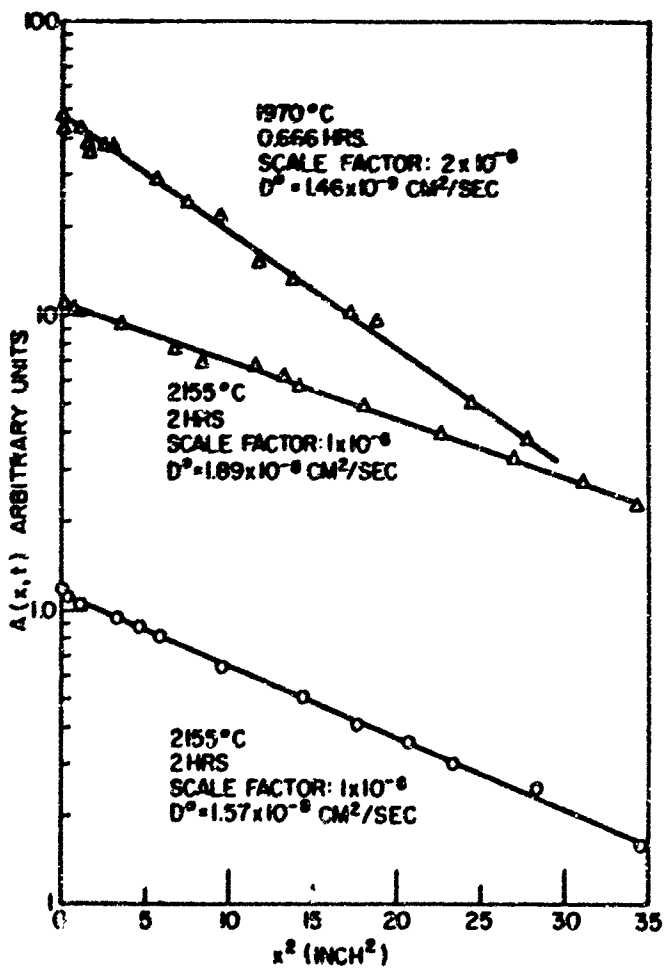

Figure 44. Portions of the Concentration Profiles for Single Crystal (Δ) and Polycrystalline (o) ZrC. Mechanically Sectioned

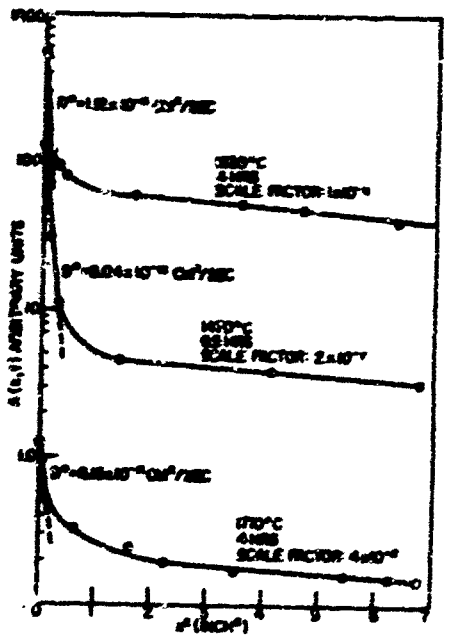

Figure 45. Portions of the Concentrative Profiles for Polycrystalline ZrC. Mechanically Sectioned

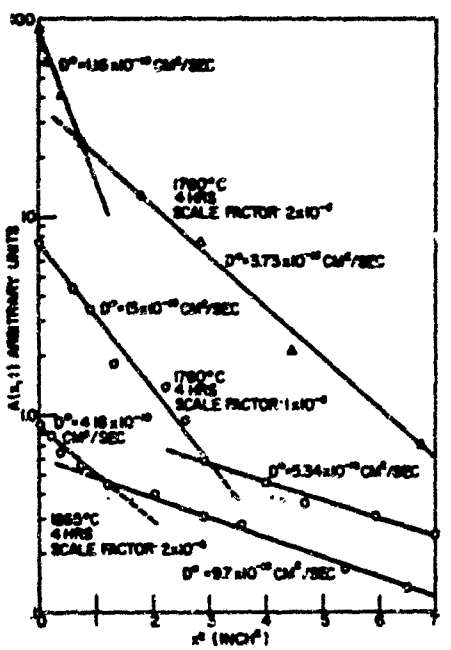

Figure 46. Portions of the Concentration Profiles for Single Crystal (Δ) and Polycrystalline (o) ZrC. Mechanically Sectioned

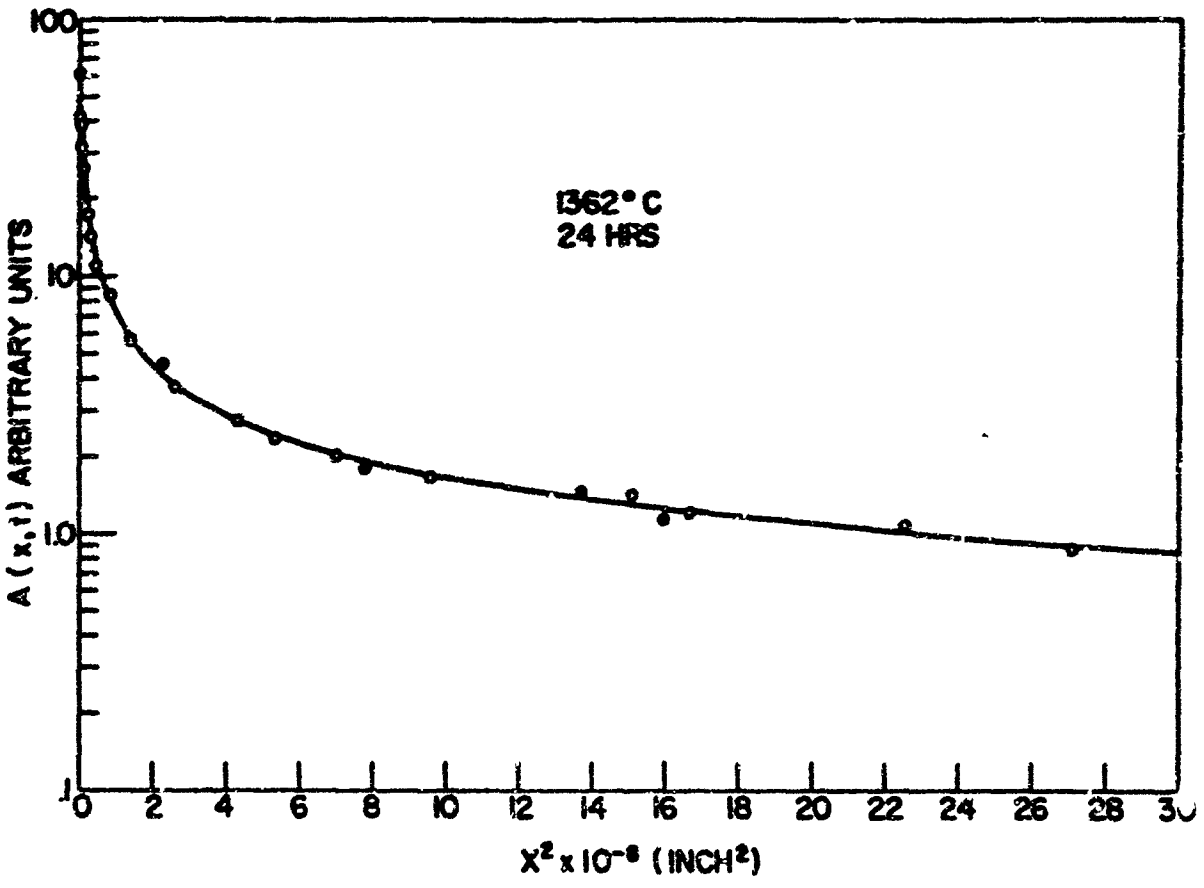

Figure 47. Portion of the Concentration Profiles for Two Polycrystalline ZrC Specimens. The Closed Circles (•) Refer to Mechanical Sectioning and the Open Circles (o) to Chemical Sectioning

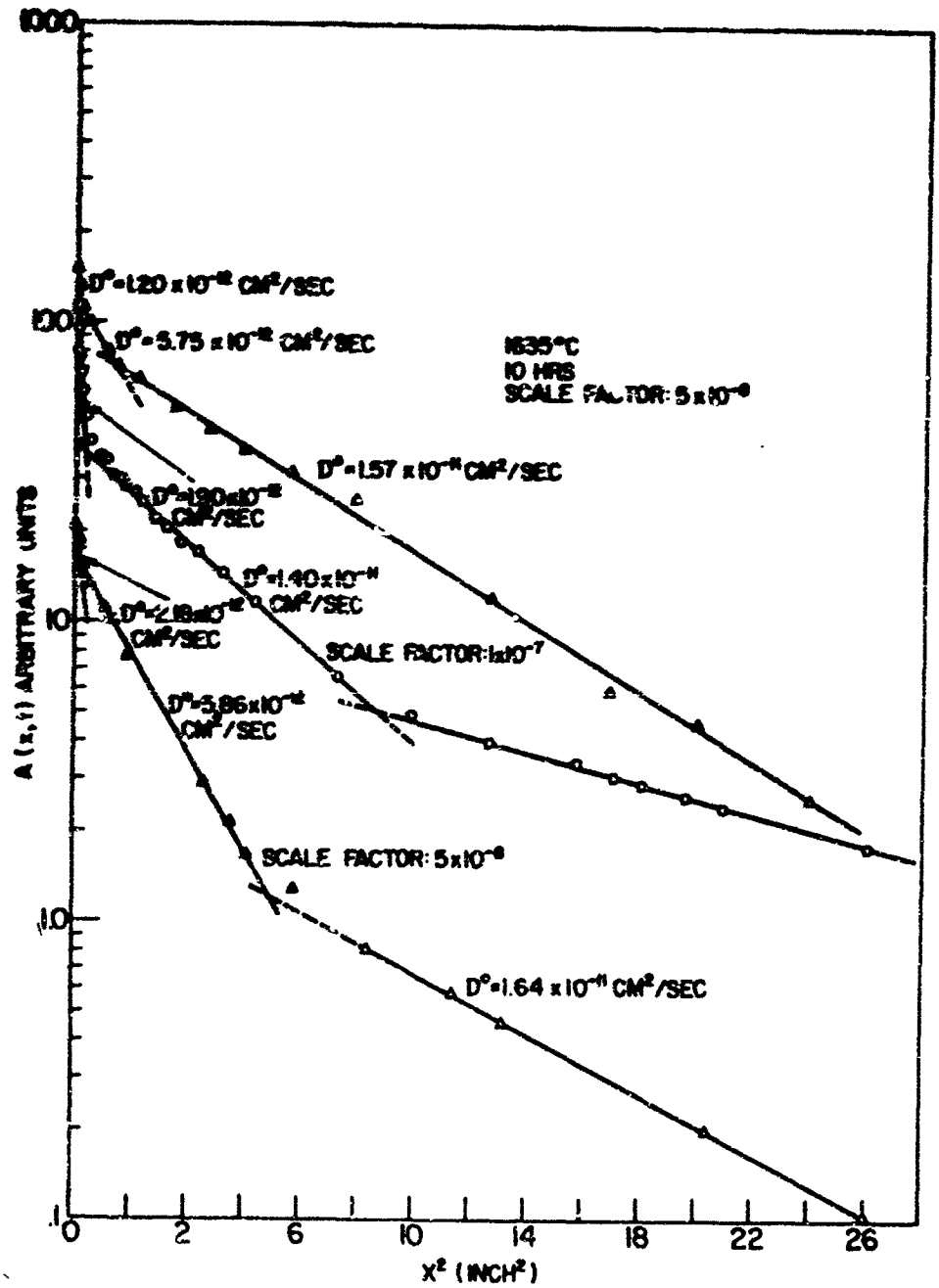

Figure 48. Portions of the Concentration Profiles for Single Crystal (Δ) and Polycrystalline (o) ZrC. Chemically Sectioned

In those instances when the in-deep region of the polycrystalline specimens was found to be curved or when the entire plot of the activity versus penetration distance squared showed nonlinearity, the data was replotted as the first power of the penetration distance and found to be linear. Typical examples are shown in Figure 49. The data obtained from such plots was too limited to permit the separation of D_b^* from D_l^*, however.

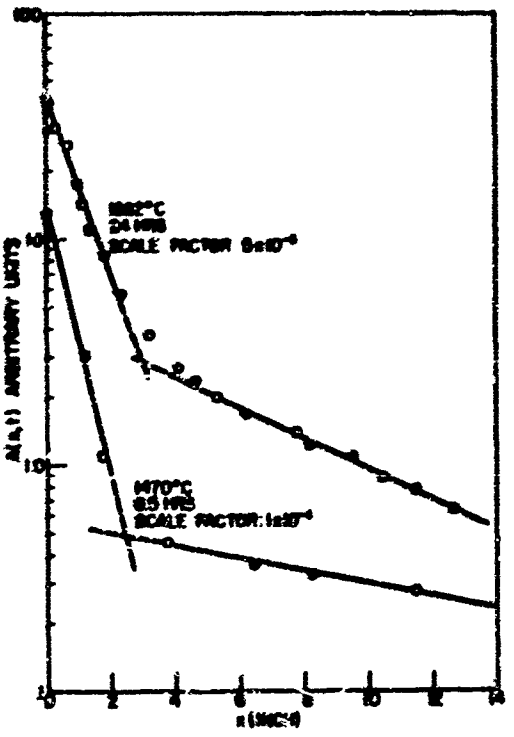

Figure 49. Portions of the Concentration Profiles for Polycrystalline ZrC. The Log of the Activity is Plotted as the First Power of Penetration Distance. The Upper Curve was Determined by Chemical Sectioning and the Lower Curve by Mechanical Sectioning

c. Analysis of Results

Using Eq. 3, diffusion coefficients were calculated for all linear portions of the penetration curves. These coefficients can be represented by two equations:

$$D^* = 1.32 \times 10^2 \exp\left(-\frac{113,200}{RT}\right) \quad (5)$$

$$D^* = 1.6 \exp\left(-\frac{90,000}{RT}\right) \quad (6)$$

and these are taken to represent volume diffusion and short-circuit enhanced volume diffusion, respectively.

The detailed physical reasons neither for the near-surface effect, common to both single and polycrystals, nor for the intermediate region found for the single crystals only, were established by this study. That these regions are reproducible by experiment was verified, however, and at 1635° C, the near-surface diffusion coefficient is only an order of magnitude smaller than that observed in the bulk.

All of the data are shown in Arrhenius form in Figure 50. Here we have assumed a mechanism of substitutional diffusion and arbitrarily multiplied the tracer lattice diffusion coefficient (Eq. 5) by the Bardeen-Herring correlation factor of f_{11}. For interstitial or sub-boundary mechanisms, the tracer diffusion coefficient equals the self diffusion coefficient.

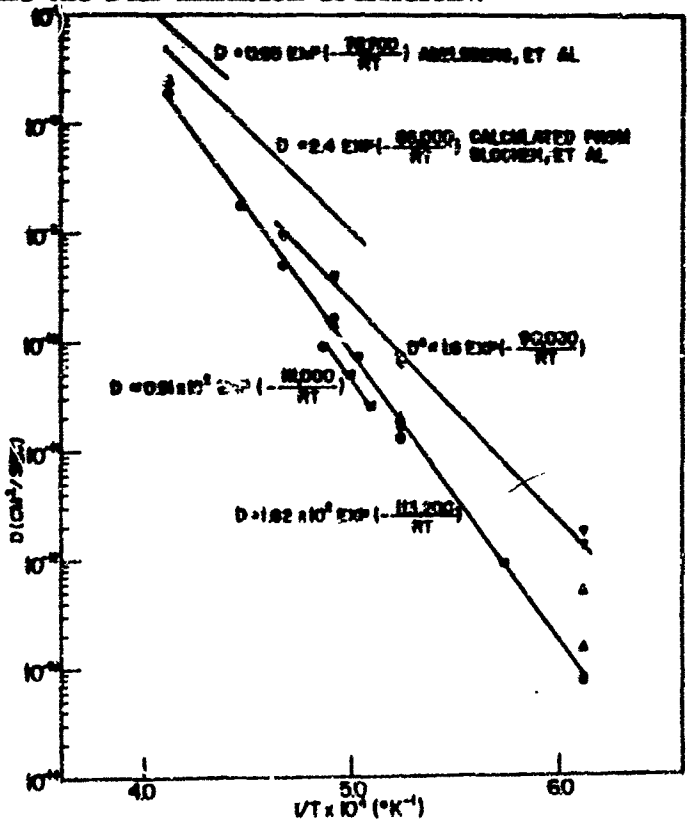

Figure 50. Diffusion Coefficients as a Function of Reciprocal Temperature. △ Single Crystal, Mechanically Sectioned; ▲ Single Crystal Chemically Sectioned; o Polycrystal Mechanically Sectioned; ● Polycrystal Chemically Sectioned. ▽ Polycrystalline, ▽ Single Crystal, Diffusivity Calculated From the In-Deep Region Using Eq. 1. ■ Calculated From the Creep Data of Keihn and Boohns (Ref. 32) Using Eq. 7

d. Comparison With Indirect Methods

Keihn and Boons [32] have measured the high temperature creep rate of a fully dense polycrystalline specimen of ZrC. Using the methods of Dorn, [33] they calculate an activation energy for creep of 111 kcal. The single specimen used by these investigators and that used in this work were from the same source and virtually identical in composition and grain size.

In some instances, [34-36] high temperature creep can be characterized by the so-called Nabarro-Herring [37,38] diffusional viscosity. The diffusion coefficients calculated from creep experiments, usually assuming equal quasi-spherical grains with relaxed boundaries, agree quite well with tracer measurements. In our case, since the length-to-diameter ratio of the grain is greater than 10, comparison will be made using the Herring [38] expression relating the equivalent viscosity, η, of a filament with "bamboo-like" structure to the diffusivity:

$$\eta = \frac{RL}{3B} \quad \frac{KT}{D\Omega} \qquad (7)$$

In the above expression, Ω is the molar volume, 2R, the grain diameter, L the grain length and B takes the asymptotic value of 12.37 for $L \gg R$. For a compound $A_\alpha B_\beta$, Eq. 7 will contain the factor, α, on the right hand side. The Ω term is to be interpreted as the molar volume of the molecular unit and D is the molecular diffusion coefficient. [35] For $\alpha = \beta = 1$, the molecular diffusion coefficient is usually taken as that of the lowest moving species.

Using the suggestion by Farnsworth and Coble [34] that the viscosity coefficient for viscous flow in terms of a tensile stress, σ, and tensile strain rate, $\dot{\epsilon}$, be taken as $\eta = \frac{\sigma}{3\dot{\epsilon}}$, we calculate a diffusion coefficient for creep:

$$D' \simeq 0.91 \times 10^2 \exp\left(-\frac{111,000}{RT}\right) \qquad (8)$$

which agrees with Eq. 5 by a factor of less than 1.5. Herring [38] estimates that the diffusivity calculated from Eq. 7 for boundaries which are normal to the tensile axis, may be smaller by a factor of 2-3 than for the real case in which the boundaries are irregular.

Use of a quasi-spherical grain model, on the other hand, leads to values of D' smaller by a factor of 10 than that given by Eq. 8. In reality, a value intermediate between the extreme limiting cases of quasi-spherical and "bamboo-like" grains might be expected. It would appear, then, that high temperature creep in dense polycrystalline ZrC occurs by a diffusion mechanism and that the rate is controlled by the flux of carbon atoms.

In contrast to these results, Leipold and Nielson [39] measured creep in ZrC which contained appreciable quantities of free carbon along the grain

boundaries. These investigators report an activation energy for creep of about 260 kcal above 2150°C and 75 kcal below that temperature. They suggest, on the basis of comparison of activation energies, that at high temperatures the process is one primarily of deforming the free carbon at the grain boundaries and an unknown process at the lower temperatures. Coble[60] and Ruoff[61] have suggested a modification of the Nabarro-Herring mechanism to account for grain boundary, rather than volume, diffusion controlled creep. Unfortunately, the details of the Leipold-Nielson work are too sketchy (viz. uncertainty of grain size, porosity, etc) to allow a fair test of this model except perhaps to state that the low temperature activation energy which they calculate is in fair agreement with that observed for the grain boundary diffusion of carbon in ZrC.

Blocher, et al.,[42] have measured the rate of carburization of ATJ graphite tubes heated in a ZrI_4 atmosphere. They show that between 1700°C and 2100°C, the formation of ZrC can be expressed as:

$$\frac{w^2}{4t} = 1.74 \exp\left(-\frac{91,500}{RT}\right) \qquad (9)$$

where w is the width of the carbide layer formed in time, t. It is easy to show that the steady-state solution for a hollow cylinder, where diffusion is everywhere radial, reduces to that for diffusion through a plane sheet provided the thickness of the layer is small. Furthermore, Vansant and Phelps[43] have shown that for the diffusion of carbon in TiC, the simplification of a quasi-steady state assumption leads to practically the same result as the Wagner[44] equation for diffusional phase formation. That Blocher, et al., found parabolic layer growth, indicates that a quasi-steady state solution for a plane sheet can be used as an approximation. From Eq. 9, and using the carbon solubility limits given by Vil'k, et al.,[22] and Farr,[23] the apparent diffusivity of carbon, assuming that layer growth is due to a surplus of carbon atoms only, in zirconium carbide is:

$$D'' \simeq 2.4 \exp\left(-\frac{86,000}{RT}\right) \text{ cm}^2/\text{sec} \qquad (10)$$

Adelsberg, et al.,[45] have measured carbide layer growth during the reaction of ZTA graphite with liquid zirconium above 2000°C and report an apparent diffusivity of:

$$0.95 \exp\left(-\frac{78,700}{RT}\right) \text{ cm}^2/\text{sec}.$$

Comparison of the apparent activation energies for carbide formation with Eq. 6 indicates that the carburization process is considerably enhanced by the diffusion of carbon along grain boundaries. Although it may well be fortuitous, Eq. 10 agrees remarkably well with the diffusion coefficients calculated for the in-deep linear portion of the penetration curves, Eq. 6, even ignoring possible correlation effects.

2. CARBON DIFFUSION THROUGH ZIRCONIUM DIBORIDE

The materials procurement problem proved to be more acute in the case of ZrB_2 than it was for ZrC. A wide variety of diboride specimens were obtained from a number of sources. Most of these either contained microcracks or were too small to be of use, and were not further evaluated. The remainder of the specimens, regardless of the source or method of fabrication, contained an included second phase. This phase remained after prolonged high temperature annealing. Polished sections and Laue back-reflection photographs of a variety of these samples are shown in Figures 51 through 59. This second phase was not identified but the lamellar structure suggests ZrB_{12} or free boron. Lynch, et al., [46] have observed Widmenstatten precipitates in single crystal TiB_2 and have concluded, on the basis of electron diffraction patterns of some of the extracted particles, that the included second phase which they observed was nonstoichiometric TiB_2. Nonstoichiometric compounds are also found in Zr, Hf, and Th oxides. This may be true in our case also. Using methods similar to that described by Lynch, et al., work was initiated to extract some of the second phase observed in ZrB_2 but was not completed before the expiration date of this program.

Using the geometry and experimental conditions devised in the study of carbon diffusion in ZrC, diffusion anneals were made with two polycrystalline ZrB_2 specimens. One anneal was conducted at 1840°C for 5 hours and the second at 1860°C for 2 hours. In both cases, the surface activity dropped from about 30,000 cpm to less than 10 cpm upon annealing. The activity of end-faces of the serially-sectioned (chemical sectioning was employed) specimens remained at this level - no concentration profiles were obtained. The physical reasons for this are not immediately obvious but one possibility is that the diffusion of carbon through ZrB_2 is rapid - perhaps several orders of magnitude larger than that of carbon through ZrC. This is mere speculation, however.

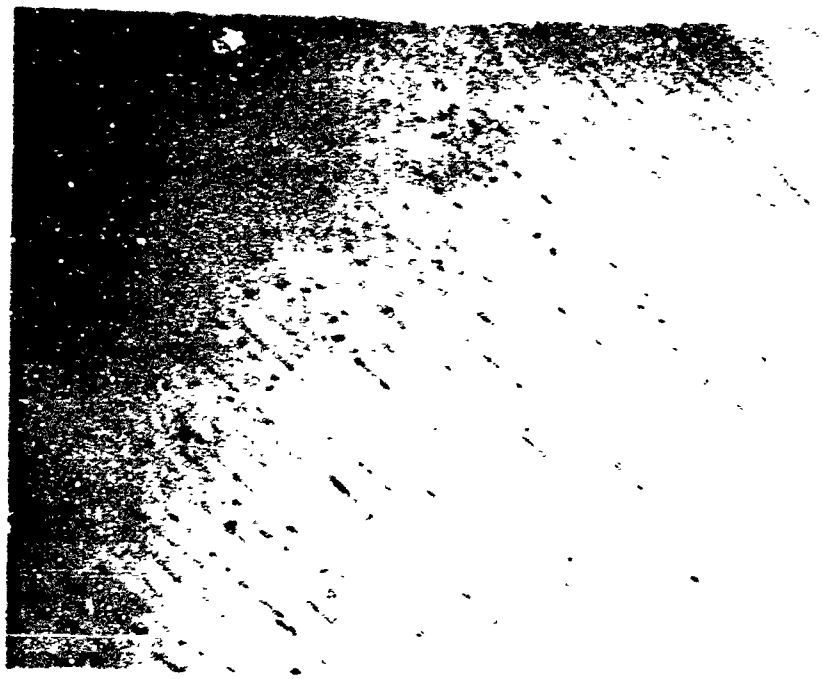

Figure 51. Photomicrograph of Single Crystal ZrB_2 Showing Lamellae of ZrB_{12} or B

Figure 52. Photomicrograph of a Bicrystal or ZrB_2 Showing Lamellae of ZrB_2 or B

Figure 53. Photomicrograph of Polycrystalline ZrB_2 Showing Lamellae of ZrB_{12} or B

Figure 54. Photomicrograph of a ZrB_2 Specimen Showing What Appears to be Free Boron in a Single Crystal Matrix of ZrB_2 (150 X Magnification)

Figure 55. Photomicrograph of the Same ZrB_2 Specimen as Shown in Figure 54, but Showing the Small Amount of Crystallinity Which Exists (150 X Magnification)

Figure 56. Photomicrograph of the Same ZrB_2 Specimen but at High Magnification Illustrating Not Only the Presence of a Free Second Phase but Also of Some Other Perturbation in the Matrix. That This Perturbation Is Real Can Be Seen by Close Examination of the Laue Spots (Figure 57) Which Show a "Spotty" Texture or Nonuniform Blackening

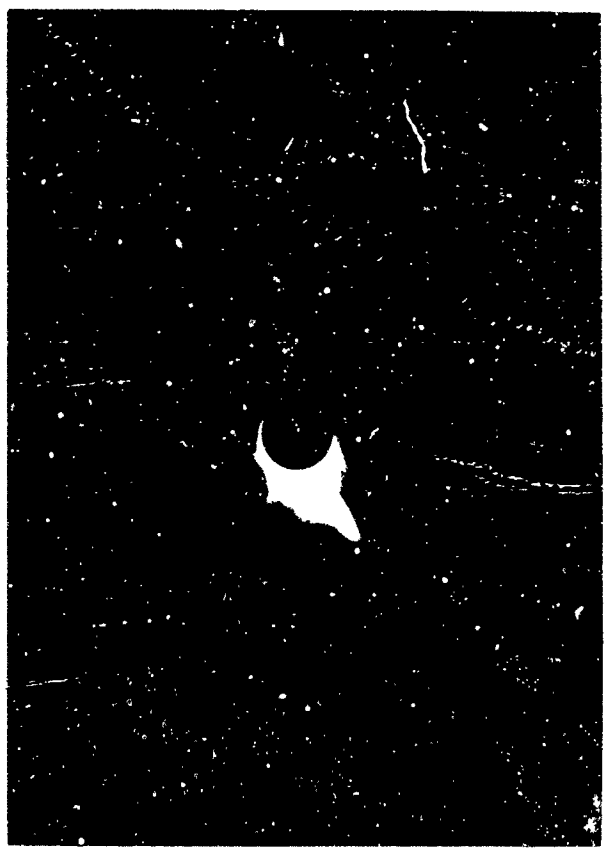

Figure 57. Laue Back-Reflection Photograph of Single Crystal ZrB_2. The Axis of the Crystal Is Nearly Parallel to the (00.1) Pole. The Area Corresponds to That Shown in Figure 54

Figure 58. Laue Back-Reflection Photograph of the Same ZrB_2 Specimen But the Area Exposed to the X-ray Beam Is That Shown In Figure 5. Note the Multiplicity of Spots and Apparent Lack of Hexagonal Symmetry Which Is Readily Apparent in Figure 57

Figure 59. Photomicrograph of a Polycrystalline Specimen of ZrB_2 Which Has Been Heat-Treated at 2130° For Two Hours in an Attempt to Anneal Out the Included Second Phase. The Annealing Appears to be Unsuccessful. The Structure Prior to Annealing Is Shown in Figure 53

IX. STUDIES ON MULTILAYER COATINGS

TASK E-3

1. OXYGEN PERMEABILITY THROUGH ZIRCONIA AND THORIA COATED WITH ZIRCONIUM DIBORIDE

a. Introduction

It was determined previously that the permeabilities of thoria, yttria-stabilized zirconia, and calcia-stabilized zirconia are low enough to permit their use as oxygen barriers in a coating system.[1,2] The object of this work was to determine whether the presence of a ZrB_2 coating influences the permeability of zirconia or thoria to oxygen. Such an influence was, in fact, established.

b. Materials Characterization

The calcia and yttria-stabilized zirconia tubes were identical with those used and characterized previously.[1,2] The thoria tubes were obtained from the Zirconium Corporation of America and were similar to those used previously in the program.[1,2] The density of the thoria, as determined from its buoyancy in water, was 8.80 g/cc, corresponding to a porosity of approximately 12 percent. The material contained few impurities, as shown by the semiquantitative spectroscopic analysis given in Table 13.

TABLE 13

SEMIQUANTITATIVE SPECTROSCOPIC ANALYSIS OF THORIA

Element	Percent
Th	major
Si	~ 0.1
Mg	0.01 to 0.1
Al	0.01 to 0.1
Fe	~ 0.01
Cu	~ 0.01

The zirconium diboride used for coating, obtained commercially, (U. S. Borax Research) had the following analysis: Zr: 79.3%; B: 18.33%; C: 0.65%; N: 0.25%; and O: 0.67%. The theoretical percentages are: Zr: 80.8%; B: 19.2%.

c. Experimental Procedure

The experimental procedure was identical with that described in Section V for oxygen permeation through alumina. Briefly, oxygen was admitted on the inside of the tube and the quantity of oxygen permeating through the tube walls was determined using the ion-gage or the omegatron mass spectrometer. The oxygen reservoir connected to the inside of the tube was fitted with a manometer; oxygen consumption due to permeation and/or chemical reaction could therefore be calculated from the pressure drop and the known volume of the system. A thoria-coated iridium susceptor was used for heating the tubes. Permeability measurements first were made on uncoated zirconia or thoria tubes; the tubes were then coated and the measurements repeated. The coatings were applied by dipping the tubes in a slurry of ZrB_2 powder in xylene with subsequent drying and sintering in vacuum or argon to 1600°-1800°C. An alternate coating method consisted of vapor-depositing ZrB_2 via the decomposition of $Zr(BH_4)_4$ at 600°C in vacuum (see Section VII). The vapor-deposited coating thus consisted of a mixture of ZrB_2 and boron.

d. Results

(1) Calcia-Stabilized Zirconia

When the ZrB_2 coatings were sintered, the calcia-stabilized zirconia tubes all became embrittled and either shattered from thermal shock or developed leaks. The X-ray diffraction patterns showed that the originally cubic (calcia-stabilized) zirconia had been destabilized and had reverted to the monoclinic form. Subsequently, it was found that ZrB_2 does indeed react with CaO at elevated temperatures. A sample of an equimolar powder mixture of CaO (Fisher reagent grade) and ZrB_2 (contained in a ZrB_2 crucible) was held at ~1800°C for 0.5 hours under 0.5 atmospheres of He. A Debye-Sherer powder pattern showed ZrB_2 and $Ca_2B_2O_5$ as identifiable constituents of the reaction product.

(2) Yttria-Stabilized Zirconia

The yttria-stabilized zirconia tubes did not shatter and remained impervious to argon. However, coating with ZrB_2 caused a color change of the oxide from white-yellow to black, indicating that a change in the stoichiometry had occurred. Simple heating in vacuo in the absence of ZrB_2 did not change the color of the tubes. When oxygen permeability measurements were attempted at 1430°C, an initially rapid oxygen absorption occurred (see Figure 60). During the first two hours, no oxygen penetrated the sample. The quantity of oxygen consumed during this time corresponded to the amount of oxygen required to oxidize completely the ZrB_2 coating to ZrO_2 and B_2O_3 (weight of coating, 70 mg; theoretical oxygen consumption, 49.5 mg; experimental, 48 mg). Based on permeability measurements on the same tube prior to the coating application, complete oxidation of the coating should have required approximately 60 hours.

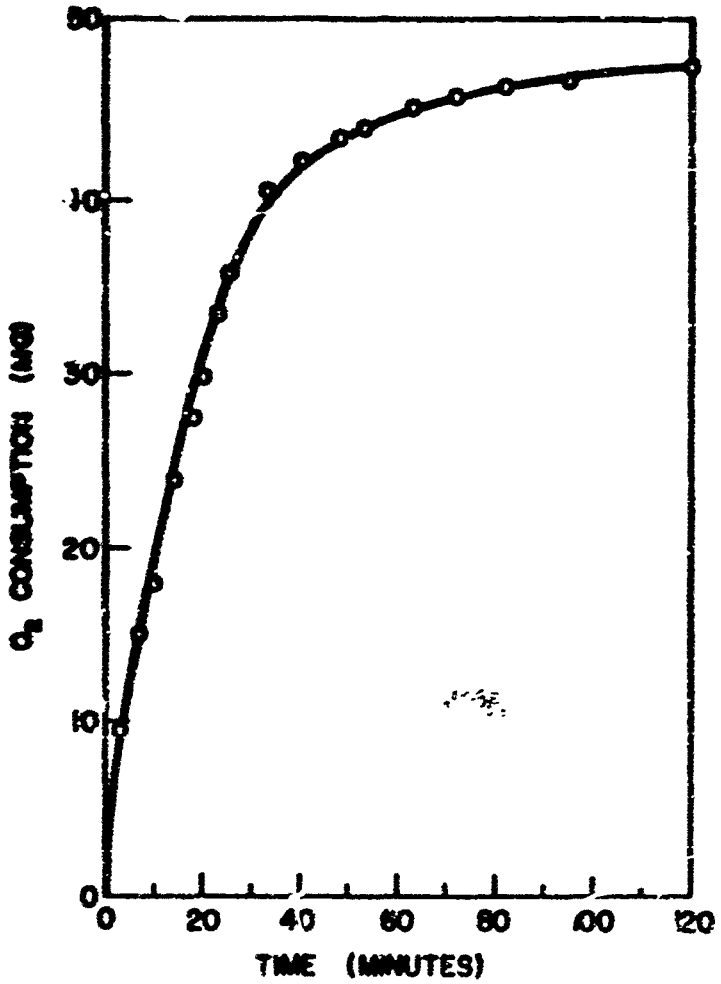

Figure 60. Oxygen Consumption Versus Time for Y_2O_3 Stabilized ZrO_2 Coated With ZrB_2

After oxidation of the coating, the permeability of the tube was identical with that measured before the coating application and the quantity of oxygen consumed (determined from the pressure drop) agreed closely with the permeation rate as determined with the ion-gage.

In order to demonstrate further the oxygen deficiency created by sintering ZrB_2 on ZrO_2, a yttria-stabilized zirconia tube was slurry dip coated in the manner previously described; after the sample was sintered, the coating was mechanically removed before oxygen diffusion measurements were made. Again, oxygen was initially rapidly consumed, but the quantity of oxygen consumed was much smaller; and, after one hour, the tube was completely reoxidized and the permeability was identical with that of uncoated yttria-stabilized zirconia. After this experiment, the color of the material reverted to white-yellow. The coated section of the zirconia tube weighed 7.40 g; oxygen consumption was 0.0165 g. If one ignores the presence of Y_2O_3, the change in stoichiometry of zirconia on sintering in the presence of ZrB_2 was approximately one percent, or, $ZrO_2 \rightarrow ZrO_{1.98}$.

To determine if the oxygen deficiency of zirconia was due to the carbon impurity in ZrB_2, two yttria-stabilized zirconia tubes were vapor coated with carbon-free ZrB_2 by decomposing $Zr(BH_4)_4$. Oxygen permeability measurements at 1430°C were then performed on these tubes. Again, oxygen was initially absorbed very rapidly, and, after the coating was completely oxidized, diffusion proceeded as in uncoated ZrO_2. The amount of oxygen consumed corresponded to the amount calculated to oxidize the coating completely. This result was qualitatively the same as that obtained on slurry dip coated tubes, indicating that the reduction of ZrO_2 was caused not by the carbon content of the ZrB_2 but, rather, by the ZrB_2 itself.

The zirconia used for these investigations contained approximately eight percent Y_2O_3 as a stabilizer. It is not known to what extent (if any) yttria contributed to the observed results.

(3) Thoria Coated With ZrB_2

Oxygen permeability measurements on ZrB_2 coated thoria tubes were carried out at 1660° and 1790°C. The coatings were sintered for three hours in vacuo at the same temperature at which the permeability measurements were to be made, i.e., at 1660°C and 1790°C, respectively.

The results are shown in Figures 61 and 62. The lower (straight line) curve denotes the oxygen consumption determined on the uncoated tubes, which was equal to the permeability. The oxygen consumption determined on the coated tubes was initially approximately three times higher, as shown by the upper curves in Figures 61 and 62. For several hours oxygen did not actually permeate the samples. The time interval after which oxygen appeared in the detection system is also indicated in Figures 61 and 62; the quantity of oxygen consumed up to this point is equal to the amount required for oxidation of the ZrB_2 coating to ZrO_2 and B_2O_3.

After approximately six hours at 1660°C or three hours at 1790°C, the permeability of the coated samples became identical to that measured previously on the uncoated tubes, as evident from the identical slopes of the curves in Figures 61 and 62, respectively. At this point, the oxygen consumption (determined from the pressure drop) again agreed with the permeability determined from the ion-gage reading.

In analogy to the observations on the ZrO_2-ZrB_2 system, ThO_2 also turned dark gray on sintering in the presence of ZrB_2, and the color reverted to white during the permeation runs. Efforts to determine the extent of oxygen deficiency by the method used for the ZrB_2-ZrO_2 system were unsuccessful because the ZrB_2 coating adhered so strongly that it could not be mechanically removed without damaging the thoria tubes.

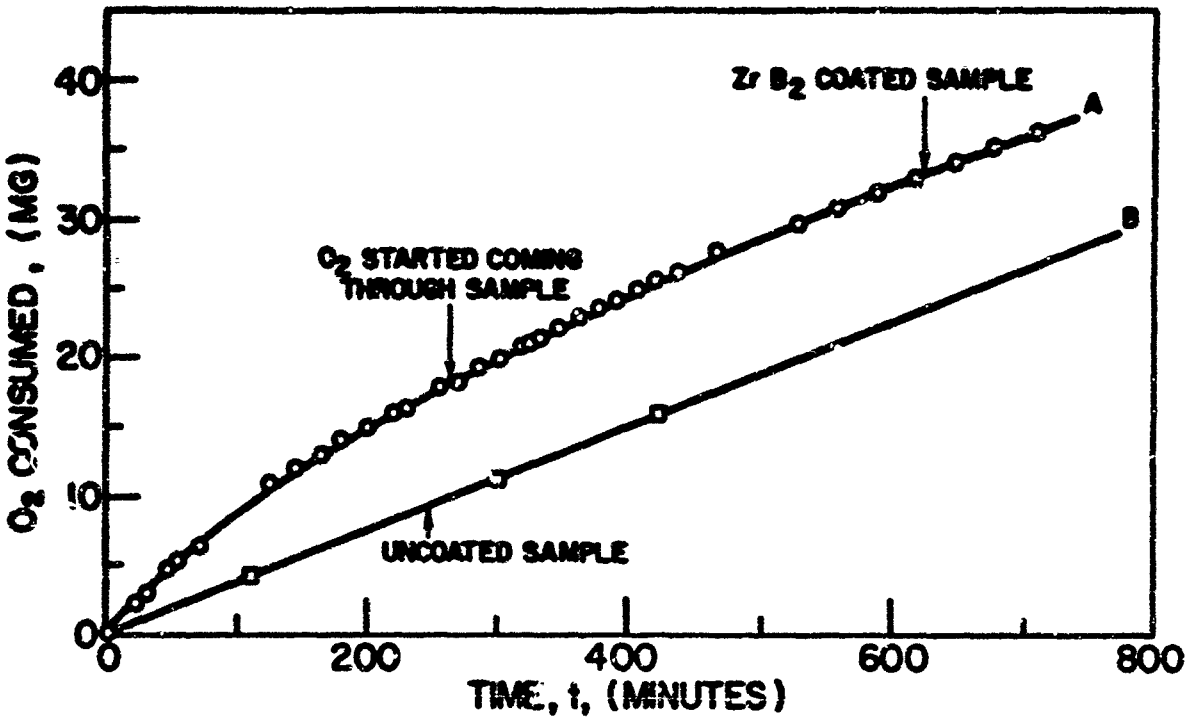

Figure 61. Oxygen Consumption Versus Time for Thoria Coated With ZrB_2 (A) and for Uncoated Thoria (B), Runs at 1660°C

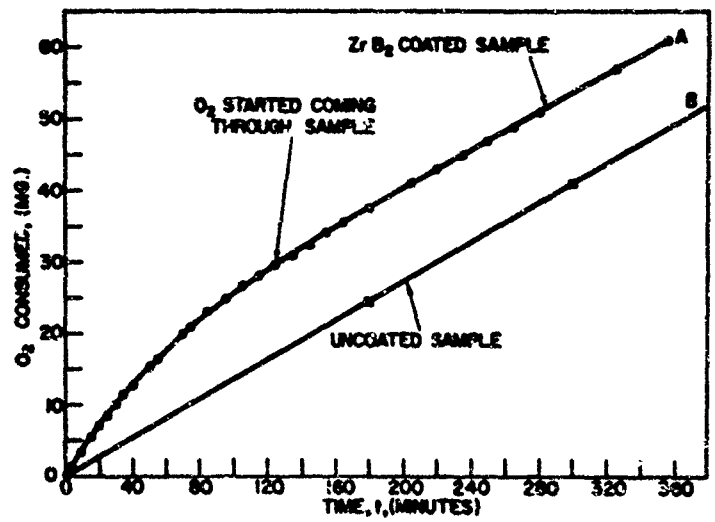

Figure 62. Oxygen Consumption Versus Time for Thoria Coated with ZrB_2 (A) and for Uncoated Thoria (B), Runs at 1790°C

e. Discussion and Conclusions

The time required to oxidize a ZrB_2 coating on ZrO_2 or ThO_2 is substantially shorter than the time calculated from oxygen permeability measurements on the uncoated oxides. The oxygen permeability through ThO_2 and ZrO_2 is therefore enhanced by the presence of ZrB_2.

This result can be qualitatively explained on the basis of thermodynamic considerations. The free energies of formation per mole compound at 1500°C[49] for ZrB_2, ZrO_2, and B_2O_3 are -68, -183, and -204 kcal, respectively. There is, therefore, no extensive chemical reaction between ZrO_2 and ZrB_2. For the hypothetical reaction $3/2\ ZrO_2 + ZrB_2 \rightarrow 5/2\ Zr + B_2O_3$ the free energy change $\Delta F = +138$ kcal and the equilibrium is therefore entirely on the side of ZrO_2 and ZrB_2. However, ZrO_2 and, to a lesser extent, ThO_2 exist over a fairly wide stoichiometry range and become oxygen deficient at low partial pressures of oxygen. The free energy change for the reaction $2/3\ B + O_2 \rightarrow 2/3\ B_2O_3$ at 1500°C is -136 kcal per gram-mole oxygen, corresponding to an equilibrium oxygen pressure in the order of 10^{-16} atmospheres. Similarly, ΔF for the reaction $2/5\ ZrB_2 + O_2 \rightarrow 2/5\ ZrO_2 + 2/5\ B_2O_3$ is -127.6 kcal per gram-mole oxygen at 1500°C, corresponding to an equilibrium oxygen pressure of less than 10^{-15} atmospheres. Vacuum sintering of ZrO_2 or ThO_2 in the presence of ZrB_2 or ZrB_2 + free boron should therefore cause these oxides to become oxygen deficient, and this was indeed observed.

Since it is known that oxygen diffusion in ZrO_2 and ThO_2 occurs by an oxygen vacancy mechanism, the presence of additional vacancies in the oxygen deficient oxides should increase the oxygen permeation rate. More importantly, the presence of an oxygen "sink" (ZrB_2) increases the oxygen vacancy gradient. In a dynamic system, i.e., after oxygen has been admitted to the inside of the tubes, the thermodynamic equilibrium considerations given above are, of course, no longer applicable. The partial pressure of oxygen on the low pressure side (and therefore the vacancy gradient) will be dependent on how fast oxygen is being consumed by reaction with ZrB_2. This is a complicated function of the quantity, density, and particle size of ZrB_2, the rate of diffusion of oxygen through the $ZrO_2 + B_2O_3$ layer and the geometry of the system. In general, as ZrB_2 is oxidized, the oxygen pressure will increase and the vacancy concentration gradient and the permeation rate will decrease. However, as long as unoxidized ZrB_2 remains, the permeation rate will be enhanced. Finally, one would expect this effect to be larger in ZrO_2 than in ThO_2, since the latter oxide is more stable thermodynamically and exhibits smaller variations from stoichiometry. All of our experimental observations are in accordance with these considerations.

The use of iridium as a barrier layer should have negligible effect on the permeability of the oxides. Although accurate thermodynamic data are not available, the oxidation resistance of iridium suggests that the free energies of formation of the iridium oxides are quite small. Iridium should therefore not effect the stoichiometry of the oxides. This is again in accordance with our observations, since ThO_2 coatings on an iridium susceptor remained pure white on vacuum sintering.

The foregoing discussion was intended to show that caution must be exercised in using the available oxygen permeation data. However, neither the thermodynamic calculations nor the experimental observations should be interpreted as automatically eliminating the use of ZrB_2 as a barrier layer on graphite. As was already pointed out, in a dynamic system, the vacancy concentration gradient and, therefore, the oxygen permeation rate will depend critically on how fast oxygen is removed by reaction with ZrB_2. Among other factors, this is dependent on the composition and density (available surface area) of the boride as well as on the composition and structure of the oxide subscale which is formed on oxidation. Recently, some compositions of ZrB_2 and, particularly, of HfB_2 have been found to be quite oxidation resistant[50] and the possible use of compositions of this type as barrier layers on graphite need to be investigated.

REFERENCES

1. Criscione, J.M., Mercuri, R.A., Schram, E.P., Smith, A.W., and Volk, H.F., High Temperature Protective Coatings for Graphite, Technical Documentary Report No. ML-TDR-64-173, Part II (October 1964).

2. Criscione, J.M., Volk, H.F., Nuss, J.W., Mercuri, R.A., Sarian, S., and Meszaros, F.W., High Temperature Protective Coating for Graphite, Technical Documentary Report No. ML-TDR-64-173, Part III (October 1965).

3. Howard, R.A., and Piper, E.L., Research and Development on Advanced Graphite Materials, Volume XIII - Development of a Fine-Grain Isotropic Graphite for Structural and Substrate Applications, Union Carbide Corporation, Contract No. AF 33(616)-6915. WADD TR 61-72, Volume XIII.

4. "Refractory Ceramics for Aerospace," Compiled by Battelle Memorial Institute. Published by the American Ceramic Society, Inc., Columbus Ohio (1964).

5. The Industrial Graphite Engineering Handbook, Published by Union Carbide Corporation, Carbon Products Division, New York (1965).

6. Foster, L.M., Long, G., and Hunter, M.S., J. Am. Cer. Soc. 39, 1 (1956).

7. Campbell, I.E., High Temperature Technology, J. Wiley and Sons, New York (1956), p. 61.

8. Handbook of Chemistry and Physics, Forty-fourth Edition, The Chemical Rubber Publishing Company (1962), 526.

9. Davies, M.O., "Transport Phenomena Aluminum Oxide," NASA TN D 2765, April 8.

10. Oishi, Y., and Kingery, W.D., J. Chem. Phys. 33, 480 (1960).

11. Fryer, T.M., Budworth, D.W., and Roberts, J.P., Trans. Brit. Cer. Soc., 62, 525 (1963).

12. Keihn, F.G., "Research on Physical and Chemical Principles Affecting High Temperature Materials for Rocket Nozzles," Union Carbide Research Institute and Parma Technical Center, Quarterly Progress Report, March 31, 1964, Contract No. DA-30-069-ORD-2787, Pt. III-54.

REFERENCES (Cont'd)

13. Houska, C., and Keplin, E., "Research on Physical and Chemical Principles Affecting High Temperature Materials for Rocket Nozzles," Union Carbide Research Institute, Quarterly Progress Report, September 30, 1963, Contract No. DA-30-069-ORD-2787, Pt. III-51.

14. Richardson, T.H., J. Am. Ceram. Soc., 48, 497 (1965).

15. Grisaffe, S.J., J. Am. Ceram. Soc., 43, 494 (1960).

16. Houska, C.R., J. Am. Ceram. Soc., 47, 310 (1964).

17. Mauer, F.A., and Bolz, L.H., Measurement of Thermal Expansion of Cermet Components by High Temperature X-ray Diffraction, Air Research and Development Command, Wright-Patterson Air Force Base, Ohio, Report No. WADC-TR-55-473, Contract No. AF 33(616)-53-12 (December 1955).

18. Lowrie, Robert, "Research on Physical and Chemical Principles Affecting High Temperature Materials for Rocket Nozzles," Pt. III., p. 26-29, Quarterly Progress Report, Union Carbide Research Institute, Tarrytown, New York, Contract No. DA-30-069-ORD-2787, (30 June 1962).

19. Goldsmith, A., Waterman, T.E., and Hirschborn, H.F., Handbook of Thermophysical Properties of Solid Materials, Macmillan Company (1961).

20. Reid, W.E., Bish, J.M. and Brenner, A., J. Electrochem. Soc. 104, 21 (1957).

21. Bardeen, J., and Herring, C., in Atom Movements (ASM, Cleveland, 1951), Pp. 87; Imperfections in Nearly Perfect Crystals (J. Wiley and Sons, New York, 1952)pp. 261.

22. Vil'k, Yu. N., et al., Zhurnal Prikladnoi Khimii 38, 1500 (1965).

23. Farr, J., data reported by E. K. Storms, USAEC, LAMS-2674, 87 (1962).

24. Lundy, T.S., et al., in: Diffusion in Body-Centered Cubic Metals (ASM, Metals Park, 1965) p. 35.

25. Homan, C.G., Acta Met. 12, 1071 (1964).

REFERENCES (Cont'd)

26. Styris, D. L., and Tomizuka, C. T., J. Appl. Phys. 34, 1001 (1963).

27. Feldman, M. H., et al., J. Appl. Phys. 23, 1200 (1952); Atomic Energy Research Department, North American Aviation, Inc., Report No. NAA-SR-167.

28. See for example the discussion by Tomizuka, C. T., Lundy, T. S., and James, D. W., in: Diffusion in Body-Centered Cubic Metals (ASM, Metals Park, 1965) p. 379.

29. Fisher, J. C., J. Appl. Phys. 22, 74 (1951).

30. Whipple, R. T., Phil. Mag. 45, 1225 (1954).

31. Levine, H. S., and MacCallum, C. J., J. Appl. Phys. 31, 595 (1960).

32. Keihn, F., and Boohns, D, Union Carbide Research Institute, Contract DA-34-069-ORD-2787, Vol. II, Appendix XV (1965).

33. Dorn, J. E., Creep and Recovery (ASM, Cleveland, 1956), p. 255.

34. Farnsworth, P. L., and Coble, R. L., J. Am. Ceram. Soc., 49, 264 (1966).

35. Ruoff, A. L., J. Appl. Phys. 36, 2903 (1965).

36. Folweiler, R. C., J. Appl. Phys. 32, 773 (1961).

37. Nabarro, F. R. N., Report of a Conference on the Strength of Solids, (The Physical Society, London 1948) p. 75.

38. Herring, C., J. Appl. Phys. 21, 437 (1950).

39. Leipold, M. H., and Nielson, T. H., J. Am. Ceram. Soc., 47, 419 (1964).

40. Coble, R. L., J. Appl. Phys. 34, 1679 (1963).

41. Ruoff, A. L., Materials Science Center Report No. 298, Cornell University, Ithaca, New York.

42. Blocher, J. M., et al., BMI-1200 (June, 1957).

43. Vansant, C. A., and Phelps, Jr., W. C., ASM (Transactions Quarterly) 59, 105 (1966).

44. Wagner, C., results published in W. Jost, Diffusion in Solids, Liquids, Gases, (Academic Press, New York, 1960) Pp. 69.

45. Adelsberg, L.M., Cadoff, L.H., and Tobin, J.M., Trans. AIME 236, 972 (1966).

46. Lynch, C.T., Mersol, S.A., and Vahldiek, F.W., J. Less Common Metals, 10, 206 (1966).

47. Ackerman, R.J., Raub, E.G., Thorn, R.J., and Cannon, M.C., J. Phys. Chem. 67, 762 (1963).

48. Ackerman, R.J., and Thorn, A.J., in: Progress in Ceramic Science, Vol. I, (Pergamon Press, New York, 1961), Pp. 39.

49. JANAF, Thermochemical Tables.

50. Kaufman, L., and Clougherty, E.V., Investigation of Boride Compounds for Very High Temperature Applications, RTD-TDR-63-4096, Part III, March 1966.

APPENDIX A

OXIDATION OF IRIDIUM - GASEOUS OXIDES OF IRIDIUM*

J. L. Margrave
Department of Chemistry
Rice University
Houston, Texas

A number of investigators have demonstrated[1, 2, 3] that the only stable crystal lattice in the Ir-O_2 system is that of IrO_2-x, where x ≈ 0 to 0.5. The oxygen pressure over the solid is one atmosphere at ≈ 1375°K.

At higher temperatures and lower oxygen pressures, the existence of several gaseous oxides has been demonstrated. In the range 1300° - 1480°K and oxygen pressures ranging from 35-700 mm, for example, the transpiration studies of Schafer and Heitland[4] and of Alcock and Hooper[5] establish the volatile species as Ir_xO_3 (g) with a standard heat of formation of +3±3 kcal/mole but with x undetermined. Cordfunke and Meyer[6] studied the transpiration of Ir_xOy (g) over the temperature range 1290°-1690°K at O_2 pressures from 157-762 mm with Ir (s) and IrO_2-x (s); they reported that x = 0.976 and that y = 2.990. Thus, they concluded IrO_3 (g) to be the major volatile species and, from the temperature coefficient, deduced a standard heat of formation of +4.65 kcal/mole, a value which is in good agreement with that of other workers. However, in their evaluation of the x-value in Ir_xOy, Cordfunke and Meyer[6] appear to have ignored the variation in IrO_2 (s) stoichiometry which they had established by their own dissociation pressure studies. With this variation, one must increase the range of possible x-value up to 1.15. A more recent study[7] appears to require that x be more nearly equal to 1.

The next definitive study of gaseous iridium oxides was that of Norman, Staley, and Bell,[8] which demonstrated the existence of IrO_3 (g), IrO_2 (g), and IrO (g) as vapor species in the range 1830-2030°K and established the following thermodynamic values:

(1) Ir (s) + O_2 (g) = IrO_2 (g)
$\Delta H_{1900°K} = +48.5 \pm 0.8$ kcal/mole
$\Delta S_{1900°K} = +3.9 \pm 2.0$ e.u.

(2) Ir (s) + $^3/_2$ O_2 (g) = IrO_3 (g)
$\Delta H_{1900} = +5.5 \pm 1.5$ kcal/mole
$\Delta S_{1900} = -13.1 \pm 2.5$ e.u.

---

* Work performed under subcontract with the Carbon Products Division of Union Carbide Corporation, Parma, Ohio, sponsored by the United States Air Force.

At 2033°K, the equilibrium pressures of O_2, IrO_2, and IrO_3 which satisfy the equilibrium $IrO_2(g) + \frac{1}{2} O_2(g) = IrO_3(g)$ were found to be 4.3×10^{-4} atm. for O_2, 1.9×10^{-8} atm. for IrO_3, and 3.1×10^{-9} atm. for IrO_2. The IrO (g) pressure was estimated to be 4×10^{-10} atm. at this temperature, and the mass spectrometric study definitely showed IrO^+ peaks originating from neutral IrO molecules.

From the appearance potential data, one can deduce the stability of IrO (g) as follows:

(3) $IrO_2 + e \rightarrow IrO^+ + O + 2e$ $\qquad AP_2 = 15.1$ ev

(4) $IrO + e \rightarrow IrO^+ + 2e$ $\qquad AP_1 = 10.1$ ev

(3-4) $IrO_2 \rightarrow IrO + O$ $\qquad \Delta(AP) = 5.1$ ev

Thus, 5.1 ev = 115 kcal/mole = $\Delta H_f(IrO) + \Delta H_f(O) - \Delta H_f(IrO_2)$

$$\Delta H_f [IrO(g)] = 105 \text{ kcal/mole.}$$

From these heats of formation and the heat of sublimation of iridium, one derives an average Ir-O bond energy of 110 ± kcal/mole, a value which seems to fit all three gaseous oxides.

It would appear, then, that at high temperatures (~2000°K) and relatively low oxygen pressure (~10^{-4} atm.), IrO_2 (g) and IrO_3 (g) are the major vapor species with IrO (g), because of the highly positive heat of formation (+105 kcal/mole) of IrO (g), which increases rapidly and becomes predominant at temperatures of ≃ 2500°K. At lower temperatures (1300-1700°K) and high oxygen pressures (35-760 mm), the data support Ir_xO_y, where y is almost certainly 3.00 and x lies in the range 0.976 to 1.15.

Alcock and Hooper[5] suggested that x might equal two; tentative confirmation of this possibility in terms of a species Ir_2O_3 (g) was provided by the mass spectrometer studies of Ehlert, Kent, Kuriakose, and Margrave.[9] At ~1173°k and 1 atm. O_2 pressure, extensive transfer of Ir via gaseous oxides was observed; and, with a leak system into the mass spectrometer, the species $Ir_2O_2^+$, with an appearance potential of ~14 ev, was observed. An iodine catalyst was necessary to produce the species, but no oxyiodide peaks were observed. The $Ir_2O_2^+$ signal increased with O_2-pressure and with temperature, as expected from the estimated properties based on bond energy considerations and either the structure

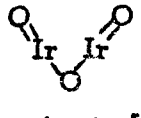

or

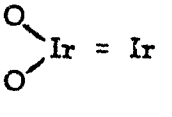

resulting in $\Delta H^\circ_{298} [Ir_2O_3(g)]$ in the range 0-30 kcal/mole.

Norman[9] reports no evidence for $Ir_2O_x^+$ ions with 20 ev electrons at

1373°K and 10^{-4} atm. O_2 pressure, i.e., $P_{Ir_zO_x} + < 10^{-9}$ atm., and, further, claims that $P_{IrO_3} \approx 10^{-10}$ atm. at 1000°K. Consider the equilibrium (5) $Ir_2O_3(g) + {}^3/_2\ O_2(g) = 2IrO_3(g)$ at 1000°K, and let $P_{O_2} = 10^{-4}$ atm., $P_{IrO_3} = 10^{-10}$ atm. and $P_{Ir_2O_3} = 10^{-12}$ atm.

Then, (6) $K_{1000} \approx \dfrac{10^{-20}}{(10^{-12})\ \ (10^{-4})^{3/2}} \approx 10^{-2}$

From the available heats of formation, $\Delta H_{reaction}$ is in the range +10 to -20 kcal/mole; thus K_{eq} could either increase or decrease, but not very fast. If one assumes $K = 10^{-2}$, $\Delta H_r \approx 0$, and $P_{O_2} = 1$ atm.,

$$P^2_{IrO_3} = 10^{-2}\ P_{Ir_2O_3} \text{ or } P_{IrO_3} = 10^{-1}\sqrt{P_{Ir_2O_3}}.$$

For $P_{O_2} = 10^{-4}$ atm., $P_{IrO_3} = 10^{-4}\ \sqrt{P_{Ir_2O_3}}$.

One can calculate the ratios and total pressures as shown in Table 1.

TABLE 1

CALCULATED Ir_xO_y PRESSURES

(a) $P_{O_2} = 1$ atm.

$P_{Ir_2O_3}$ (atm.)	P_{IrO_3} (atm.)	$R = P_{Ir_2O_3}/P_{IrO_3}$
10^{-14}	10^{-8}	10^{-6}
10^{-10}	10^{-6}	10^{-4}
10^{-6}	10^{-4}	10^{-2}
10^{-4}	10^{-3}	10^{-1}
10^{-2}	10^{-2}	1
10^{-0}	10^{-1}	10^{+1}

(b) $P_{O_2} = 10^{-4}$ atm.

$P_{Ir_2O_3}$ (atm.)	P_{IrO_3} (atm.)	R = Ir_2O_3/Ir_2O_3
10^{-14}	10^{-11}	10^{-3}
10^{-10}	10^{-9}	10^{-1}
10^{-6}	10^{-7}	10
10^{-4}	10^{-6}	10^{2}
10^{-2}	10^{-5}	10^{3}
10^{0}	10^{-4}	10^{4}

In the studies of Cordfunke and Meyer[6], P_{IrO_3} (g) was calculated to be in the range 0.8 to 1.15 mm ($\approx 10^{-3}$ atm.) for oxygen pressures near one atm. In this range, according to the Table 1, there would be ≈ 10 percent Ir_2O_3. This result would lead to a gaseous phase of composition $\approx Ir_{1.1}O_{3.0}$, a result which is in agreement with their reinterpreted data. In the studies of Norman, Staley, and Bell, [8,9] $P_{IrO_3} \approx 10^{-10}$ atm. and $P_{Ir_2O_3} \leq 10^{-12}$ atm. at 1000°K. These species, then would not have been detected mass spectrometrically. The fact that Ir_2O_3 (g) is not an important species at higher temperatures is evidence for a heat of formation for Ir_2O_3 (g) near zero, a condition which is in contrast with the definitely endothermic IrO_3, IrO_2, and IrO species. In order that

$$\frac{P_{Ir_2O_3}}{P_{IrO_3}} \leq 10^{-2} \text{ at } 2000°K,$$

it is necessary that $K_{2000} \approx \frac{(10^{-8})^2}{(10^{-10})\ (10^{-4})^{3/2}} \approx 1$. This reasoning implies that ΔH_r = + 18 kcal/mole and, thus, that $\Delta H°_f[Ir_2O_3\,(g)]$ = -8 ±10 kcal/mole.

In summary, there are apparently three and probably four gaseous oxides of iridium: IrO, Ir_2O_3, IrO_2, and IrO_3; the major low temperature species apparently is IrO_3, and IrO_2 and IrO occur at a temperature significantly above 2000°K. The species Ir_2O_3 (g) is apparently formed exothermally and is usually a minor species; however, at high O_2 pressures and temperatures low enough that Keq ≤ 1, it is possible for Ir_2O_3 (g) to be the major species.

REFERENCES

Appendix A

1. Wöhler, L., and Witzmann, W., Z. Elektrochem. 14, 97 (1908).
2. Wöhler, L., and Jochum, N., Z. Physik. Chem. 167A, 169 (1933).
3. Cordfunke, E. H. P., and Meyer, G., Rec. Trav. Chim. 81, 495 (1962).
4. Schafer, H., and Heitland, H., Z. anorg, allgem. Chemie. 304, 249 (1960).
5. Alcock, C. B., and Hooper, G. W., Proc. Roy. Soc. 254A, 557 (1960).
6. Cordfunke, E. H. P., and Meyer, G., Rec. Trav. Chim. 81, 670 (1962).
7. Bell, W. E., Tagami, M., and Ianyard, R. E., J. Phys. Chem. 70 2048 (1966).
8. Norman, J. H., Staley, H. G., and Bell, W., J. Chem. Phys. 42, 1123 (1965).
9. Ehlert, T. C., Kent, R. A., Kuriakose, A. K., and Margrave, J. L., in Appendix A, High Temperature Protective Coatings for Graphite, Technical Documentary Report No. ML-TDR-64-173, Part III, (December 1965).
10. Norman, J. H., Private Communication (May 24, 1965).

APPENDIX B

MASS SPECTROMETRIC STUDIES OF THE VAPORS OVER THE REFRACTORY OXIDES $CaZrO_3$ AND $HfSiO_4$

P. Ficalora, C. H. Williams, K. Zmbov and J. L. Margrave
Department of Chemistry
Rice University
Houston, Texas

Among the possible refractory coatings for graphite are various high melting oxides, both binary and ternary. Clearly, their use will be limited either by the production of stable, volatile species or by the attainment of a rapid rate of reaction with the graphite layer on which they are deposited. Since unexpectedly stable, complex molecular species have recently been reported in the gases over refractory molybdates, tungstates, stannates, etc.,[1,2] this work on $CaZrO_3$ and $HfSiO_4$ was undertaken to see if these oxides, too, volatilize appreciably in the form of ternary molecular species.

EXPERIMENTAL

The Knudsen cell sampling system for the Bendix time-of-flight mass spectrometer was used for the $CaZrO_3$ studies to temperatures of ~1900°K, limited by the LUCALOX supports; the $HfSiO_4$ study was conducted in the magnetic mass spectrometer up to ~2300°K, with the Knudsen cell impaled on W support rods. Various containers were tried (Ta, ZrO_2, and ThO_2); and since the least reaction was observed for ThO_2 containers, they were used.

With a Ta-cell, Ca^+/Ca was the only species observed over $CaZrO_3$; with ZrO_2 and ThO_2, both CaO+/CaO and Ca+/Ca were observed at 1325° and 1500°C, respectively. For $HfSiO_4$ heated in a ThO_2 cell, the only ions observed were SiO+, SiO_2^+, and $Si_2O_2^+$. No gaseous species containing Zr or Hf were observed in either set of experiments.

In the mass spectrometric experiments with $CaZrO_3$ in a ZrO_2 or ThO_2 linear, shutterable peaks of Mg+, Ns+, SiO+, and SiO_2^+ were seen and attributed to the ceramic linears in addition to the shutterable peaks for Ca^+ and CaO+. The CaO+ peak was first observed at ~1326°C and was monitored against temperature through 1550°C. The slope of log IT versus 1/T, the ion current times the temperature, versus 1/T plot was linear and gave $\Delta H_s = 90 \pm 3$ kcal/mole^{-1} whereas ΔH_s for pure CaO is ~139

* Work performed under subcontract with the Carbon Products Division of Union Carbide Corporation, Parma, Ohio, sponsored by the Unites States Air Force.

kcal/mole^{-1}, as reported by Babeliowsky[3]. When the sample was heated above 1550°C, a change in acitivity of CaO was indicated by curvature in the IT versus 1/T plot toward lower slopes. The results were the same for either ZrO_2 or ThO_2 liners.

The Ca^+ signal in both experiments was appreciable by the time the temperature reached 1500°C and it increased rapidly with the temperature, but with decreasing activity as indicated. The log IT versus 1/T plot for the Ca^+ signal yields $\Delta H = 53 \pm 3$ kcal/mole^{-1} from the slope.

Appearance potentials for Ca^+ and CaO^+ were measured using O_2^+ and Ag^+ as standards. The appearance potential of CaO^+ was found to be 8.7 e.v., whereas that of Ca^+ was essentially the same as that of Ca-metal atoms determined from optical spectroscopy. The Ca^+ signal may, therefore, be from Ca-metal produced by reduction of CaO^+ on the Ta heat shields. The total absence of the CaO^+ peak when a Ta Knudsen cell without a liner is used supports this viewpoint.

As $HfSiO_4$ was heated in a ThO_2 Knudsen cell at temperatures up to 2300°K, the only ionic species due to molecules effusing from the cell were SiO^+, $SiO_2O_2^+$, and SiO_2^+. No ions containing Hf were identified in the mass spectrum even at low bombardment voltages.

The ion currents for SiO^+ and SiO_2^+ were recorded over the temperature range 1600-2300°K, and plots of log IT versus 1/T gave straight lines from which one may calculate "heats of sublimation" for SiO, and SiO_2 of 94 ± 3 and 68 ± 3 kcal/mole^{-1}, respectively. The heat of sublimation for forming SiO_2 (g) from cristobalite was reported by Porter, Chupka, and Inghram[4] as $\Delta H_{298} = 136 \pm 8$ kcal/mole^{-1}.

DISCUSSION OF RESULTS

In evaluating these experiments, one must first consider that the samples studied were not ideal. From X-ray diffraction, for example, the $CaZrO_3$-sample was shown to be mainly calcium zirconate, but there were also present significant amounts of two uncombined oxides. The $HfSiO_4$ (s) was the only phase detected in the $HfSiO_4$ studied. There is no detailed information on the stoichiometry of either solid, and, since both ZrO_2 and HfO_2 show homogeneity ranges of some breadth, it is appropriate to describe the samples studied as Ca_xZrO_y, where $x \approx 1$ and $y \approx 3$ and as $HfSi_uO_v$, where $u \approx 1$ and $v \approx 4$.

If $x = 1$ and $y = 3$, exactly, then one could write a straightforward equation for the high-temperature decomposition:

$$CaZrO_3 \text{ (solid)} \rightleftharpoons CaO \text{ (gas)} + ZrO_2 \text{ (solid)};$$

this equation would be correctly descriptive unless a stable $CaZrO_3$ (g) molecule exists . The low appearance potential of CaO^+ and the non-observation of any gaseous species containing Zr seem to eliminate the possibility of a gaseous $CaZrO_3$ species at the temperatures and pressures of this study.

For the exactly stoichiometric case, assuming that $CaZrO_3$ (s) forms from the oxides in a slightly exothermic process, one predicts that the slope of a log IT versus 1/T plot for CaO^+ should be equal to or greater than 139 kcal/mole^{-1}, i.e., the energy to sublime CaO (g) from pure CaO (s).

The observations are clearly in disagreement with this expectation, since the slope of the plot for $CaO^+/CaZrO_3$ is only 90 ± 3 kcal/mole^{-1}. This result is apparently another example of the complex behavior of transition metal oxides already observed in studies of binary systems (ZrO_2, TiO, U_xO_y, etc.) discussed recently by Kubaschewski[5]. One can expect large deviations from the behavior of stoichiometric solids.

The process studied is more appropriately written

$$Ca_xZrO_y\,(\text{solid}) \rightleftharpoons b\,CaO\,(\text{gas}) + Ca_{x-b}ZrO_{y-b}\,(\text{solid})$$

or $$(\text{solid I}) \rightleftharpoons CaO\,(\text{gas}) + (\text{solid II})$$

and $$\Delta H_{1300\text{-}1500^\circ K} \approx 90 \text{ kcal/mole}^{-1}.$$

Further studies of $CaZrO_3$ samples of various known stoichiometries are required to evaluate these data in detail and provide a complete thermodynamic description of the sublimation process.

A similar approach is required for the $HfSiO_4$ data. In this case, the temperature-dependence of the SiO_2^+ signal from $HfSiO_4$ (s) is 68 ± 10 kcal/mole^{-1} less than the SiO_2^+/SiO_2 heat of sublimation reported[4] Thus,

$$HfSi_uO_v\,(\text{solid}) = bSiO_2\,(\text{gas}) + HfSi_{u-b}O_{v-2b}\,(\text{solid});$$

and the energy of the volatilization process can be less than the enthalpy of sublimation of pure SiO_2, even though the ternary oxide is formed exothermically in oxygen deficient compounds. The SiO+ comes from the equilibrium

$$SiO_2\,(\text{gas}) \rightleftharpoons SiO\,(\text{gas}) + \tfrac{1}{2}\,O_2 \text{ or } O\,(\text{gas})$$

which has a high positive heat but also a high positive entropy so that appreciable dissociation occurs at temperatures of 2000°K and low oxygen pressures.

CONCLUSIONS

Both $CaZrO_3$ and $HfSiO_4$ vaporize appreciably at temperatures of 1500-2300°K by evolution of gaseous CaO and SiO, SiO_2, respectively. The temperature dependences suggest that these gaseous species are more easily evolved from the ternary systems than from the respective pure binary oxides. This result can be explained if the ternary oxides have wide homogeneity ranges, small exothermic to fairly endothermic heats of formation from the binary oxide, and/or positive entropies of formation from the binary systems.

No ternary gaseous oxide molecular species were detected in this study.

REFERENCES

Appendix B

1. Vaporization of Compounds and Alloys at High Temperatures, Part XXIV. Mass Spectrometric Determination of the Stability of Gaseous Molybdates, Tungstates, Molybdites, and Tungstites of Magnesium, Calcium, Strontium, and Tin. Verhaegen, G., Colin, R., and Drowart, J., Wright-Patterson Air Force Base, Ohio, TDR No. WADD 60-782, Part XXIV.

2. Berhaegen, G., Colin, R., Exsteen, G., and Drowart, J., Trans. Farad. Soc., 61, 1372 (1965).

3. Babeliowsky, T.P.J.H., J. Chem. Phys. 38, 2035 (1963).

4. Porter, R.F., Chupka, W.A., and Inghram, M.G., J. Chem. Phys. 23, 216 (1955).

5. Kubaschewski, O., Bull. Soc. Chem. France, 1170 (1965).

Unclassified
Security Classification

DOCUMENT CONTROL DATA - R&D

(Security classification of title, body of abstract and indexing annotation must be entered when the overall report is classified)

1 ORIGINATING ACTIVITY (Corporate author)
Union Carbide Corporation
Carbon Products Division,
Parma, Ohio

2a. REPORT SECURITY CLASSIFICATION
Unclassified

2b GROUP

3 REPORT TITLE

High Temperature Protective Coatings for Graphite (Part IV)

4 DESCRIPTIVE NOTES (Type of report and inclusive dates)
Final Summary Technical Report 1 June 1965 to 31 May 1966

5. AUTHOR(S) (Last name, first name, initial)
Criscione, J.M., Sarian, S., Volk, H.F., Mercuri, R.A., Nuss, J.W., and Meszaros, F.W.,

6. REPORT DATE	7a. TOTAL NO. OF PAGES	7b. NO. OF REFS
November 1966	111	50

8a. CONTRACT OR GRANT NO.	9a. ORIGINATOR'S REPORT NUMBER(S)
AF 33(657)-11253	ML-TDR-64-173 Part IV
b. PROJECT NO. 7350	
c. Task No. 735002	9b. OTHER REPORT NO(S) (Any other numbers that may be assigned this report)
d.	

10. AVAILABILITY/LIMITATION NOTICES This document is subject to special export controls and each transmittal to foreign governments or foreign nationals may be made only with prior approval of the Metals and Ceramics Division, Air Force Materials Laboratory (MAMC), Wright-Patterson Air Force Base, Ohio 45433.

11 SUPPLEMENTARY NOTES	12. SPONSORING MILITARY ACTIVITY
	Air Force Materials Laboratory, Research and Technology Division, Air Force Systems Command, Wright-Patterson AFB, Ohio

13. ABSTRACT

The final annual report of a three-year program concerning basic factors controlling the oxidation behavior of high temperature protective coatings for graphite is presented.

The work includes: the permeability of Al_2O_3, ZrO_2 in contact with ZrB_2, and ThO_2 in contact with ZrB_2 to oxygen; the iridium-carbon eutectic temperature; the thermal expansion of ZrB_2, HfB_2, and various composites of ZrB_2 and HfB_2 with one of the rare earth hexaborides, CeB_6, YB_4, or LaB_4; the deposition of ZrB_2 on graphite via the decomposition of $Zr(BH_4)_4$; the diffusion of carbon in zirconium monocarbide and zirconium diboride; a review of the literature concerning the vapor species in the iridium-oxygen system and mass spectrometric studies involving the dissociation of $CaZrO_3$ at temperatures to 1600°C and $HfSiO_4$ at temperatures to 2000°C.

DD FORM 1 JAN 64 1473

Unclassified

KEY WORDS	LINK A		LINK B		LINK C	
	ROLE	WT	ROLE	WT	ROLE	WT
Oxidation Protection						
High Temperature Coatings						
Graphite						
Iridium						
Borides						
Carbides						
Oxides						
Reaction kinetics						
Permeability						
Diffusion Volatility						

INSTRUCTIONS

1. ORIGINATING ACTIVITY: Enter the name and address of the contractor, subcontractor, grantee, Department of Defense activity or other organization *(corporate author)* issuing the report.

2a. REPORT SECURITY CLASSIFICATION: Enter the overall security classification of the report. Indicate whether "Restricted Data" is included. Marking is to be in accordance with appropriate security regulations.

2b. GROUP: Automatic downgrading is specified in DoD Directive 5200.10 and Armed Forces Industrial Manual. Enter the group number. Also, when applicable, show that optional markings have been used for Group 3 and Group 4 as authorized.

3. REPORT TITLE: Enter the complete report title in all capital letters. Titles in all cases should be unclassified. If a meaningful title cannot be selected without classification, show title classification in all capitals in parenthesis immediately following the title.

4. DESCRIPTIVE NOTES: If appropriate, enter the type of report, e.g., interim, progress, summary, annual, or final. Give the inclusive dates when a specific reporting period is covered.

5. AUTHOR(S): Enter the name(s) of author(s) as shown on or in the report. Enter last name, first name, middle initial. If military, show rank and branch of service. The name of the principal author is an absolute minimum requirement.

6. REPORT DATE: Enter the date of the report as day, month, year, or month, year. If more than one date appears on the report, use date of publication.

7a. TOTAL NUMBER OF PAGES: The total page count should follow normal pagination procedures, i.e., enter the number of pages containing information.

7b. NUMBER OF REFERENCES: Enter the total number of references cited in the report.

8a. CONTRACT OR GRANT NUMBER: If appropriate, enter the applicable number of the contract or grant under which the report was written.

8b, 8c, & 8d. PROJECT NUMBER: Enter the appropriate military department identification, such as project number, subproject number, system numbers, task number, etc.

9a. ORIGINATOR'S REPORT NUMBER(S): Enter the official report number by which the document will be identified and controlled by the originating activity. This number must be unique to this report.

9b. OTHER REPORT NUMBER(S): If the report has been assigned any other report numbers *(either by the originator or by the sponsor)*, also enter this number(s).

10. AVAILABILITY/LIMITATION NOTICES: Enter any limitations on further dissemination of the report, other than those imposed by security classification, using standard statements such as:

(1) "Qualified requesters may obtain copies of this report from DDC."

(2) "Foreign announcement and dissemination of this report by DDC is not authorized."

(3) "U. S. Government agencies may obtain copies of this report directly from DDC. Other qualified DDC users shall request through _____."

(4) "U. S. military agencies may obtain copies of this report directly from DDC. Other qualified users shall request through _____."

(5) "All distribution of this report is controlled. Qualified DDC users shall request through _____."

If the report has been furnished to the Office of Technical Services, Department of Commerce, for sale to the public, indicate this fact and enter the price, if known.

11. SUPPLEMENTARY NOTES: Use for additional explanatory notes.

12. SPONSORING MILITARY ACTIVITY: Enter the name of the departmental project office or laboratory sponsoring *(paying for)* the research and development. Include address.

13. ABSTRACT: Enter an abstract giving a brief and factual summary of the document indicative of the report, even though it may also appear elsewhere in the body of the technical report. If additional space is required, a continuation sheet shall be attached.

It is highly desirable that the abstract of classified reports be unclassified. Each paragraph of the abstract shall end with an indication of the military security classification of the information in the paragraph, represented as *(TS), (S), (C), or (U)*.

There is no limitation on the length of the abstract. However, the suggested length is from 150 to 225 words.

14. KEY WORDS: Key words are technically meaningful terms or short phrases that characterize a report and may be used as index entries for cataloging the report. Key words must be selected so that no security classification is required. Identifiers, such as equipment model designation, trade name, military project code name, geographic location, may be used as key words but will be followed by an indication of technical context. The assignment of links, rules, and weights is optional.